SYNTHESIS OF BIOACTIVE COPPER PYRIDINE COMPLEXES AND PREPARATION OF NANOPARTICLES FOR BIOSEPARATION

THUMMARUK SUKSRICHAVALIT

A THESIS SUBMITTED IN PARTIAL FULFILLMENT
OF THE REQUIREMENTS FOR
THE DEGREE OF DOCTOR OF PHILOSOPHY
(MEDICAL TECHNOLOGY)
FACULTY OF GRADUATE STUDIES
MAHIDOL UNIVERSITY
2010

Thesis
entitled

SYNTHESIS OF BIOACTIVE COPPER PYRIDINE COMPLEXES AND PREPARATION OF NANOPARTICLES FOR BIOSEPARATION

Mr.Thummaruk Suksrichavalit
Candidate

Prof.Virapong Prachayasittikul,
Ph.D.
Major-advisor

Assoc.Prof.Chartchalerm Isarankura-Na-Ayudhya,
Ph.D.
Co-advisor

Lect.Theeraphon Piacham,
Ph.D
Co-advisor

Asst. Prof. Auemphorn Mutchimwong,
Ph.D.
Acting Dean
Faculty of Graduate Studies
Mahidol University

Prof. Virapong Prachayasittikul,
Ph.D.
Program Director
Doctor of Philosophy Program in Medical Technology
Faculty of Medical Technology
Mahidol University

Thesis
entitled

SYNTHESIS OF BIOACTIVE COPPER PYRIDINE COMPLEXES AND PREPARATION OF NANOPARTICLES FOR BIOSEPARATION

was submitted to the Faculty of Graduate Studies, Mahidol University
for the degree of Doctor of Philosophy (Medical Technology)
on
November 30, 2010

Mr. Thummaruk Suksrichavalit
Candidate

Prof. Somsak Ruchirawat,
Ph.D. (Organic Chemistry)
Chair

Prof. Virapong Prachayasittikul,
Ph.D.
Member

Assoc. Prof. Chartchalerm Isarankura-Na-Ayudhya,
Ph.D.
Member

Prof. Supaluk Prachayasittikul,
Ph.D.
Member

Lect. Lertyot Treeratanapiboon,
Ph.D.
Member

Asst. Prof. Auemphorn Mutchimwong,
Ph.D.
Acting Dean
Faculty of Graduate Studies
Mahidol University

Prof. Virapong Prachayasittikul,
Ph.D.
Dean
Faculty of Medical Technology
Mahidol University

ACKNOWLEDGEMENTS

I have been living in Faculty of Medical Technology, Mahidol University for approximately 10 years from past to present. In 2004, I was a graduate student that I would like to take this opportunity to thank all committees in the Ph.D program here. I would like to thank a number of people who helped and cheered me during my Ph.D study. First of all and above all things, I would like to express my gratitude to my major advisor Prof. Virapong Prachayasittikul for all continuous help, support, and scientific guiding. I could not manage to write and to criticize my thesis without all your supports. Especially, I really appreciate that you often have kindly shared a time whenever I needed a help or discussion. I would also like to thank two co-advisors Assoc. Prof. Chartchalerm Isarankura Na Ayuhya and Lect. Theeraphon Piacham for their extensive support, guidance, and mentor during the time of my Ph.D.

Assoc. Prof. Supaluk Prachayasittikul, I appreciate all your help, when I occasionally appeared and asked questions and helps. I would like to thank you for chemical training.

I am grateful to Prof. Leif Bülow and Lei Ye at the Department of Pure and Applied Biochemistry, Center of Chemistry and Chemical Engineering, Lund University for their support and guidance when I was in Sweden. Prof. Klaus Mosbach, I appreciate all your guidance during my time as a visiting student in Lund, Sweden. Thank you, Ulla Jeppsson Wistrand and Ingrid Nilsson, for all your help supports inside and outside of a laboratory. It was a great support particularly in the beginning when I came to Sweden and did not know the things in Lund.

I am grateful for The Ministry Staff Development Project by the Ministry of Education from Thailand for financial support during my Ph.D study.

All the friends and colleagues we had a good together in Lund and here. Since it is impossible to list all names, I would not write them here. But I hope you recognize about yourself. What I can say is that the time I spent with all of you were just a great and I appreciate the friendship.

Eventually, I would like to say my special thanks to my family for their support, care, and love. I would like to thank my sister for their wisdoms. I would like to deeply thank my parents for their devotion, care, and support throughout the years.

Thummaruk Suksrichavalit

SYNTHESIS OF BIOACTIVE COPPER PYRIDINE COMPLEXES AND PREPARATION OF NANOPARTICLES FOR BIOSEPARATION

THUMMARUK SUKSRICHAVALIT 4738067 MTMT/D

Ph.D. (MEDICAL TECHNOLOGY)

THESIS ADVISORY COMMITTEE: VIRAPONG PRACHAYASITTIKUL, Ph.D., CHARTCHALERM ISARANKURA-NA-AYUDHYA, Ph.D., THEERAPHON PIACHAM, Ph.D.

ABSTRACT

The reactive oxygen species is the most radical species of free radicals in biological systems which causes damage to DNA, proteins, and lipids. Therefore, free radical scavengers (such as vitamin E, glutathione, flavonoids, superoxide dismutase (SOD), glutathione peroxidase, and more) are essential to prevent abnormalities caused by oxidative stress. Because of this, antioxidants have been studied in attempts to find new antioxidants, to improve antioxidant activity, and to develop extraction yield as well as extraction processes. Our studies herein report the synthesis of antioxidant molecules based on copper pyridine complexes and the extraction of materials for antioxidants by molecularly imprinted polymer (MIP) and clicked boronic acid affinity Sepharose. Copper complexes of nicotinic acid (vitamin B3) with general metabolites were successfully synthesized. All complexes were characterized as tetragonally distorted geometries. The complexes exhibited superoxide-scavenging activity also known as SOD mimic. The SOD activities of the complexes were in the range of 34.42-130.20 μM. The best SOD mimic was the copper complex of nicotinic acid with phthalic acid. Moreover, the complexes also demonstrated having antimicrobial activity against B. subtilis ATCC 6633 and C. albicans ATCC 90028 with an MIC range of 128-256 μg/mL. A computer simulation was also applied to study the correlation between quantum chemical parameters and SOD activity. The results showed that the SOD activities of the complexes were well correlated with electron affinity (EA), highest occupied molecular orbital (HOMO) energy, and lowest unoccupied molecular orbital (LUMO) energy. In addition, this thesis also developed an extraction method based on molecularly imprinted polymer (MIP) for antioxidant separation. The MIP was used to generate binding pockets in the polymers by providing a specific cavity for tocopherol (vitamin E) and tocopherol acetate. The imprinted polymers for tocopherol (MIP-TP) and tocopherol acetate (MIP-TPA) were successfully prepared by using a bulk polymerization method. Moreover, tocopherol-imprinted polymer (MIP-TP) was also synthesized by the precipitation polymerization method. The MIP-TP displayed a two-fold greater binding capacity than the corresponding non-imprinted polymer and also exhibited specific binding with tocopherol as compared to MIP-TPA. While MIP-TP nanospheres were able to bind to the tocopherol template approximately 1.22-1.57 times greater as compared to the non-imprinted polymer, the highest binding capacity of the nanospheres was 1.85 times greater than the imprinted and non-imprinted polymer in the optimal rebinding solvent of ethanol:water (8:2, v/v). Furthermore, novel clicked affinity ligand based on boronic acid was successfully synthesized. The ligand was coupled to azide-functionalized Sepharose using a Cu(I)-catalyzed 1,3-cycloaddition reaction called click reaction. In this thesis, two common glycoproteins: ovalbumin and ribonuclease B (RNase B), were used as models of glycosylated and glycated biomolecules. Compared to unmodified Sepharose, the new clicked Sepharose showed good efficiency for glycoprotein separation in the presence of non-glycoproteins: bovine serum albumin (BSA), RNase A and crude bacterial proteins. The SOD mimics are expected to be useful as potential candidates for antioxidative therapeutics. The methods for bioseparation present an effective model for extracting antioxidants.

KEY WORDS: SUPEROXIDE DISMUTASE MIMIC/ NICOTINIC ACID/ MOLECULARLY IMPRINTED POLYMER/ VITAMIN E/ CLICK CHEMISTRY/ BORONIC ACID/ GLYCOPROTEIN

166 pages

การสังเคราะห์สารประกอบเชิงซ้อนโลหะของคอปเปอร์ด้วยอนุพันธ์ของไพริดีนที่มีฤทธิ์ทางชีวภาพและการเตรียมโมเลกุลขนาดนาโนเพื่อใช้ในการแยกสารทางชีวภาพ

SYNTHESIS OF BIOACTIVE COPPER PYRIDINE COMPLEXES AND PREPARATION OF NANOPARTICLES FOR BIOSEPARATION

ธรรมรักษ์ สุขศรีชวลิต 4738067 MTMT/D

ปร.ด. (เทคนิคการแพทย์)

คณะกรรมการที่ปรึกษาวิทยานิพนธ์ : วีระพงศ์ ปรัชชญาสิทธิกุล, Ph.D., ฉัตรเฉลิม อิศรางกูร ณ อยุธยา, Ph.D., ธีรพล เปียฉ่ำ, Ph.D.

บทคัดย่อ

อนุมูลอิสระกลุ่มออกซิเจน เป็นกลุ่มของอนุมูลอิสระที่พบมากที่สุดในระบบของสิ่งมีชีวิต แล้วยังเป็นสาเหตุให้เกิดความเสีย หายของดีเอ็นเอ โปรตีน และไขมัน ดังนั้นสารต้านอนุมูลอิสระ เช่น วิตามินอี กลูตาไทโอน เอนไซม์ซุปเปอร์ออกไซด์ดิสมูเตส เอนไซม์กลูตาไทโอนเปอร์ออกซิเดส เป็นต้น ถือว่าเป็นสิ่งจำเป็นที่ช่วยป้องกันความผิดปกติที่เกิดจากอนุมูลอิสระ ด้วยสาเหตุนี้สารต้านอนุมูลอิสระถูกนำมาศึกษาอย่างต่อเนื่อง เพื่อหาสารชนิดใหม่ๆ เพื่อเพิ่มประสิทธิภาพในการกำจัดอนุมูลอิสระและเพื่อพัฒนาวิธีการสกัดสารต้านอนุมูลอิสระ ก็ยังคงมีการศึกษาวิจัยอยู่จนถึงปัจจุบันในการศึกษาครั้งนี้ เราได้ทำการสังเคราะห์สารต้านอนุมูลอิสระจากสารประกอบเชิงซ้อนโลหะคอปเปอร์ของอนุพันธ์ไพริดีน และยังพัฒนากระบวนการสกัดสารต้านอนุมูลอิสระจาก 2 วิธีคือ โมเลกุลเชิงซ้อนที่มีคุณสมบัติจับจำเพาะ และโมเลกุลจับจำเพาะของอนุพันธ์กรดโบโรนิก ส่วนแรกของการศึกษาเราประสบความสำเร็จในการสังเคราะห์สารประกอบเชิงซ้อนโลหะคอปเปอร์ ของกรดนิโคตินิกหรือวิตามินบีสาม กับสารทั่วไปที่พบในกระบวนการสันดาบในร่างกาย หลังการวิเคราะห์พบว่าสารประกอบที่สังเคราะห์มีโครงสร้างเป็นปิรามิดฐานสามเหลี่ยม สารประกอบเชิงซ้อนดังกล่าวถูกพบว่ามีฤทธิ์ในการกำจัดซุปเปอร์ออกไซด์หรือสามารถเรียกได้อีกอย่างหนึ่งว่า มีฤทธิ์เสมือนเอนไซด์ซุปเปอร์ออกไซด์ดิสมูเตส โดยฤทธิ์ในการกำจัดซุปเปอร์ออกไซด์ของสารประกอบเชิงซ้อนที่สังเคราะห์ได้อยู่ในช่วง 34.42-130.20 ไมโครโมลาร์ สารประกอบเชิงซ้อนโลหะคอปเปอร์ที่มีฤทธิ์กำจัดซุปเปอร์ ออกไซด์ได้ดีที่สุดคือสารประกอบเชิงซ้อนโลหะคอปเปอร์ของกรดนิโคตินิกกับกรดทาริก นอกจากนี้สารประกอบเชิงซ้อนโลหะที่สังเคราะห์ได้ยังมีฤทธิ์ ต้านจุลชีพ *B. subtilis* ATCC 6633 และ *C. albicans* ATCC 90028 ที่ความเข้มข้นต่ำสุดที่สามารถยับยั้งการเจริญเติบโตได้ที่ 128-256 ไมโครกรัมต่อมิลลิลิตรจากนั้นฤทธิ์ในการกำจัดซุปเปอร์ออกไซด์ของสารประกอบเชิงซ้อนโลหะคอปเปอร์ยังถูกนำมาศึกษาปัจจัยต่อฤทธิ์ โดยใช้เทคนิคทางคอมพิวเตอร์ขั้นสูง ผลการทดลองพบว่าฤทธิ์ในการกำจัดซุปเปอร์ออกไซด์ของสารประกอบเชิงซ้อนโลหะคอปเปอร์ มีความสัมพันธ์กับอัตราการรับอิเล็กตรอนของโลหะ พลังงาน HOMO และพลังงาน LUMO งานวิจัยครั้งนี้ยังพัฒนาวิธีการสกัดสารต้านอนุมูลอิสระคือ วิตามินอี และ อนุพันธ์ของวิตามินอี ด้วยวิธีการสังเคราะห์โมเลกุลเชิงซ้อน ที่มีคุณสมบัติจับจำเพาะ การสังเคราะห์โมเลกุลเชิงซ้อนดังกล่าวถูกเตรียมขึ้นจาก 2 วิธีคือ วิธีดั้งเดิม bulk และวิธีการตกตะกอน เพื่อให้ได้โมเลกุลเชิงซ้อนที่เป็นทรงกลมขนาดนาโนเมตร โมเลกุลเชิงซ้อนจับจำเพาะของวิตามินอีและของอนุพันธ์ของวิตามินอี ที่เตรียมจากวิธี bulk ให้ความสามารถในการจับจำเพาะกับวิตามินอีเป็น 2 เท่าของตัวควบคุม ขณะที่โมเลกุลเชิงซ้อนจับจำเพาะของวิตามินอี ทรงกลมขนาดนาโนเมตร สามารถจับจำเพาะกับวิตามินอีได้ 1.22-1.57 เท่าของตัวควบคุม และสามารถจับกับวิตามินอีได้สูงสุดที่ 1.85 เท่าในสารละลายผสมของแอลกอฮอล์กับน้ำ สัดส่วน 8:2 วิทยานิพนธ์ฉบับ นี้ในส่วนสุดท้าย เรายังศึกษาโมเลกุลจับจำเพาะของกรดโบโรนิก ซึ่งการศึกษาครั้งนี้ได้ประสบความสำเร็จในการสังเคราะห์อนุพันธ์ของกรดโบโรนิก จากนั้นก็นำมาทำปฏิกิริยากับหมู่ azide ที่ตรึงอยู่บนโมเลกุลของเซฟฟาโรส ด้วยปฏิกิริยาเคมีคริ๊ก ในการศึกษาครั้งนี้ไกลโคโปรตีน 2 ชนิดคือ โอวอลบูมิน และเอนไซม์อาเอนเอสบี ถูกนำมาใช้เพื่อเป็นตัวแทนของสารไกลโคซิลเลสโมเลกุล และ สารไกลเคสโมเลกุล ผลการทดสอบความสามารถในการจับ จำเพาะกับไกลโคโปรตีน พบว่าสามารถแยกไกลโคโปรตีนออกจากโปรตีนที่ไม่ใช่ไกลโคโปรตีน คือ โบไวด์ซีรัมอัลบูมิน เอนไซม์อาเอนเอสเอ และ โปรตีนจากแบคทีเรีย จากวิทยานิพนธ์ฉบับนี้สารสังเคราะห์ที่มีคุณสมบัติเสมือนเอนไซม์ซุปเปอร์ออกไซด์ และ กระบวนการสกัดสารต้านอนุมูลอิสระ แสดงให้เห็นถึงตัวอย่างที่มีประสิทธิภาพ และคาดว่าน่าจะถูกนำมาใช้เป็นทางเลือกเพื่อการรักษา รวมถึงเพื่อใช้ในการสกัดสารต้านอนุมูลอิสระ

166 หน้า

CONTENTS

CONTENTS (cont.)

CONTENTS (cont.)

CONTENTS (cont.)

CONTENTS (cont.)

CONTENTS (cont.)

LIST OF TABLES

LIST OF FIGURES

LIST OF FIGURES (cont.)

LIST OF FIGURES (cont.)

LIST OF ABBREVIATIONS

Abbreviations	Term
2Am	2-Aminopyridine
2Hy	2-Hydroxypyridine
3APBA	3-Aminophenylboronic acid
Å	Angstrom
ADVN	2,2□-Azobis(2,4-dimethylvaleronitrile)
AIBN	2,2□-Azobis(isobutyronitrile)
AMP	Adenoside-5□-monophosphate
Ant	Anthranilic acid
ATP	Adenoside-5□-triphosphate
BE	Binding energy
BSA	Bovine serum albumin
B. subtilis	*Bacillus subtilis*
°C	Degree Celsius
C. albicans	*Candida albicans*
Co	Cobalt
CO_2	Carbon dioxide
CRP	C-reactive protein
CSF	Cerebrospinal fluid
Cu	Copper
$CuSO_4$	Copper sulfate
DCM	Dichloromethane
DFT	Density functional theory
DHC	3,4-dihydroxy chalcon
DMSO	Dimethyl sulfoxide
DNA	Deoxynucleic acid
DVB	Divinylbenzene

LIST OF ABBREVIATIONS (cont.)

Abbreviations	Term
E	Energy
EA	Electron affinity
E. coli	*Escherichia coli*
EDMA	Ethylene glycol dimethacrylate
eNOS	Endothelial nitric oxide synthase
et al.	Et alii (Latin: And others)
etc	Et cetera (Latin: And so forth)
eV	Electron Volt
Fe	Iron
g	Gram
h	Hour
HDL	High density lipoprotein
H^1-NMR	Proton-nuclear magnetic resonance
H_2O_2	Hydrogen peroxide
HOMO	Highest occupied molecular orbital
HPLC	High-performance liquid chromatography
HRMS	High resolution mass spectrometry
IC_{50}	Half maximal inhibitory concentration
INF-γ	Interferon gamma
IR	Infrared
KBr	Potassium bromide
kcal	Kilocalorie
kDa	Kilodalton
kJ	Kilojoule
kV	Kilovolt
LDL	Low density lipoprotein
Lp	Lipoprotein

LIST OF ABBREVIATIONS (cont.)

Abbreviations	Term
LUMO	Lowest unoccupied molecular orbital
MAA	Methacrylic acid
MeOH	Methanol
mg	Milligram
$MgCl_2$	Magnesium chloride
MH	Müeller Hinton
MHz	Megahertz
MIC	Minimal inhibitory concentration
min	Minute
MIN	Molecular-imprinted nanosphere
MIP	Molecularly imprinted polymer
mL	Milliliter
mmol	Millimole
Mn	Manganese
m.p.	Melting point
MS	Mass spectrometry
MW	Molecular weight
NA	Nicotinic acid
NAD	Nicotinamide adenine dinucleotide
NADP	Nicotinamide adenine dinucleotide phosphate
$NaHCO_3$	Sodium hydrogen carbonate
Nam	Nicotinamide
NaN_3	Sodium azide
NaOH	Sodium hydroxide
NBT	Nitro blue tetrazolium
Ni	Nickel
NIN	Non-imprinted nanosphere

LIST OF ABBREVIATIONS (cont.)

Abbreviations	Term
NIP	Non-imprinted polymer
nm	Nanometer
NO	Nitric oxide
$O_2^{\bullet -}$	Superoxide anion
oxLDL	Oxidized low density lipoprotein
PBS	Phosphate buffer saline
Ph	Phthalic acid
pH	Power of hydrogen ion
Pi	Picolinic acid
ppm	Part per million
QSAR	Quantitative structure activity relationship
QSPR	Quantitative structure property relationship
Rh	Rhodium
RNA	Ribonucleic acid
RNase A	Ribonuclease A
RNase B	Ribonuclease B
RP-HPLC	Reverse-phase high performance liquid chromatography
rpm	Resolution per minute
RT	Room temperature
Sal	Salicylic acid
S. aureus	*Staphylococcus aureus*
SDS	Sodium dodecyl sulphate
SDS-PAGE	Sodium dodecyl sulfate polyacrylamide gel electrophoresis
SEM	Scanning electron microscopy
SOD	Superoxide dismutase

LIST OF ABBREVIATIONS (cont.)

Abbreviations	Term
TE	Total energy
TP	α-Tocopherol
TPA	Tocopherol acetate
Trp	Tryptophan
μeff	Magnetic moment
μL	Microliter
μM	Micromolar
μm	Micrometer
UV	Ultraviolet
ν	Frequency
v/v	Volume by volume
VLDL	Very low density lipoprotein
Zn	Zinc

CHAPTER I
INTRODUCTION

Nowadays, in the rapid moving trend of technology and growing population, human health has been endangered by many serious factors, such as food contamination, air pollutant, socioeconomical stress, changing of life-style, radiation as well as technology burden etc. Those factors can induce free radical production leading to oxidative stress and imbalance of human functions. Superoxide radical ($\mathbf{O}_2^{\bullet -}$) is particularly considered to be one of the most prominent radical species in oxygenated biological system. Superoxide anions attack macromolecules and subsequently cause damage by autocatalytic degradation of the biomolecules (DNA damage, protein damage and lipid peroxidation) (1). It is also affected in many degenerative processes e.g. proliferation effects, activation of cell dead, activation of cell signaling, membrane damage and gene expression change. These effects may lead to many pathological conditions including Alzheimer's disease, Parkinson's disease (2), atherosclerosis (3), cardiovascular diseases (4), cancer (5), skin irritation (6), aging (7) and inflammation (8). Thus, free radical scavengers are acceptable that they are the necessity for current society to prevent abnormality causing by oxidative stress. Many molecules having free radical scavenging activity are non-enzymatic antioxidants (e.g. vitamin C, vitamin E, glutathione, anthocyanin, flavonoids, resveratrol, etc.) and enzymatic antioxidants (superoxide dismutase; SOD, catalase and glutathione peroxidase). However, many research works have been geared towards the development of antioxidants in some aspects e.g. to find new antioxidant molecules, to improve and/or to enhance antioxidant activity and to develop extraction yield and extraction process. This thesis discovered the new antioxidant compounds together with new activity based on metallovitamin complexes and also demonstrated the effective separation methods for antioxidant compounds using two nanoparticle models; molecularly imprinted polymer (MIP) and clicked boronic acid affinity matrix.

Superoxide radical is one of major reactive oxygen species (ROS) that is mainly eliminated by SOD enzyme known as endogenous antioxidant defense mechanism to form hydrogen peroxide (H_2O_2) and is then converted to water and oxygen by catalase enzyme. The employment of SOD protein in clinical trials has been reported for immunological responses deriving a non-human enzyme. Superoxide scavengers based on small molecules have been designed in the concept of metal center possessing redox potential property and binding architectures. In this research, copper as metal center and potential coordination sites of nicotinic acid and structurally related bioactive compounds (phthalic acid, salicylic acid, anthranilic acid, picolinic acid, 2-hydroxypyridine and 2-aminopyridine) were utilized to perform new copper complexes for the SOD activity.

Although the new antioxidant has been discovered, antioxidants from natural sources are still important to be used against free radical. α-Tocopherol, also known as the principle form of vitamin E, is a highly effective agent against free radical, which is typically found in vegetables and fruits. Vitamin E is interested as high-value compound for medical and cosmetic therapies. Analytical methods to determine vitamin E consist of thin-layer chromatography (TLC), supercritical fluid chromatography (SFC) and high-performance liquid chromatography (HPLC). Molecular imprinting is a technology to build template-shaped pockets in polymer matrices with memory of the template molecules. Solid phase extraction based on MIP is mainly approach for purification of interested molecules from complex matrices. Therefore, molecularly imprinted polymer (MIP) was used to produce nanosphere matrices that are expected to be highly specific to tocopherol and its derivatives (tocopherol acetate).

Furthermore, novel clickable affinity ligand based on boronic acid was synthesized which the boronic acid cloud display specific binding to molecules containing *cis*-diol groups, such as carbohydrates, nucleotides, nucleosides and glycoproteins. This ligand was coupled to azide-functionalized hydrophilic nanoparticle using Cu(I)-catalyzed 1,3-cycloaddition reaction, called “click reaction”. In this research, glycoproteins that are proteins containing oligosaccharide chains covalently attached to the polypeptide chains, are firstly focused target model. The reason is that glycoproteins play vital roles in diverse physiological and pathological

processes in eukaryotic organisms. By the way, *cis*-diol groups are also detected in antioxidant compounds, such as flavonoid-O-glucoside, leucoanthocyanidin (flavan-3,4-*cis*-diol), epicatechin, quercetin, quercetin-3-O-galactoside. Thus, clickable boronic acid affinity ligand is possibly used to extract these antioxidants.

CHAPTER II
OBJECTIVES

The objectives of this study are:

1. To synthesize superoxide dismutase mimic as designed from copper complexes of nicotinic acid with aromatic carboxylic acid (phthalic acid, salicylic acid and anthranilic acid).
2. To synthesize superoxide dismutase mimic as designed from copper complexes of nicotinic acid with 2-substituted pyridines (picolinic acid, 2-hydroxypyridone and 2-aminopyridine)
3. To correlate the calculated quantum chemical parameters with the SOD activity of the copper complexes.
4. To produce molecularly imprinted nanoparticles for extracting tocopherol and its derivatives.
5. To model of mechanistic insight of the binding mode of tocopherol-monomer complexes.
6. To construct novel clicked boronic acid nanoparticle bead for separating glycoproteins.

CHAPTER III
LITERATURE REVIEW

3.1. Physiology and biochemistry of oxygen

Oxygen is usually assumed to be used in aerobic organisms for energy production, which is released to drive anabolic and catabolic activities such as muscle activity (9). Oxygen can bind ferrohemoglobin in a reversible and pH-dependent manner in order to be primarily distributed in human body. The physically dissolved amount of oxygen in plasma is insignificant, approximately 0.13×10^{-3} $mol\cdot L^{-1}$, as compared to the total oxygen-binding capacity of the blood. Oxygen readily permeates biomembranes, with more than 90% of cellular oxygen consumed by the mitochondria (10). Oxygen in mitochondria acts as terminal electron acceptors in the electron transport chain to control ATP synthesis and to compete for cytochrome oxidase with nitric monoxide (NO). The nitric monoxide syntase (NOS) can convert L-arginine to NO in a O_2-dependent manner. Under hypoxic condition, the production of the NO is rather low. This has severe consequences on a great variety of physiological functions, while NO stimulates blood flow by vascular relaxation and downregulates platelet aggregation. Tissues are less supplied with blood and the risk of embolus pathology increases when NO cannot be generated. In addition, oxygen is critical in O_2-dependant biosynthesis of a variety of molecules, including tyrosine, nicotinic acid, sterol, polyunsaturated fatty acid, hydoxyproline, hydroxylysine and retinal (11-14).

3.2. Oxidative stress

Oxygen is converted in a step-by-step manner to superoxide radical ($O_2^{\bullet -}$) by transferring single electrons in the mitochondria. Enzymes involved in the electrons transport system includes: NAD(P)H oxidase, nitric oxide syntase and xanthine oxidase. Superoxide radical is considered to be one of the most prominent radical species in oxygenated biological systems. Superoxide anions are immediately converted to hydrogen peroxide (H_2O_2) by catalysis of superoxide dismutase (SOD).

Hydrogen peroxide is then incompletely metabolized to oxygen and water by catalase and/or glutathione peroxidase. While non-metabolized H_2O_2 can induce reactive hemolytic cleavage in the presence of transition metal, the reaction between H_2O_2 and iron, known as "Fenton's reaction", can generate highly reactive oxygen such as hydroxyl radical. Thus, in thalassemia patient with iron overload, iron is easily catalyzed by hydrogen peroxide to perform hydroxyl radical. Hydroxyl radicals possessing the highest oxidation potential of aerobic metabolites, attack all biomolecules, followed by autocatalytic degradation of the respective molecules (e.g. DNA damage, protein damage and lipid peroxidation) (1). Additionally, free radical can be generated by exogenous sources, such as ionizing radiation, UV light, environmental toxicants, chemotherapeutics as well as inflammatory cytokines (e.g. TNF-γ, NF-κB and iNOS). An uncontrolled increase of free radical concentration is definitely affected in many degenerative processes, such as proliferation effects, activation of cell dead, activation of cell signaling, membrane damage and gene expression change. These effects lead to many diseases including Alzheimer's disease, Parkinson's disease (2), atherosclerosis (3), cardiovascular diseases (4), cancer (5), skin irritation (6), aging (7) and inflammation (8). Free radical scavenger is a necessity for the elimination of free radicals in the human body.

3.3. Antioxidants

An increased production of radicals and other forms of reactive oxygen species (ROS) has led organisms to develop a series of defense mechanisms, which encompasses preventative mechanisms, repair mechanism, physical defense and antioxidant defenses. There are two antioxidant systems including enzymatic antioxidants (e.g. superoxide dismutase; SOD, catalase and glutathione peroxidase; GPx) and nonenzymatic antioxidants (vitamin C, vitamin E, glutathione, carotenoids, flavonoids and other antioxidants) as shown in Table 3.1. Balancing of the activity and levels of free radical and antioxidants is essential for organisms and their health (15, 16).

Table 3.1. Major enzymatic and nonenzymatic physiological antioxidants

Antioxidants	**Functions**
Enzymatic	
Superoxide dismutase	- located in both cytosol and mitochondria
	- dismutates superoxide anion
Glutathione peroxidase	- located in both cytosol, mitochondria and cell membrane
	- removes hydrogen peroxide and organic hydroperoxides
Catalase	- located in peroxisomes
	- removes hydrogen peroxide
Thioredoxin	- repairs oxidized sulfhydryl proteins
	- eliminate hydrogen peroxide and other radical
Glutaredoxin	- protect protein and non-protein thiols under oxidative stress
Nonenzymatic	
Vitamin E	- mainly protect lipid peroxidation
Vitamin C	- located in aqueous phase of cell; acts of radical scavenger and recycles vitamin E
Vitamin A	- derived from cleavage of carotene in intestine
	- show biological activity of retinol
	- inhibits lipid peroxidation
Uric acid	- scavenges hydroxyl radicals
Glutathione	- nonprotein thiol in cells; serves multiple roles in the cellular antioxidant defense
α-Lipoic acid	- effective as an antioxidant and in recycling vitamin C
	- potent pro-glutathione agent
Carotenoids	- protects lipid peroxidation
Flavonoids and polyphenols	- major component of "phytochemicals"
	- perform lipid soluble radical scavenger and metal chelators
Bilirubin	- serves as an extracellular antioxidant

3.3.1 Enzymatic antioxidant (Superoxide dismutase; SOD)

SOD is a critical enzyme for disproportionating superoxide anion radicals, which can be distinguished into three classes depending on the protein folding and catalytic metal ions: Cu,ZnSOD, MnSOD/FeSOD and NiSOD (as demonstrated in Figure 3.1). Cu,ZnSOD, also known as SOD_1 and SOD_3 in humans, is also found in eukaryotes and some prokaryotes. MnSOD/FeSOD, called SOD_2 in humans, is presented to have evolved from a common ancestral gene, with the FeSOD gene found in primitive eukaryotes, in the plasmids of plants and in bacteria (17). NiSOD have been observed only in bacteria. Basically, all kinds of SODs are the disproportionation reaction, happening through alternate oxidation and reduction of their catalytic metal ions and rather remarkably. The catalytic rate of SOD closes to diffusion rate of radicals. Although the structures of all three classes are distinct, all interestingly provide electrostatic guidance for the superoxide substrate and alter the metal ion redox potential to a range suitable for superoxide elimination (18). The mechanism of dismutation involves binding of prosthetic group of SOD in the oxidized form (Mn^{3+}) to superoxide anion and a proton. The reduced form (Mn^{2+}) then binds to a second superoxide anion and a proton followed by a release of the less reactive hydrogen peroxide (H_2O_2) and finally returning to the oxidized state. Hydrogen peroxide then serves as a substrate of catalase for further conversion to O_2 and H_2O. MnSOD, as an example, is summarized by the following equations of the two-step reactions (19):

$$Mn^{3+} + O_2^{\bullet -} + H^+ \leftrightarrow Mn^{2+}(H^+) + O_2 \qquad \text{Step 1}$$

$$Mn^{2+}(H^+) + O_2^{\bullet -} + H^+ \leftrightarrow Mn^{3+} + H_2O_2 \qquad \text{Step 2}$$

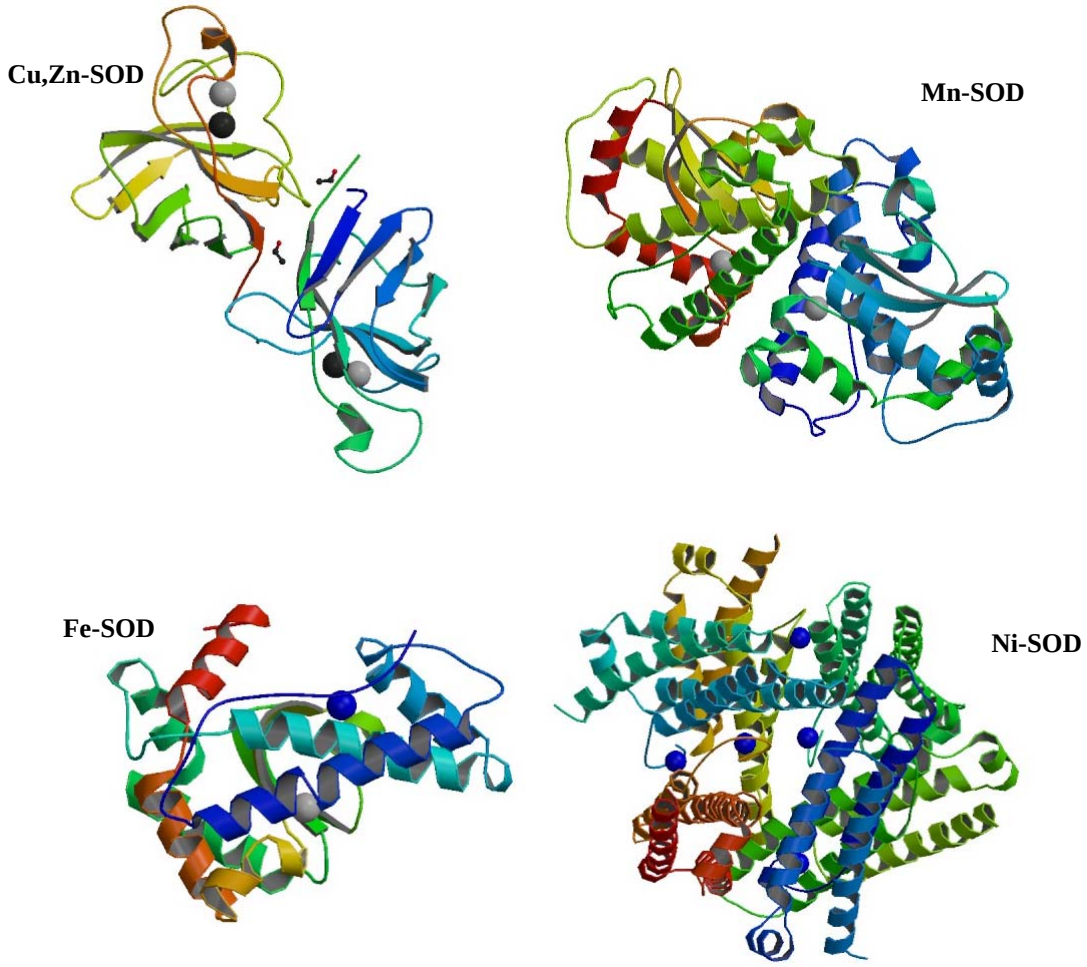

Figure 3.1. Three-dimentional structure of the four-types of SODs containing different metal ions is vital for the architecture and/or catalytic activity (Protein Data Bank, Accession code PDB ID 2SOD (Cu,Zn-SOD); 3K9S (Mn-SOD); 3JS4 (FeSOD); 1T6U (Ni-SOD))

3.3.2 Non-enzymatic antioxidants

The non-enzymatic antioxidants are divided into metabolic antioxidants (e.g. endogenous antioxidants: lipoid acid, glutathione, L-arginine, coenzyme Q10, melatonin, etc.) and nutrient antioxidant (e.g. exogenous antioxidants: vitamin E, vitamin C, carotenoids, flavonoids and trace metals) being provided through food and supplements. Nutrient antioxidant from diet plays a vital role in helping endogenous antioxidants in detoxifying free radicals. Exogenous antioxidant insufficiency is one of the major causes of many diseases derived from oxidative stress (2, 5).

3.3.2.1 Vitamin E and its derivatives

Vitamin E is a well-known vitamin that possesses high antioxidant property. During the past nine decades, vitamin E has been identified, purified, elucidated, synthesized and characterized for its biological functions. At least eight stereoisomers have been isolated from plant foods possessing vitamin E activity. All contain a 6-chromanol ring structure and a variant side chain. Furthermore, two commercial vitamin E are *RRR*-α-tocopherol and all-rac-α-tocopherol, which is generally synthesized from esterification of acetate and succinate. The esters are not found in natural foods and leads to a loss of biological activity. Dietary needs of α-tocopherol requires a recommended intake level of 15 mg/day. Vegetable oils are the major sources of vitamin E such as wheat germ oil and sunflower oil (20). Small amounts of their fat have to be absorbed with vitamin E from the proximal small intestine. Additionally, vitamin E esters have to be digested by esterase from pancreas and eventually absorbed. Vitamin E is mixed with chylomicrons and transported into lymph and finally blood circulation. Basically plasma vitamin E is combined with low-density lipoprotein (LDL) and high-density lipoprotein (HDL), which are transported and stored in adipose tissue, liver and muscle as the major storage deposits of the vitamin E (21). The well-known biological activity of vitamin E is an antioxidant. This action plays a protective role against lipid peroxidation, which causes atherosclerosis. Moreover, loss of this preventive role can also affect the neurological function such as abetalipoproteinemia and nerve damage. High levels of any supplement form (>1000 mg) can effect with blood clotting, which increase risk of hemorrhagic stroke (22). Interestingly, tocotrienols possess powerful neuroprotective,

antioxidant, anticancer and cholesterol lowering properties that often differed from the properties of tocopherols. Figure 3.2 showed vitamin E and its derivatives. As an antioxidant, vitamin E has been used either as medical or cosmetic therapies. For medical therapy, supplementation with vitamin E can reduce the risk of cardiovascular diseases, cancer and neurodegenerative diseases (e.g. Alzheimer's disease). For cosmetics, vitamin E has been employed for acne and scars treatments as well as for promoting healing of eczema, burns and other skin ailments.

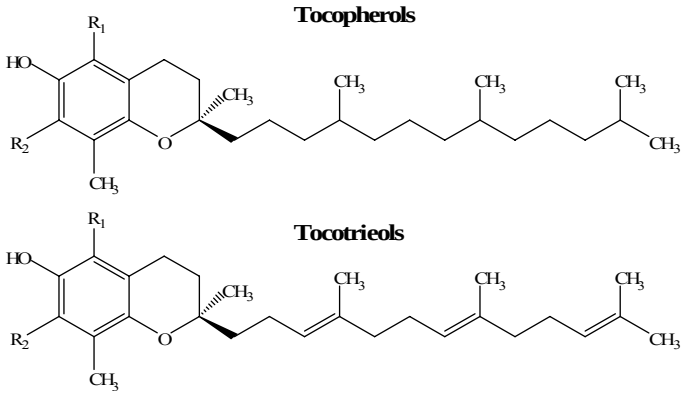

Tocochromanol	R_1	R_2
α	CH_3	CH_3
β	CH_3	H
γ	H	CH_3
δ	H	H

Figure 3.2. Vitamin E and its derivatives.

3.3.2.2 Phenolic compounds

Phenols or phenol groups are a typical structure of several plants metabolites. This functional group is characterized by at least one hydroxyl group bound to a benzene ring. Many phenolic compounds possess free radical scavenging activity for several ROS. According to chemical structure, more than 4,000 flavonoids have been isolated and classified into flavanol (catechin, epicatechin), flavanones also known as flavanone glycoside (e.g. hesperidin), flavones (e.g. apidenin), isoflavones, flavonols (e.g. quercetin), anthocyanidins (e.g. malvedin) and phenylpropanoids (e.g. caffeic acid) as shown in Figure 3.3 and Table 3.2

(23-25). Advantages of flavonoids in human mainly reside in their potent antioxidant activity, resulting in the prevention and reduction of degenerative ailments. The major sources of flavonoids include green tea, grapes, apple, cocoa, soybean, curcuma, berries, onion, etc. Phenolic compounds are commonly taken to the human body mostly from the diet by gastrointestinal tract. Mechanisms of absorption are active as well as passive absorptions, depending on chemical formula and its environment (26-30).

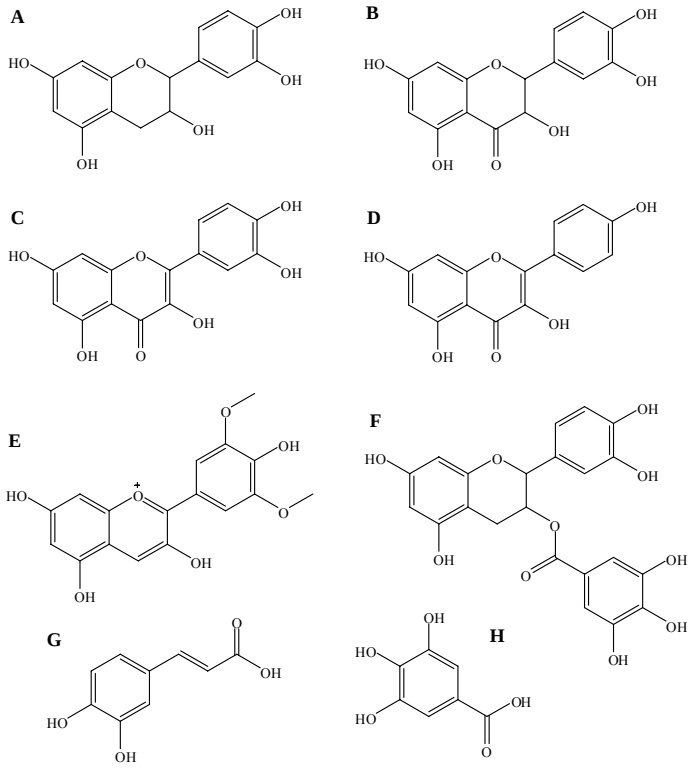

Figure 3.3. Structures of phenolic compounds, epicatechin (A), taxifolin (B), quercetin (C), apigenin (D), malvedin (E), epicatechingallate (F), caffeic acid (G) and gallic acid (H) (26-30).

Table 3.2. Structures of flavonoid glycosides (25).

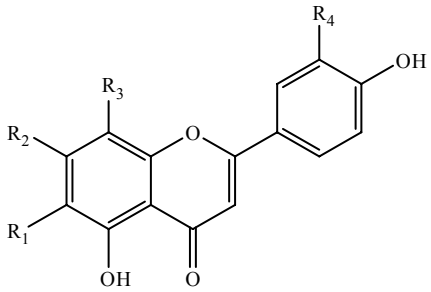

Compound	R_1	R_2	R_3	R_4
Schaftoside	*C*-β-D-glucopyranosyl	OH	*C*-α-L-arabinopyranosyl	H
Isoschaftoside	*C*-α-L-arabinopyranosyl	OH	*C*-β-D-glucopyranosyl	H
Orientin	H	OH	*C*-β-D-glucopyranosyl	OH
Isovitexin	*C*-β-D-glucopyranosyl	OH	H	H
Isoorientin	*C*-β-D-glucopyranosyl	OH	H	OH
Luteolin 7-O-sophoroside	H	*O*-β-D-glucopyranosyl (1 →2) glucopyranoside	H	OH
Vitexin	H	OH	*C*-β-D-glucopyranosyl	H

3.3.3 Synthetic antioxidants (Superoxide dismutase mimetics)

As an endogenous antioxidant defense, SODs have shown the beneficial role in fighting a wide range of diseases, including cancer, inflammation and AIDS. However, the utilization of native enzymes in clinical trials has been reported in a variety of immunological responses deriving from a non-human enzyme and the problem of penetrating membrane barriers to reach targeted sites. To mimic SOD activity, synthetic compounds have been studied in order to be developed pharmaceutical candidates. The SOD mimics have been designed from the concept of metal center having redox potential property and binding architectures of potential coordination sites of ligands containing nitrogen, oxygen and sulfur atoms. The researches were started with Fe-EDTA as an SOD mimic in 1980 (31). The result showed that the activity of iron-EDTA complex exhibited only 0.01% activity as compare to the native SOD. After that, there were many ligands bearing the potential coordination sites which were complexed with metals for SOD-like activity, such as porphyrin (32) and salen (33) complexes (Figure 3.4). However, the activity was still much smaller than that of the native enzymes. Interestingly, the potential coordination sites are also found in nicotinic acid (NA: vitamin B3) and bioactive compounds including phthalic acid, salicylic acid, anthranilic acid, 2-picolinic acid, 2-hydroxypyridine and 2-aminopyridine. Therefore, this thesis has focused on using metal complexes of nicotinic acid with bioactive compounds as SOD mimics demonstrated in **Paper I and II** (Chapter 4 and 5). The SOD activity was investigated to observe a correlation with the computational data consisting of electron affinity, HOMO and LUMO. Moreover, these copper complexes were also tested for antimicrobial activity. The vitamin-metal complexes described in this thesis are great example of the value-added benefits of vitamins for medicinal applications.

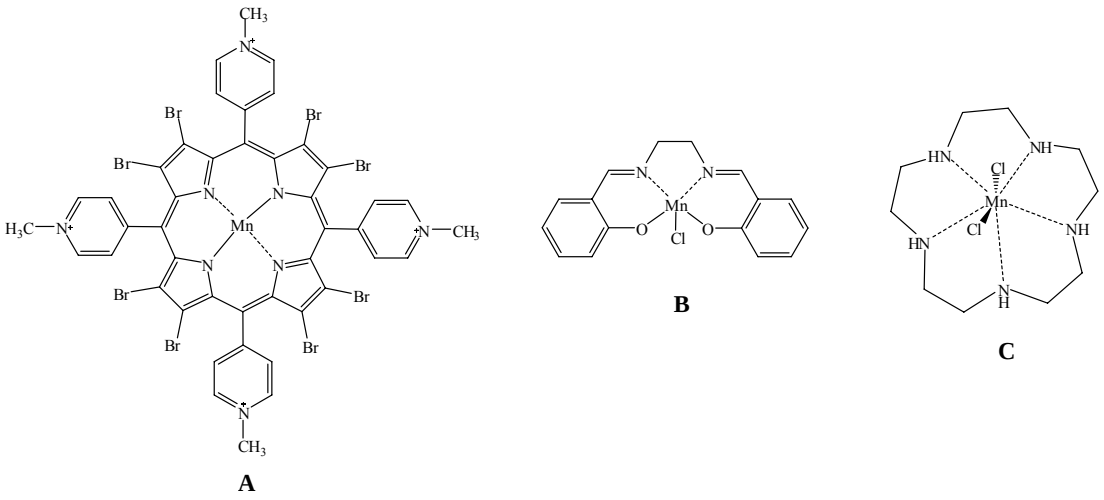

Figure 3.4. The structure of SOD mimics. (A) metalloporphyrin namely Mn(II)OBTM-4-PyP, (B) salen complex called EUK-8 and (C) macrocyclic complex MnPAM.

3.4 Nutrients

Foods that are consumed are mashed by mechanical grinding, digested by enzymatic digestions, sorted by particular absorption and converted by metabolic reactions. Nutrients originated from foods and bacteria are the essential chemicals for normal physiological functions of organism to live and grow, to assist in metabolism, to serve in specific cellular function, to build and repair cellular structure and to be used for energy production. At least 6 different elements from absorbable nutrients are utilized for building 99% of the mass of the human body; oxygen (65%), carbon (18%), hydrogen (10%), nitrogen (3%), calcium (1.5%) and phosphorus (1.0%) (34).

3.5 Vitamins

As an essential nutrient excluding other nutrients such as dietary minerals, essential fatty acids or essential amino acids, the term “vitamin” is a well-known keyword in daily language also usually in minute amounts. However, dietary deficiencies of vitamins can widely effect in physiological functions (35). A vitamin can’t be synthesized by the host in amount sufficient to meet normal function needs and must be come from daily intake of food. Thirteen categories are now typically

recognized as vitamins that are classified by their biological and chemical activity, but not their structure. In case, a precursor of a vitamin is referred to a pro-vitamin; such some carotenoids can be metabolized to active form of vitamin A. Solubility of vitamins is usually utilized to classify vitamins into two groups; water-soluble (Vitamin A, D, E and K) and fat-soluble (Vitamin B and C) (36).

3.6 Niacin

3.6.1 Source and Synthesis

The term niacin, also known as vitamin B_3, comprises the two main forms; nicotinamide (3-pyridinecarboxamide) and nicotinic acid (3-pyridine-carboxylic acid). Niacin can be obtained by two sources consisting of metabolized tryptophan and foods. Although the small proportion of the available tryptophan is metabolized, L-tryptophan, both from foods and from tissue protein breakdown, is an important alternative for synthesizing niacin. Tryptophan (Trp), nicotinic acid (NA) and nicotinamide (Nam) are employed through distinct metabolic pathways to perform NAD^+, which is controlled by gene products of many enzymes. Trp is firstly converted by indoleamine dioxygenase (INDO) or tryptophan dioxygenase (TDO2) to *N*-formylkynurenine, which is a precursor for kynurenine (Kyn) using the product of arylformamidase gene (*AFMID*). Kynurenine monooxygenase (KMO) is utilized to form 3-hydroxykynurenine (3-HK), which is used as a substrate of kynureninase (KYNU) and forms 3-hydroxyanthranilate (3-HAA). 3-Hydroxyanthranilate dioxygenase (HAAO) then forms quinolinate (Quin), which is continuously converted to nicotinic acid mononucleotide (NaMN) using the products of quinolate phosphoribosyltransferase (QPRT) gene. NaMN is converted to nicotinic acid adenine dinucleotide ($NaAD^+$) and then to NAD^+ by *NMNAT1-3* and *NADSYN1* gene, respectively. In addition, nicotinic acid (NA) is used in the three-step Preiss-Handler pathway. NA is used as a substrate of nicotinic acid phosphoribosyltransferase (NAPRT1) and forms NaMN by addition of the 5-phosphoribose group from 5-phosphoribosyl-1-pyrophosphate to NA. NaMN is then converted to $NaAD^+$ and NAD^+ by activity of NMNAT1-3 and NADSYN1, respectively. Nam is utilized by nicotinamide phosphoribosyltransferase (Namt), which catalyzes the addition of a phosphoribose group into Nam to form nicotinamide mononucleotide (NMN). NAD^+

is readily formed from NMN by NMNAT1-3. Nam can be also converted to NA by nicotinamase. The intracellular NAD^+ synthetic pathway in human is presented in Figure 3.5 (37).

Niacin-rich foods include liver, meat and fish, mainly as NAD^+, $NADP^+$, nicotinate, nicotinamide. The outer layer of grains is relatively niacin-rich, though much of this may be in the form of complexes with carbohydrates (niacytins) or peptides (niacinogens). Since, both niacin and tryptophan can contribute to niacin adequacy. Intakes are often assessed in niacin equivalence. Calculation of niacin equivalences is based on the assumption that 60 mg of tryptophan contribute as much as 1 mg nicotinamide or nicotinic acid. Daily intake of niacin was reported to be around 21 mg in women and 25 mg in men (38).

3.6.2 Digestion, absorption and transportation

Nucleotide pyrophosphatase from pancreatic and intestinal secretions metabolize NAD/NADP into 5'-AMP and nicotinamide ribonucleotide. An intestinal brush border enzyme can then release nicotinamide with low activity. Nicotinamide and nicotinate are absorbed from stomach and proximal small intestine. Uptake of these compounds proceeds by sodium-dependant, by facilitated diffusion at low concentrations and by passive diffusion at higher concentrations. Both nicotinate and nicotinamide are transported into blood circulation, into brain and into other tissues (39). Nicotinate and nicotinamide are readily converted to NAD^+ and $NADP^+$, which are also synthesized from L-tryptophan-derived nicotinate mononucleotide in many tissues. Liver, kidney, heart and skeletal muscle contain relatively concentrations of NAD^+, which can become available in times of low niacin intake (40).

3.6.3 Functions

Also known as an enzyme cofactor, more than 200 well-characterized NAD^+-dependent dehydrogenase use NAD^+ as electron acceptor or NADH as a hydrogen donor for intracellular respiration and oxidoreductive reactions. Additionally, the functions of NADP are mainly analogous to those of NAD^+, which many enzymes actually are equally active with NADP and NAD^+. $NADP^+$ has an additional specific role as a hydrogen donor for the reductive synthesis of fatty acid

and steroids. At present, niacin and various related derivatives (Figure 3.6) (41, 42) in daily dose of one to several grams are utilized for the treatment of hyperlipidemias. General effects of niacin include decreases of LDL cholesterol concentration and increases of HDL cholesterol concentrations (Figure 3.7) (43).

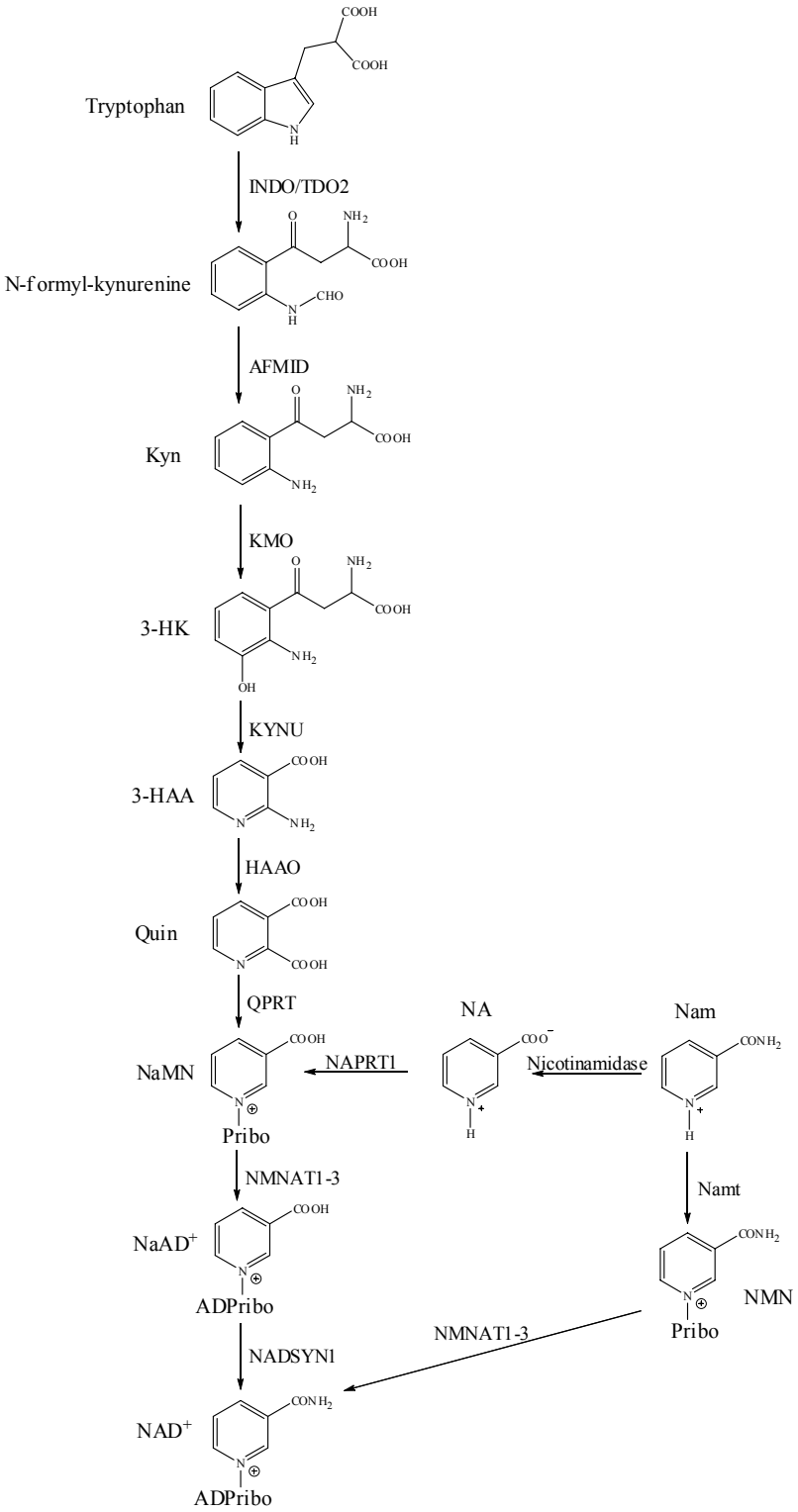

Figure 3.5. Intracellular NAD^+ metabolisms in human (37).

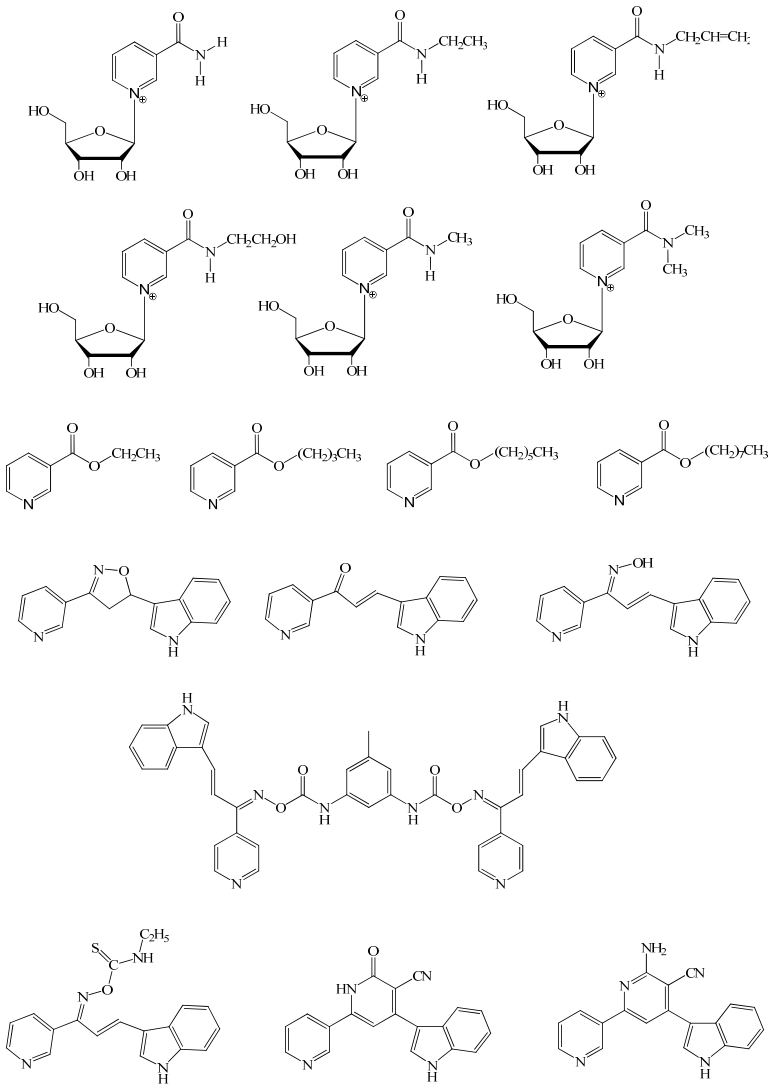

Figure 3.6. Chemical structures of niacin derivatives and related compounds (41, 42).

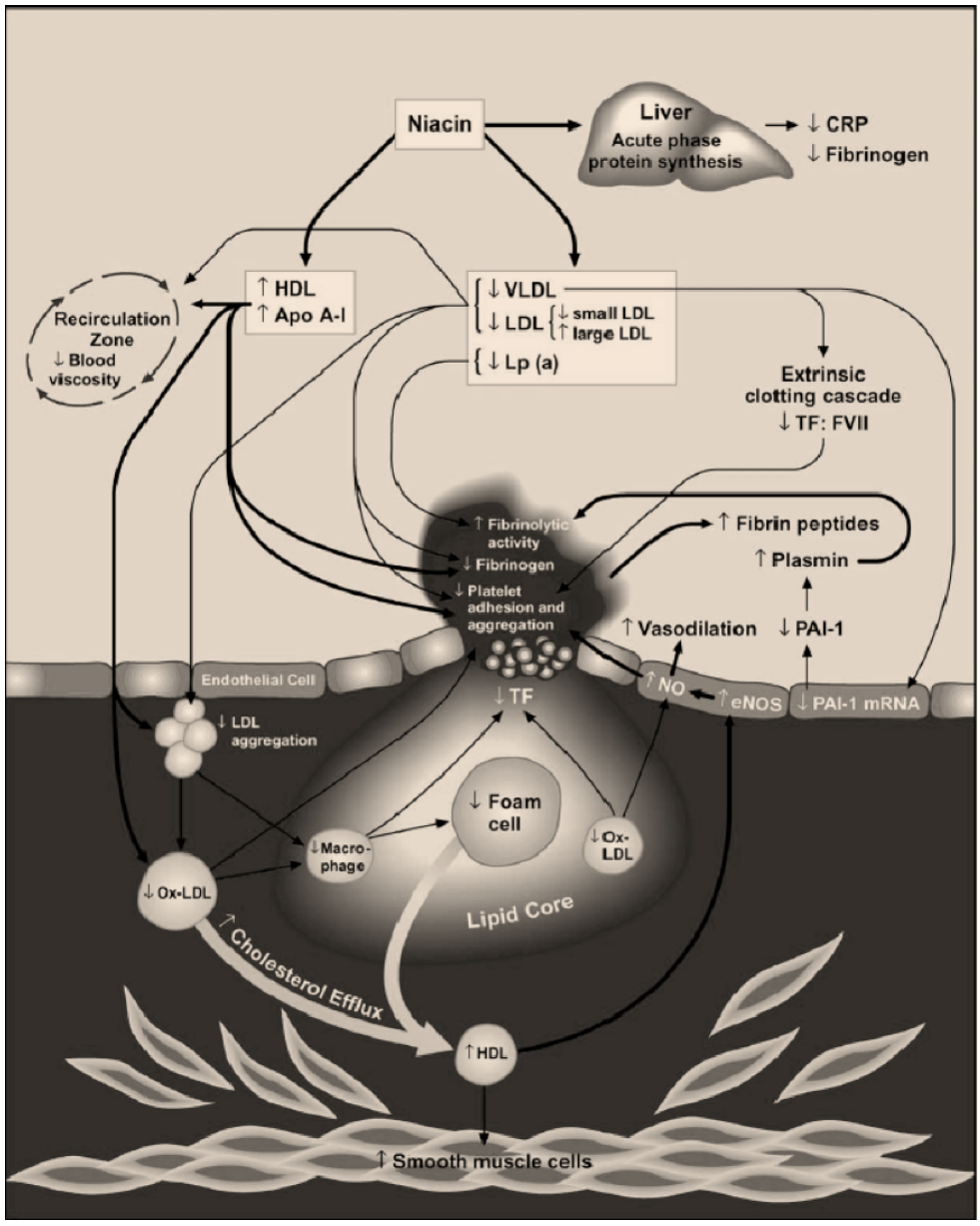

Figure 3.7. Antiatherothrombotic effects of niacin. Illustration of the influence of niacin on atherosclerotic plaque stability, thrombogenesis and fibrinolysis. The arrows are classified as (↑) component increased by niacin; (↓) component decreased by niacin; (↑) activity increased by niacin; (↓) activity decreased by niacin. CRP indicates C-reactive protein; HDL, high-density lipoprotein; Apo AI, apolipoprotein AI; VLDL, very low-density lipoprotein; LDL, low-density lipoprotein; Lp(a), lipoprotein (a); TF, tissue factor; FVII, factor VII; PAI-1, plasminogen activator inhibitor; NO, nitric oxide; eNOS, endothelial nitric oxide syntase; and Ox-LDL, oxidized LDL (43).

3.7 Pyridine derivatives

3.7.1 Picolinic acid

Picolinic acid (Figure 3.8a), an isomer of nicotinic acid, has been observed in blood stream, cell-free supernatants, CSF, human milk and pancreatic fluid. Endogenous of this molecule is not fully understood. Picolinic acid is synthesized through a side branch of *L*-tryptophan metabolism. Experimentally, picolinic acid seems to have a number of potential effects within the body, particularly involving the immune system and macrophage function. This compound can induce macrophage INF-γ dependant gene expression and selectively enhance expression of macrophage inflammatory proteins 1α and 1β. In addition, picolinic acid in high concentration can also inhibit virus growth (e.g. HIV, Herpes simplex virus and Simian virus-infected cell line) and has been reported to display antimicrobial activity against *Mycobacterium avium*. Moreover, picolinic acid has also been shown to affect tumor growth (44).

3.7.2 2-Hydroxypyridine

2-Hydroxypyridine can easily convert to form 2-pyridone as tautomer by delocalization of hydrogen (Figure 3.8b). This compound has been used to coordinate with transition metal resulting in antitumor activity against human ovarian cancer cell line and for urease inhibitory activity (45). For example, *cis*-planaramineplatinum (II) complexes like *trans* isomers are often found to be active against cancer cell. These kinds of the complexes have been synthesized and investigated the anticancer activity (46). Moreover, 2-pyridone has also been used as a pharmacophore for chemical substitution or modification, which 2-pyridone derivatives was reported to show the antihepatitis B virus activity (47).

3.7.3 2-Aminopyridine

Aminopyridine is a pyridine with an amino substitution. The nitrogen atom of amino functional group contributes the free electron pair to the proton of an acid. Three positional isomers consist of 2-, 3- and 4-aminopyridines as shown in Figure 3.8c. 4-Aminopyridine is a very effective avicide and bird repellent, but it is toxic to CSF of human (48). 3-Aminopyridine has been utilized as an intermediate for

colorants, agochemicals and pharmaceuticals (49, 50). 2-Aminopyridine has also been employed in the synthesis of drugs, particularly for antihistamines, anti-inflammatories and other drugs (51, 52). Aminopyridines can be coordinated to form a complex with transition metals, involving photosensitizer chemistry and luminescent materials (53). Additionally, these compounds can be used as a monomer for polymerization.

3.8 Aromatic carboxylic acid derivatives

3.8.1 Phthalic acid

Phthalic acid is aromatic dicarboxylic acid (Figure 3.8d), which was reported to possess for pharmacological properties. Two-carboxylic acid groups are potential to coordinate with transition metals, such as Cu(II), Co(III), Rh(III) and Pt(IV). These complexes represented as antifungal, antimicrobial and antitumor agents (54). Its derivative, phthalic anhydride has biochemical importance. In addition, phthalate or phthalic acid ester are widely utilized in plastic production to enhance the flexibility, transparency, longevity and durability of consumer products, food packaging materials and polyvinyl chloride (PVC) plastic (55).

3.8.2 Salicylic acid (Figure 3.8d)

Plants are a major source for pharmaceuticals and medicines, such as digitalis, quinine, taxol, morphine, opiates codeine and aspirin. The aspirin, a synthetic derivaive of salicylic acid, is a simple drug for reducing plain, inflammation and fever (56) and for decreasing the risk of heart attack, stroke and cancers (57). Over 400 years ago, willow leaves were firstly used to relieve the plain of childbirth. Willow leaves were employed until German scientists, in 1828, extracted the leaves to obtain a small quantity of a yellowish compound called salicin. Salicin was then converted into an acid form, namely acid salicylic. Thirty years later, Hermann Kolbe and coworkers firstly chemically synthesized salicylic acid, finally leading to large-scale production of economically priced salicylic acid. Although salicylic acid possesses side effects, for example chronic stomach inflammation and arthritis, this compound was even greater medicinal use. To prevent the vascular disorders (e.g. coronary heart disease, stroke and peripheral arterial disease), acetyl salicylic acid therapy (aspirin) was

demonstrated for antiplatelet activity (58). Thus, salicylic acid was chemically modified to give diverse derivatives, which exhibited different biological activities, for instance cytotoxicity against prostate cancer cells, human breast adenocarcinoma cells and other tumor cells including antioxidant and antimicrobial activities (59).

3.8.3 Anthranilic acid

Anthranilic acid (Figure 3.8d), referred to as vitamin L, is the organic compound consisting of a benzene ring with two adjacent functional groups; a carboxylic acid and an amine. Anthranilic acid has been detected in the tryptophan synthetic pathway by attachment of phosphoribosyl pyrophosphate to the amine group (60). Anthranilic acid, biosynthesized from chrosmic acid, has been utilized as an intermediate for production of dyes (61), pigments (62) and saccharin (63). Anthranilic acid and its esters has been employed in preparing perfumes to imitate jasmine and orange, pharmaceuticals and UV-absorber.

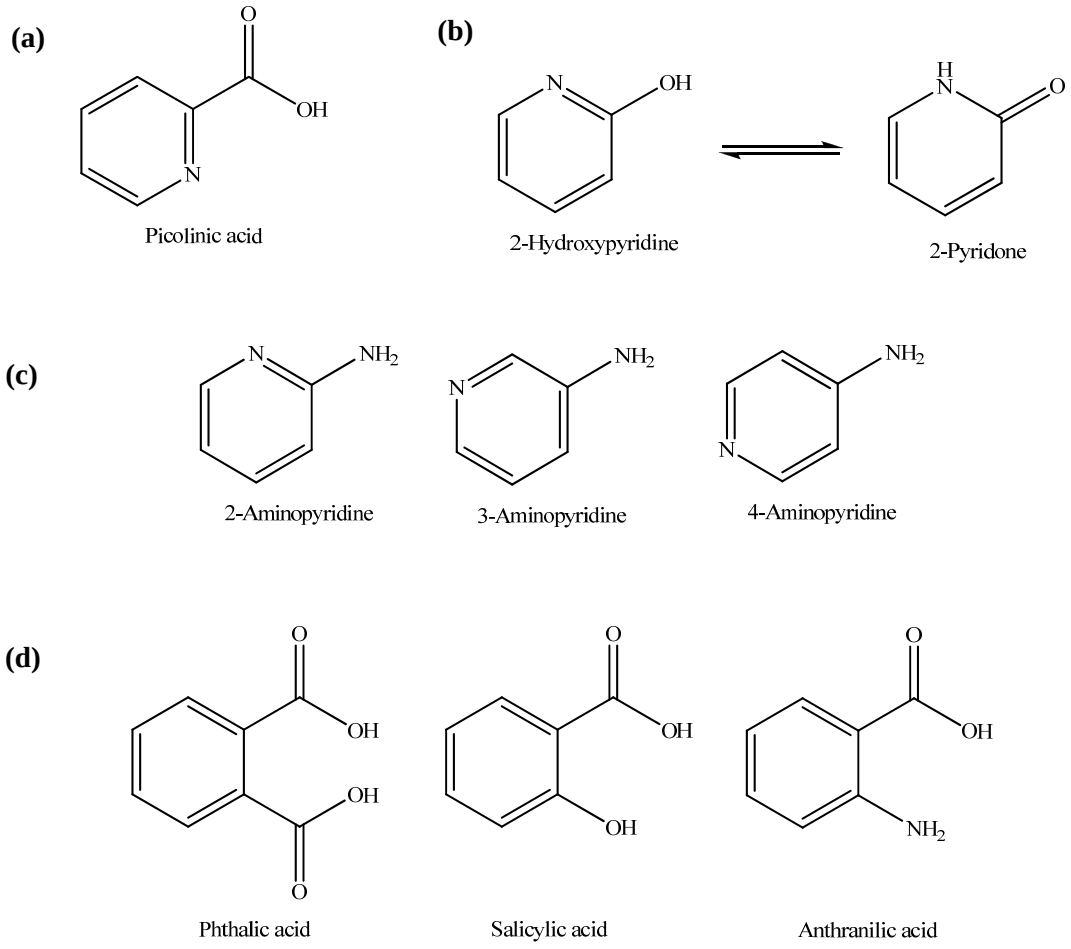

Figure 3.8. Bioactive compounds: (a) picolinic acid, (b) tautomer forms of 2-hydroxypyridine and 2-pyridone, (c) aminopyridine derivatives and (d) aromatic carboxylic acid derivatives.

3.9 Molecular recognition

Most of the molecules are randomly moving around in liquids and gases, but no in solids. Complexes between the molecules are accidentally formed between them. However, some kinds of molecules, known as receptor molecules or receptors, precisely differentiate one molecule from another. These complexes are adequately stable and their equilibrium concentrations are considerable. Such discrimination between molecules is called “molecular recognition” and is one of the essential keys to the existence of living things. Most of these molecular recognition events may trigger subsequent biological events. Well example is the protein synthetic pathways that are started from transcription and translation processes of DNA/RNA by many enzymes, including protein modification, such as phosphorylation, glycosylation, etc. Additionally, the complexes between antigen and antibody are also involved. Molecular imprinting method has been recently developed to mimic biological events that will be described in next topic (64).

3.10 Molecular imprinting

Molecular imprinting is a technique, being able to be described in the concept of “lock and key” model, to create template-shaped binding cavity produced by polymerization methods. The molecular imprinting processes are comprised of the following three steps: 1) covalent conjugate or non-covalent adduct between functional monomer and template, 2) polymerization and 3) removal of the template from the polymer (Figure 3.9). The cavity in the polymer originally occupied by the template molecule is left. Under suitable conditions, these cavities satisfactorily remember the size, structure and other physiochemical properties of the template and bind this molecule efficiently and selectively (65).

In past ten years, the current status of research in molecular imprinting technique has concerned with MIP characterizations, modification of polymerization (bulk, precipitation, core-shell emulsion, etc.), ingredients development (functional monomer, cross-linker, initiator, etc.) and computational analysis (66).

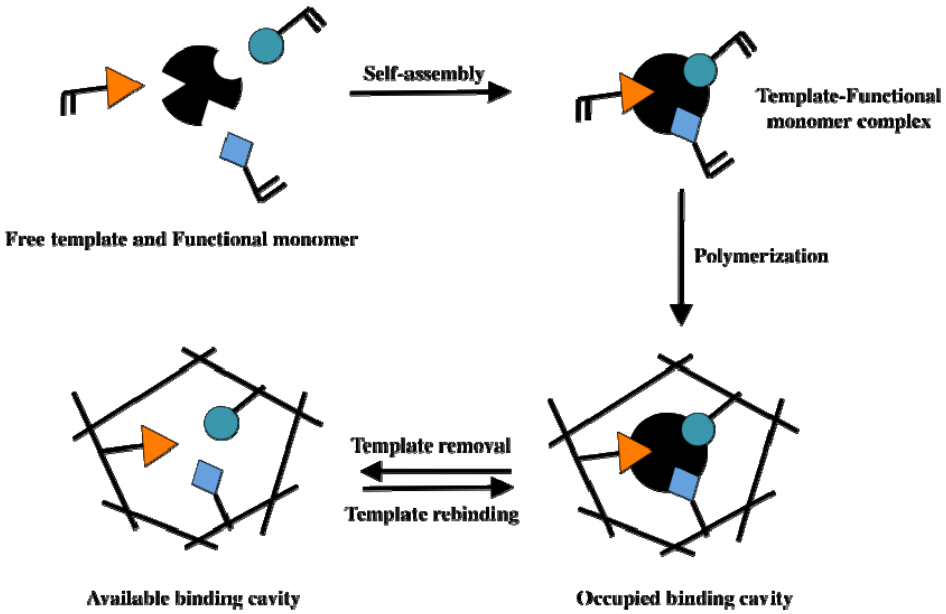

Figure 3.9. Concept of the molecular imprinting method.

3.10.1 Molecular binding between functional monomer and template

Typically, the molecular imprinting method is of two types, depending on the natural adducts between functional monomer and template; covalent and non-covalent conjugates. After that, hybridization of covalent imprinting and non-covalent imprinting has been discovered also known as semi-covalent imprinting.

3.10.1.1 Covalent imprinting

Prior to polymerization, functional monomer and monomer are conjugated by covalent bond in the first step and then is polymerized under this condition. After polymerization, the covalent linkage is cleaved to remove the template from the polymer (Figure 3.10). Upon the guest binding by the imprinted polymers, the same covalent linkage is formed. On the other hand, the template is reconnected with the imprinted polymer by non-covalent bonding called semi-covalent imprinting.

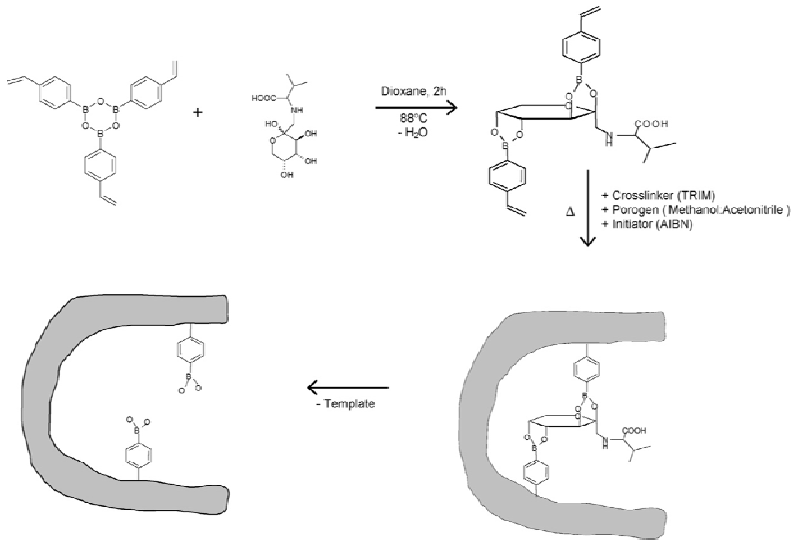

Figure 3.10. Covalent imprinting of fructosyl valine binding polymers (67).

3.10.1.2 Non-covalent imprinting

In order to connect a functional monomer with a template, non-covalent interaction such as hydrogen bonding, electrostatic interaction, Van der Waals, hydrophobic interaction and coordination-bond formation, are used here. The conjugation can be easily obtained by adding all ingredients to the reaction mixtures. After polymerization, the template is removed by suitable condition. The guest rebinding of the polymer occurs through the corresponding non-covalent interaction (Figure 3.11).

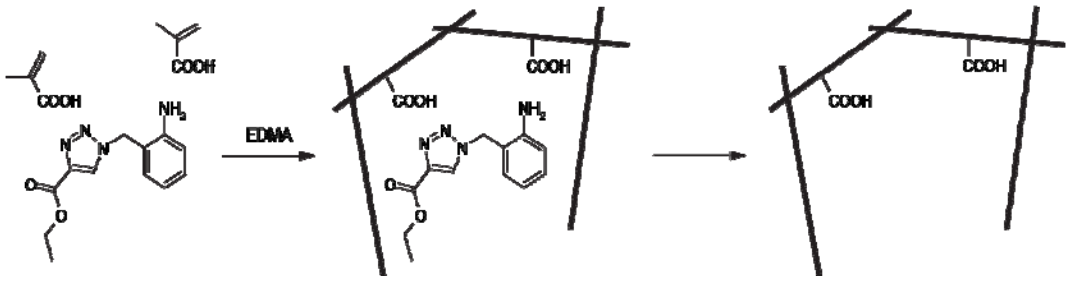

Figure 3.11. Non-covalent imprinting of drug candidate obtained from click chemistry reaction (68).

3.10.2 Ingredients for molecular imprinting

The common ingredients for technique of molecular imprinting include template, functional monomer, crosslinking monomer, initiator and solvent.

3.10.2.1 Template molecule

Template molecule acts as a center molecule for forming the polymerization. In addition, the template also acts as a rebinding molecule interacted in the hollow binding pocket. Up to now, there are many molecules that have been used for molecular imprinting researches, for example cells, proteins, nucleic acids, carbohydrates, lipids, amino acids, drugs, cholesterol, antioxidants, pesticides, insecticides, herbicides, neurotransmitters, pollutants, metal ions, etc. Many researchers have targeted the small molecules, because they are able to simply penetrate and remove of the MIP matrices easier than the lager molecules. Additionally, the large molecules in fact contain many binding recognition sites that are difficult to obtain well binding properties for the polymer. These problems have been solved by various strategies to allow the imprinting of large molecules more feasible (66).

3.10.2.2 Functional monomers

Functional monomers are the chemical compounds containing the complementary functional groups of template molecules. The functional monomers can form complexes with template and then are polymerized by crosslinking monomers. The functional monomers are presented in the binding pocket being available for template binding. Basically, the functional groups possessing in the functional monomers are acidic, basic, hydrophobic, hydrophilic groups, etc. Figure 3.12 showed typical functional monomers that have been utilized in molecularly imprinted polymers.

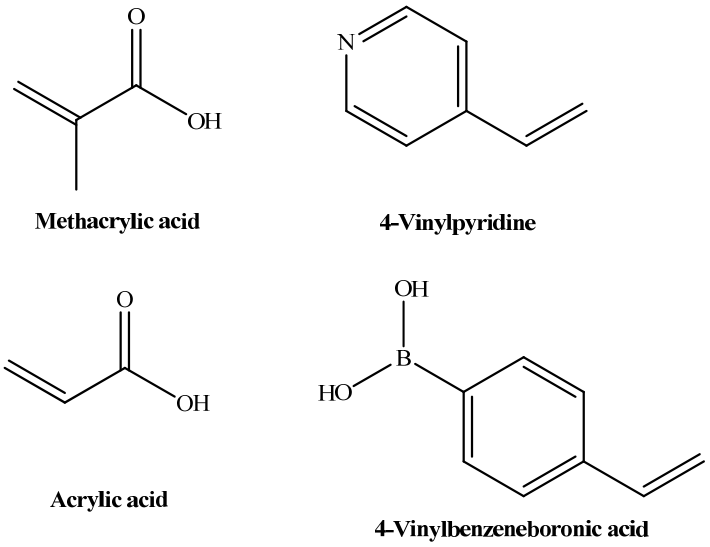

Figure 3.12. Common functional monomers.

3.10.2.3 Crosslinking monomers

In organic condition, ethylene glycol dimethacrylate (EDMA) and divinylbenzene (DVB) are typically used (Figure 3.13). *N, N'*-methylene-bisacrylamide in aqueous condition, is often used. The principle function of these ingredients is to fix the binding cavities firmly in desired structure. The mole ratios of crosslinking monomers are also important for the guest-binding sites. If the ratios are too small, the binding site are located so closely to each other resulting that cannot work independently. In extreme ratios, the binding cavity by one site can be completely blocked by the neighboring sites.

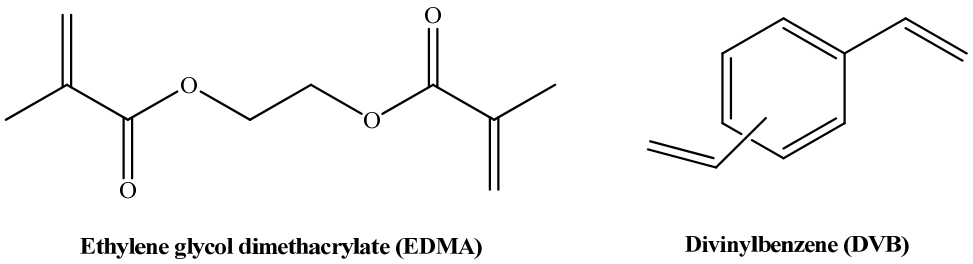

Figure 3.13. Crosslinking monomers.

3.10.2.4 Porogens or Solvents

The role of solvents is to dissolve all ingredients for polymerization, to provide porous structures to imprinted polymers and to promote their rates of guest binding. Release of the bound guest from the polymer is also facilitated by the porosity. In the polymerization, solvent molecules are incorporated inside the polymers and generate pores in the polymers after removal of solvent. Choice of solvents is depended on the kind of imprinting. In covalent imprinting, many kinds of solvents are usable as long as they satisfactorily dissolve all the components. In non-covalent imprinting, the choice of solvent is very critical to promote the formation of non-covalent linkage between the functional monomers and the template. The solvent is also important to increase the binding efficiency. For example, chloroform is preferred for the imprinting involving the ionic interaction because of low dielectric constant. Another is hydrogen bond interaction, which appropriates for low hydrogen-bond acidity or basicity resulting in a better imprinting efficiency.

3.10.2.5 Polymerization

Radical polymerization is usually initiated by using thermal decomposition of radical initiators. Illustrates are 2,2′-azobis(isobutyronitrile) (AIBN) and 2,2′-azobis(2,4-dimethylvaleronitrile) (ADVN) that are often used (Figure 3.14). The initiation radicals attack both functional monomer and crosslinker to polymerize them together. The reactions are very simple and economical. However, the critical point is oxygen, which can trap and retard the polymerization. In order to remove oxygen, degassing with argon or nitrogen, as well as freeze-and-thaw cycle under reduced pressure, is more effective. In addition, non-covalent conjugates between functional monomer and template are unstable at higher temperature, including thermal-sensitive template. One answer of this problem is to use the initiator decomposed with UV-light irradiation.

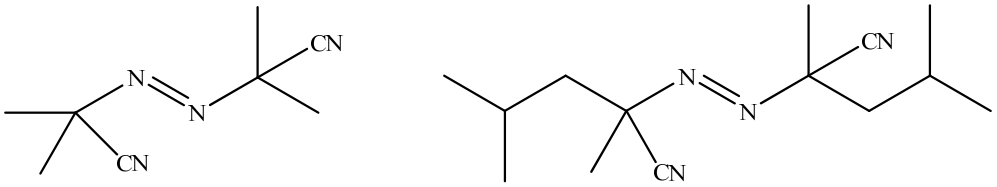

2,2'-azobis(isobutyronitrile (AIBN) **2,2'-azobis(2,4-dimethylvaleronitrile) (ADVN)**

Figure 3.14. General initiators.

Traditional polymerization method for the molecular imprinting is bulk polymerization. Polymers obtained by bulk polymerization are the monolithic blocks and need to grind the polymeric block into small heterogeneous MIP particle. Then the particle is filtered into a narrow size distribution by sieving. Irregularly sized particles are not suitable to be used for chromatography because of heterogeneous binding sites. At the present, most polymerization method used to perform uniformly sized MIP particles is the precipitation polymerization. This technique produces the micro- or nano-spheres of the polymers.

3.10.3 Characterization of molecular imprinting

The synthetic polymers are characterized the binding efficiency by column chromatography. The MIP particles are packed into the column and used as the stationary phase where the column is analyzed by a high-performance liquid chromatography (HPLC). The retention factor is a measure of the affinity of the imprinted polymer towards the template molecule and can be calculated with following equation:

$$k' = (t_{template} - t_{void})/ t_{void}$$

where $t_{template}$ and t_{void} denotes the retention times of the template molecule and void marker, respectively.

The efficiency of molecularly imprinted polymers can be obtained from the ratio of the retention factors between molecularly imprinted polymer (MIP) and non-imprinted polymer (NIP), called "imprinting factor". The imprinting factor is a measure of the selectivity of the imprinted polymer for the template molecule. To improve the recognition abilities of MIP, many techniques have been used to analyzed template-functional monomer adducts for example H^1-NMR and infrared spectroscopy.

3.10.4 Applications of molecular imprinting

The molecular imprinting method produces polymer that is specific for imprinted molecule and its derivatives. Thus, the polymers have been used as a potent separation media. Solid phase extraction is the most applications of molecular imprinting, which have been applied for separation and purification, such as racemic compounds (69), natural compounds (70), etc. Specific properties of molecular imprinting have been also acted as the recognition site applied in sensor techniques (71), as the active site of enzyme promoting the enzyme catalytic activity (72) and as the antibodies or the receptors used in drug discovery (73-75). In this research, the concept of molecularly imprinted polymers (MIPs) was used for the synthesis of nanoparticles for separating tocopherol and its derivatives (tocopherol acetate) as discussed in **Paper III** (chapter 6).

3.11 Glycosylation

Many proteins (e.g. the enzyme ribonuclease A and chymotrypsinogen) contain only amino acid residues and no other chemical constituents. However, some proteins contain permanently associated chemical components by conjugation to amino acid, referred to as conjugated proteins. The conjugated proteins are classified on the basis of the chemical groups, for example, lipoproteins contain lipids, glycoproteins contain carbohydrate groups and metalloproteins contain a specific metal. Basically, conjugated residues play a vital role in the protein's biological functions. Particularly, glycoproteins have one or several oligosaccharides of varying complexity conjugated covalently to a protein. They are observed on the outer face of the plasma membrane (76), in the extracellular matrix (77) and in the blood (78). For

intracellular, they are found in particular organelles such as Golgi complexes, secretory granules and lysosomes.

Glycoproteins are carbohydrate-protein conjugates in which the carbohydrate moieties are smaller and more structurally diverse than glycoaminoglycans of proteoglycans. The carbohydrate is attached at its anomeric carbon through a glycosidic joint to the hydroxyl group of a serine or theonine residues, also known as *O*-linked, or through an *N*-glycosyl link to the amide nitrogen of an asparagine residue, called *N*-linked. Some glycoproteins possess a single oligosaccharide chain, but not only one sugar. The carbohydrate can conjugate up to 70% of the glycoprotein by mass. The structures of *O*- and *N*-linked oligosaccharides from a diversity of glycoproteins are known (79-82).

There are many secreted proteins in the eukaryotic cell that are glycoproteins, including most of the proteins of blood, for instance, immunoglobulin (antibodies) (83) and some certain hormones (e.g. follicle-stimulating hormone, luteinizing hormone and thyroid-stimulating hormone) (84-86). Moreover, milk proteins, consisting of lactabumin and some of secreted proteins in pancreas (such as ribonuclease), are glycosylated proteins. Mammalian glycoprotein is controlled by enzymes, including glycosyltransferase and glycosidase. Glycosyltransferases synthesize glycan chain, whereas glycosidases specifically hydrolyze glycan linkages. The biosynthesis of both *N*-glycan and *O*-glycan is the same pathway in mammalian (87). Although one enzyme or one saccharide linkage paradigm applies to almost all biosynthetic steps, many glycosyltransferase isozymes exist and these underlie the breadth of glycan participation among different cell types and processes. Figure 3.15 showed cellular regulation of glycan expression.

The biological advantages of adding oligosaccharides to proteins are not completely understood. The very hydrophilic clusters of carbohydrate alter the polarity and solubility of the conjugated proteins. Oligosaccharide chains, that are attached to newly synthesized proteins in endoplasmic reticulum and elaborated in the Golgi complex, probably influence the sequence of polypeptide-folding events. Steric interactions between peptide and oligosaccharide may preclude one folding route and favor another. When diverse negatively charged oligosaccharide chains are clustered in a single region of a protein, the charge repulsion among them favors the formation

of an extended form. The bulkiness and negative charge of oligosaccharide chains also protect some proteins from attack by proteolytic enzymes (e.g. protease). Beyond these physical effects on the protein structure, there are also more specific biological effects of oligosaccharide chains in glycoproteins (Figure 3.16) (88).

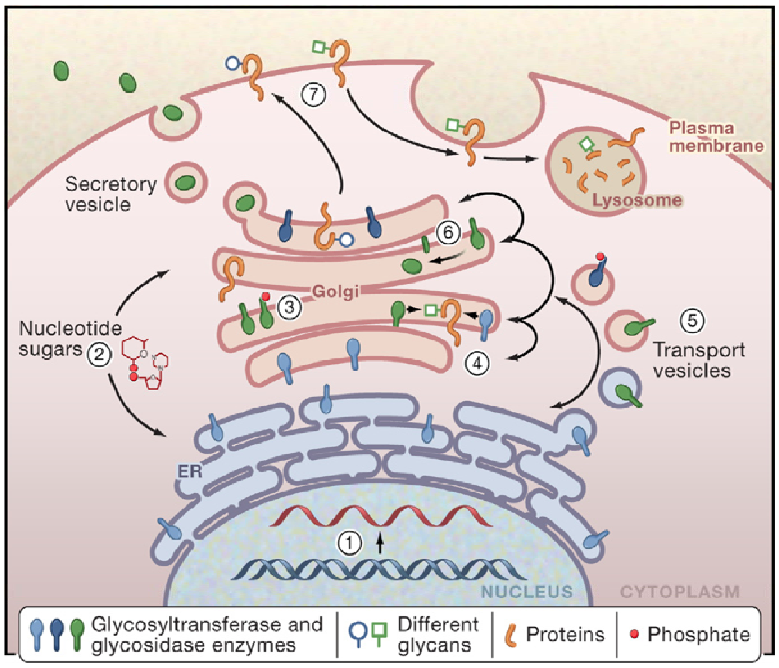

Figure 3.15. Cellular regulation of glycan expression (88).

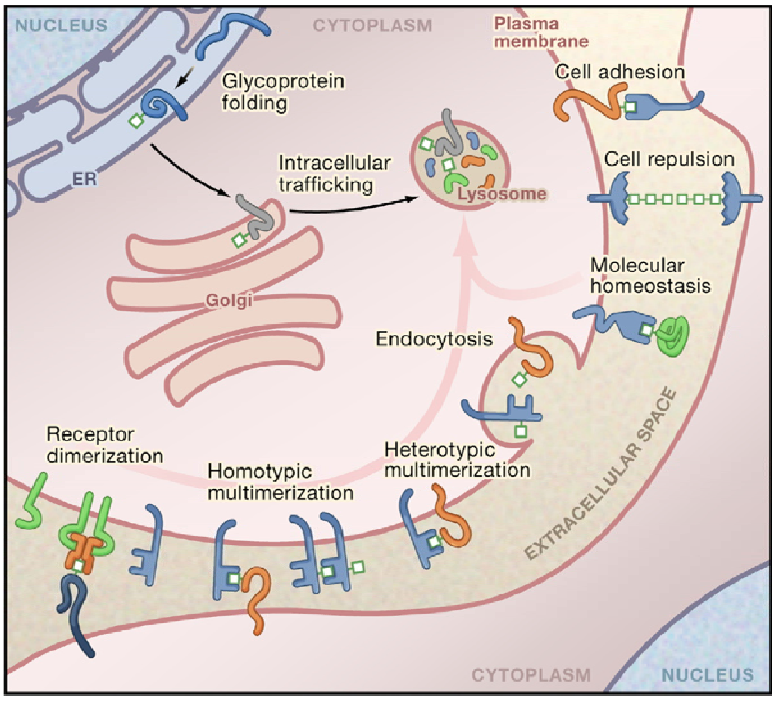

Figure 3.16. Cellular mechanism of glycoprotein function (88).

3.12 Boronic acid

Boronic acid has been used as affinity ligand for chromatography more than a century ago, also known as boronate affinity chromatography. Boronic acid specifically interacts with *cis*-diol compounds. Focusing on sugar, the interaction between boronate and *cis*-diol was firstly used in the analysis of carbohydrate in the 1940's. Until the 1970's, boronate affinity chromatography was utilized for separating sugar and nucleic acid. Up to now, this technique has been applied for the separation of many kinds of *cis*-diol compounds, such as nucleotides, nucleosides, nucleic acids, carbohydrates, glycoproteins and enzymes (89). Although the mechanism of interaction between boronic acids and *cis*-diols is not completely understood, the key interaction is covalent ester bond under basic condition. In aqueous solution under basic conditions, the boronate is hydrolyzed to form a tetrahedral boronate anion, which can form esters with *cis*-diols. This covalent ester bond is reversible by hydrolysis under neutral or acid condition. In addition, there are many secondary interactions that is important in some case, such as hydrophobic interactions, ionic interactions, hydrogen bonding and coordination interactions (Figure 3.17) (90-92).

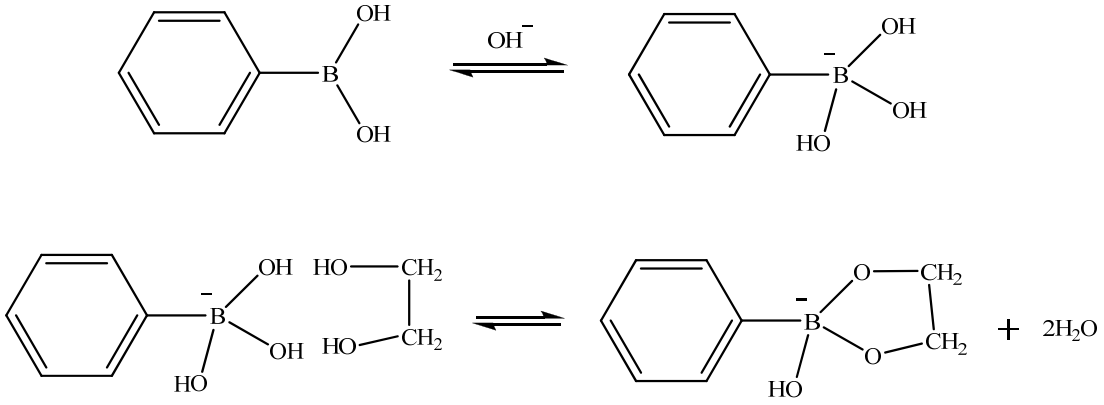

Figure 3.17. Proposed mechanism of esterification between boronic acid and *cis*-diol in aqueous solution.

The most common ligand for boronate affinity chromatography is 3-aminophenylboronic acid (3APBP), which is easy to modify at amino group of this compound for coupling it with solid supports. 3APBA possesses the pKa about 8.8 for optimum binding to analysts, which the pH of mobile phase should be as high as

possible (89). In many applications using 3APBA, the mobile pH is greater than 8.0. Figure 3.18 displayed structures of diverse boronic acid ligands (93).

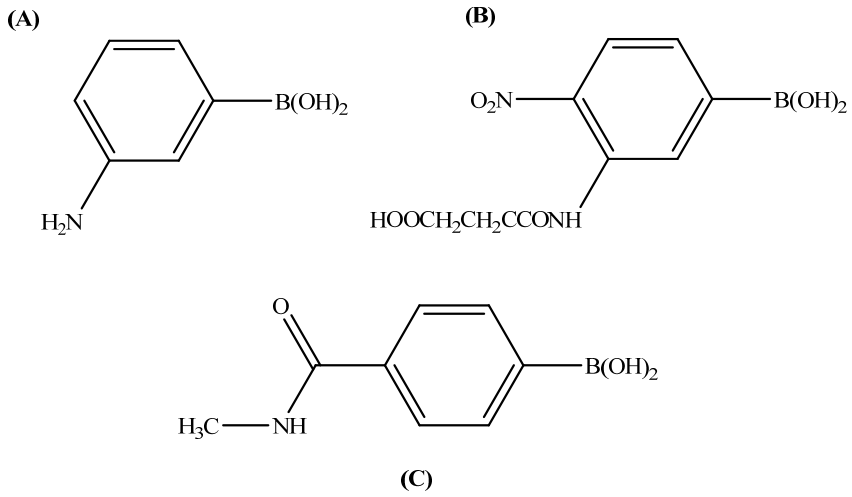

Figure 3.18. Structures of various boronic acid ligands. (A) 3-aminophenylboronic acid, (B) *N*-(4-nitro-3-dihydroxyborylphenyl) succinamic acid and (C) 4-(*N*-methyl)-carboxamidobenzene boronic acid (93).

3.13 Click chemistry

In history of modern chemistry, great many techniques for joining molecular pieces to each other have been developed. Many of these are quite sophisticated, requiring the delicate handling of highly reactive reagents under tightly controlled conditions. Until 2001, Sharpless promoted one of the best chemical reactions, namely "Click Chemistry". They are simple to make, produce in high yields with little or no byproducts, work well in various conditions and are not influent to other components (94).

Huisgen's 1,3-dipolar cycloaddition of alkynes and azides yielding triazoles is, undoubtedly, the primary example of a click reaction (Figure 3.19). Azides and alkynes are simple to install and they are also the least reactive functional groups in organic chemistry. With the recently discovered dramatic rate acceleration of the azide-alkyne coupling event under Cu(I)-catalysis and the beneficial effects of water, this unique connection process seems to be redefining the concept of a perfect reaction (95).

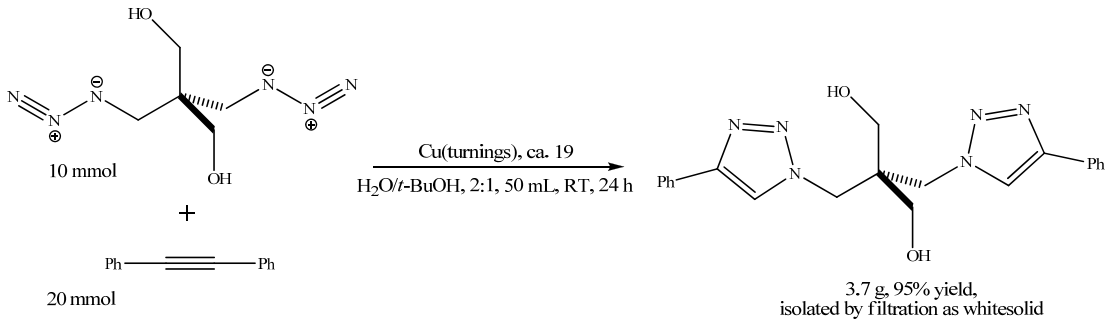

Figure 3.19. The premier click chemistry reaction.

Click chemistry has been widely used in many applications, for example, preparative organic synthesis of 1,4-substituted triazoles, peptide modifications, natural product modifications, drug discovery (95), macrocyclizations, DNA and nucleotide modifications, supramolecular chemistry, dendrimer designs, carbohydrate conjugations, polymers, material sciences and nanotechnology (96-100) based on Cu(I) catalyzed triazole ligation. In this thesis, (**Paper IV** or Chapter 7) the click chemistry was employed to immobilize stable boronate ligand onto the polymeric matrix for glycoprotein separation.

3.14 Theoretical and computational chemistries

Theory deals with using computers to model or simulate molecular behaviors that are only partly true. Theory actually contains under its broad umbrella the computational simulations. In recent year, there are the powerful computer and software packages that have become widely available. The basic equation for performing the simulations is derived from the Schrödinger equation, which is represented molecular systems in terms of the electrons and nuclei, or from classical mechanics. Thus, theory is also applied in diverse field of chemistry using physics, mathematics and computers to help scientists understand molecular behavior, to simulate molecular structures and to predict molecular properties. This context is also known as theoretical and computational chemistry.

$$i\hbar\frac{\partial}{\partial t}\Psi = \hat{H}\Psi$$

where Ψ is the wave function; the probability amplitude for different configurations of the system at different times, $i\hbar\frac{\partial}{\partial t}$ is the energy operator (i is the imaginary unit and $\hbar$ is the reduced Planck constant) and $\hat{H}$ is the Hamitonian operator. In three decade, quantum chemistry is the primary key word in the theoretical chemistry study (101, 102). Other researches in theoretical chemistry include molecular modeling, molecular dynamics, molecular mechanics, mathematical chemistry, theoretical chemical kinetics, cheminformatics, etc. All branch of theoretical and computational chemistry have been applied in broad researches, for example, protein-protein interaction, drug-protein interaction, drug design, drug properties, DNA/RNA interaction, etc. According to quantum chemistry, molecules are treated as electrons and nuclei. This thesis used quantum chemistry to discover the molecular geometry, the interatomic distances, the internal angles, occupied- and unoccupied-molecular orbitals, electronic atomic charges and the total electronic energy comparing to experimental biological activities (**Paper I-III;** Charpter 4-6).

CHAPTER IV
COPPER COMPLEXES OF NICOTINIC-AROMATIC CARBOXYLIC ACIDS AS SUPEROXIDE DISMUTASE MIMETICS

4.1 Abstract

This study reports the synthesis of novel mixed ligand complexes of copper with nicotinic and other select carboxylic acids (phthalic, salicylic and anthranilic acids). The tested copper complexes exhibited superoxide dismutase (SOD) mimetic activity and antimicrobial activity against *Bacillus subtilis* ATCC 6633, with a minimum inhibition concentration of 256 μg/mL. Copper complex of nicotinic-phthalic acids (CuNA/Ph) was the most potent with a SOD mimetic activity of IC_{50} 34.42 μM. The SOD activities were observed to correlate well with the theoretical parameters as calculated using density functional theory (DFT) at the B3LYP/LANL2DZ level of theory. Interestingly, the SOD activity of the copper complex CuNA/Ph was positively correlated with the electron affinity (EA) value. The two quantum chemical parameters, highest occupied molecular orbital (HOMO) and lowest unoccupied molecular orbital (LUMO), were shown to be appropriate for understanding the mechanism of the metal complexes as their calculated energies show good correlation with the SOD activity. Moreover, copper complex with the highest SOD activity were shown to possess the lowest HOMO energy. These findings demonstrate a great potential for the development of value-added metallovitamin-based therapeutics.

4.2 Introduction

Nicotinic acid (NA) or vitamin B3 is essential for many biological processes namely for the production of energy (103), signal transduction, regulation of gene expression (104) and involvement in the synthetic pathway of lipids (105). The oxidation of lipoproteins, low density lipoprotein and very low density lipoprotein, by free radical, particularly superoxide radical ($O_2^{\bullet -}$), causes vascular inflammation, which is involved in the early stage development of atherosclerosis, a disease affecting arterial blood vessels (106). In developed countries such as the United States, atherosclerosis is the leading cause of illness and death accounting for 44% of deaths and morbidity (107). Nicotinic acid has been reported to decrease the production of free fatty acids and lipoproteins (43), despite of this free radical continues to appear in the human body. To eliminate such superoxide radicals, transition metal complexes were developed as superoxide dismutase mimics. Some examples include metalloporphyrin (108) and metal-drug complexes (109).

Complexation of nicotinic acid with various metals (e.g. manganese, cobalt, nickel, copper and zinc) had been previously reported (110). Nicotinic acid-copper complex (CuNA) has been shown to exert diverse bioactivities. In particular, it can stimulate blood flow and prevent gastric congestion (111), reduce total lipids in sera hepatic tissue as well as regulate levels of alanine transaminase, aspartate transaminase, alkaline phosphatase, gamma glutamyl transpeptidase and oxidative markers such as nitric oxide (NO) and lipid peroxidation in rat models (112). Additionally, it also exhibits SOD mimic activity in patients with hepatocellular carcinoma. The metal complexes of nicotinic acid with other small molecules such as isonicotinate and acetylacetonate were previously reported (110, 113). The aforementioned nicotinic acid-copper complexes were formed through coordination with the carboxylate oxygen- and/or pyridine nitrogen-atoms (113, 114), which are electron donors. These electron-donating groups are commonly found in many natural compounds such as flavonoids (rutin, taxifolin, epicatechin and luteolin), phenolics (catechol and resveratrol) and drugs (aspirin, ibuprofen and oxaprozin), all of which were reported to form metal complexes with potent superoxide scavenging capacities (115-117). For example, flavonoid copper complexes were shown to exhibit higher SOD activity than the parent free flavonoids (116). A series of simple Cu carboxylate

(acetate, salicylate or benzoate) complexes synthesized by Devereux *et al*., were reported to exhibit excellent SOD mimic activity (118). Salicylic acid, one of the metal-chelating ligands used in this study, is a natural compound found in most fruits and vegetables and functioning as a plant growth hormone. The compound was shown to possess promising anti-cancer activity by modulating the inhibition of the P form of phenolsulphotransferase, thus preventing excessive carcinogen activation (119). Anthranilic acid (also known as vitamin L), another ligand used in the study, is a natural ingredient essential for lactation. Its derivatives have been found to activate soluble guanylyl cyclase, a ubiquitous NO receptor involved in vasorelaxation and hypertension (120). In addition, copper atom is an essential nutrient involved in the catalytic function of many enzymes such as copper-zinc superoxide dismutase (CuZnSOD) (121, 122). Copper deficiency has been reported to cause hematologic disorders, hypopigmentation, defective connective tissue cross-linking and ataxia (123, 124).

The ideal SOD-mimic should be a low molecular weight metal complex that possesses high membrane permeability. However, very few Cu-carboxylate complexes had been reported (118). In an attempt to obtain small molecule-based metal complexes, we now report the synthesis of novel copper complexes as potent SOD mimics. Such complexes are based on the coordination of nicotinic acid-Cu with the small molecule carboxylates phthalic acid (Ph), salicylic acid (Sal) and anthranilic acid (Ant). Computational chemistry has found extensive applications for studying molecular structure and reactivity (125). Some usage examples include studying the mechanism of protein receptor-inhibitor interaction (126), development of quantitative structure-activity/property relationship (QSAR/QSPR) (127) and elucidation of enzymatic reaction (128), etc. To shed light on the underlying mechanisms of the superoxide radical scavenging activities, quantum chemical parameters were calculated at DFT level. Results indicated that the calculated physicochemical parameters were well correlated with the experimental SOD activities. Such theoretical parameters included energies of HOMO and LUMO as well as EA. Furthermore, to confer value-added benefits to the copper complexes as well as explore the possibility of using such compounds as a multifaceted drug the antimicrobial activity of the novel complexes was also determined.

4.3 Materials and methods

4.3.1 Materials

Melting points of the complexes were determined on the Griffin capillary melting point apparatus and are reported uncorrected. Infrared (IR) spectra were obtained on a Perkin Elmer System 2000 FTIR using potassium bromide (KBr) pellet. Mass spectra were recorded on a Bruker Daltonics (MicroTOF) instrument. Magnetic moments were measured with a Mark 1 Magnetic Susceptibility Balance (Sherwood Scientific, Cambridge, UK). Nicotinic acid, phthalic acid, salicylic acid and anthranilic acid were of analytical grade and purchased from Sigma-Aldrich, as was bovine erythrocyte superoxide dismutase.

4.3.2 Synthesis of mixed-ligand complexes of copper with nicotinic acid and phtalic acid (1)

Nicotinic acid (0.123 g, 1 mmol) dissolved in methanol (30 mL) was heated (70°C) and stirred under reflux until a clear solution was obtained. Cupric chloride dihydrate (0.170 g, 1 mmol) dissolved in methanol (2 mL) and then added dropwise to the prepared nicotinic acid solution. After heating for 45 min, the reaction mixture was added dropwise to a solution of phthalic acid (1 mmol, 0.166 g) in methanol (2 mL), then the mixture was heated for 1 h under the same conditions. The precipitated solid was collected by filtration, washed with cold methanol and dried under vacuum over silica gel at room temperature. Complex **1** was obtained as an aquamarine powder; m.p. > 300°C; IR (KBr, cm^{-1}): 2,565-3,080 (m, OH), 1,685 (s, CO), 1,701 (s, CO), 1,718 (s, CO), 1,418 (m, OH), 1,333 (w, CN), 1,298 (m, C-O); HRMS (TOF) calculated for $C_6H_5NO_2$ $[M+H]^+$ 124.0399, found: 124.0399.

4.3.3 Synthesis of mixed-ligand complexes of copper with nicotinic acid and salicylic acid (2)

Complex **2** was prepared in the same way as complex **1** using nicotinic acid (0.123 g, 1 mmol), cupric chloride (0.170 g, 1 mmol) and 1 mmol (0.138 g) of salicylic acid. Product **2** was obtained as an aquamarine powder by filtration, washing with cold methanol and dried over silica gel; m.p. > 300°C; IR (KBr, cm^{-1}): 2,567 (sh, w, OH), 2,682 (sh, w, OH), 1,717 (s, CO), 1,700 (s, CO), 1,685 (s, CO), 1,454

(m, OH), 1,420 (m, OH), 1,332 (m, CN), 1,298 (s, C-O), 1,201 (w, C-O), 1,144 (w, C-O), 1,126 (w, C-O); HRMS (TOF) calculated for $C_6H_5NO_2$ $[M+H]^+$ 124.0399, found: 124.0399.

4.3.4 Synthesis of mixed-ligand complexes of copper with nicotinic acid and anthranilic acid (3)

Complex **3** was prepared by an analogous procedure, but changing from Ph and/or Sal to anthranilic acid (1 mmol, 0.137 g) as a ligand. The precipitate of complex **3** was received as an aquamarine powder; m.p. > 300°C; IR (KBr, cm^{-1}): 3,275 (m, NH), 3,400 (br, OH), 2,681 (w, OH), 2,565 (w, OH), 1,718 (s, CO), 1,700 (s, CO), 1,608 (s), 1,558 (vs), 1,458 (m, OH), 1,420 (m, OH), 1,386 (s, CN), 1,332 (m, CN), 1,298 (s, C-O); HRMS (TOF) calculated for $C_6H_5NO_2$ $[M+H]^+$ 124.0399, found: 124.0396.

4.3.5 Determination of superoxide dismutase (SOD)-like activity

The complexes were tested for SOD activity using the previously described method (109). The SOD activity of copper complexes was assayed by measuring the inhibition of the photoreduction of NBT. This indirect assay is comprised of several reactions: the photochemically excited riboflavin was first reduced by methionine to a semiquinone, which donated an electron to oxygen to form the superoxide source. The superoxide readily converted NBT into a purple formazan product, which was spectrophotometrically detected at 550 nm. In this regard, the SOD activity was inversely related to the amount of formazan formed and expressed in term of IC_{50} of NBT reduction.

4.3.6 Antimicrobial activity

The antimicrobial activity of the complexes was investigated against representative microorganisms using the method previously reported (129). One milliliter of Müeller Hinton (MH) broth was mixed with the tested complexes dissolved in DMSO. The MH broth of the tested sample was then mixed with MH agar solution and placed onto the plates with the final concentrations (64, 128 and 256 μg/mL) as agar dilution. The microorganisms, cultured in the MH broth at 37°C

for 24 h, were diluted with 0.9% normal saline solution to 3×10^8 cells/mL. The organisms were inoculated onto each plate and incubated at 37°C for 18-48 h. Complexes found to be effective against the tested strains were selected for further investigations. The inhibition of microbial cell growths was also determined. Twenty-seven strains of microorganisms were used as shown in Table 4.1.

4.3.7 Molecular modeling of superoxide dismutase mimics

The molecular models of the copper complexes were constructed with GaussView 3.09 (130) based on the IR and magnetic moment data which indicated that the coordination complexes were of distorted tetrahedral conformation. Full geometry optimizations without symmetry constraints were performed *in vacuo* using Becke's three-parameter hybrid Lee-Yang-Parr (B3LYP) (131) functional and the LANL2DZ (132-134) basis set under Gaussian 03W (135). The LANL2DZ basis set was selected as it could handle high Z atoms (136), particularly atoms that are beyond the third row. Electron affinity was computed by taking the difference of the total energies of the coordination complexes Cu(II) and Cu(I) as summarized by the following equation:

$$EA = TE_{Cu(I)} - TE_{Cu(II)}$$

where EA represents the electron affinity, $TE_{Cu(I)}$ represents the total energy of the Cu(I) coordination complex, $TE_{Cu(II)}$ represents the total energy of the Cu(II) coordination complex. HOMO and LUMO energies were derived from geometrically optimized Cu(I) coordination complex as it is the active form of the SOD mimetics.

4.4 Results and discussion

4.4.1 Synthesis and characterization

Three copper-based complexes, copper complexes of nicotinic-phthalic acids (CuNA/Ph, **1**), nicotinic-salicylic acids (CuNA/Sal, **2**) and nicotinic-anthranilic acids (CuNA/Ant, **3**), were synthesized by the reaction of 1:1:1 ratio of cupric chloride with nicotinic acid and aromatic carboxylic acids (phthalic, salicylic and anthranilic acids). The complexes were obtained in excellent yields (82-91%) as aquamarine

powder, highly polar, insoluble in methanol and water, but soluble in dimethyl sulfoxide (DMSO). Their melting points (m.p.) and magnetic moments (μ_{eff}) are listed in Table 4.2.

Infrared spectra

Coordination of the copper atom with the functional groups of the ligands was established from the IR spectra (Table 4.3). From the data of complex **1**, it can be seen that the C-O stretching vibration frequency was located at 1298 cm^{-1}, while the free phthalic acid and nicotinic acid absorptions υ(C-O) appeared at 1282 and 1299 cm^{-1}, respectively. In addition, disappearance of the hydroxyl group bending vibration (δO-H) of Ph at 1404 cm^{-1} was observed. For the carbonyl group (C=O), the stretching vibrations of both NA and Ph still exhibited intensive bands at 1685, 1701 and 1718 cm^{-1}. The weak band at 1333 cm^{-1} could be ascribed to C-N stretching vibration of complex **1** as compared with the spectra of NA, which shows strong band υ(C-N) at 1324 cm^{-1}. Thus, complex **1** was formed using pyridine ring nitrogen atom of NA and two hyd[r]oxyl groups of Ph to coordinate with copper atom.

In a similar fashion, the IR spectra of complex **2** were interpreted by comparison of its spectra with those of the free ligands. It was apparent that the hydroxyl and carbonyl absorptions of salicylic acid were at 3471 cm^{-1} υ(O-H) and 1655, 1662 cm^{-1} υ(C=O), respectively, suggesting that Cu-complex formation took place via the phenolic and carbonyl functionalities. The IR spectra of complex **2** still displayed strong absorptions at 1700, 1717 cm^{-1} υ(C=O), 1298 cm^{-1} υ(C-O) and 1420 cm^{-1} δ(O-H). However, the C-N stretching vibration of complex **2** was observed at 1332 cm^{-1} whereas the C-N absorption of free NA appeared at 1324 cm^{-1}. Based on the IR spectra, complex **2** was observed to be formed through the carbonyl and the phenolic hydroxyl group of Sal and the pyridine ring nitrogen atom.

The IR spectra of complex **3** exhibited disappearance of the anthranilic acid carbonyl (C=O) absorption at 1654 and 1679 cm^{-1}. Additionally, the amino (NH) absorption of complex **3** appeared at 3275 cm^{-1}, while the NH_2 absorption of Ant was observed at 3239 and 3325 cm^{-1}. Strong C-N stretching of Ant was displayed at 1371 and 1319 cm^{-1} with a very strong NH bending observed at 754 cm^{-1}. The IR spectra of complex **3** showed strong absorptions at 1718, 1700 (C=O), 1298 (C-O), medium bending band of OH at 1420 cm^{-1} and C-N stretching of ring N-atom at 1332 cm^{-1}.

The characteristic free NA C-N stretching absorption of the pyridine ring (υ 1324 cm^{-1}) was shifted to higher frequency at 1332 cm^{-1}. The C-N stretching of NH group of complex **3** was observed at 1386 cm^{-1}. It was suggested that complex **3** was formed through coordination of pyridine ring nitrogen atom; carbonyl and NH groups of Ant with Cu centered atom.

It is noted that these Cu-complexes were formed via monodentate interaction of the ring nitrogen atom of NA resulting in a υ(C-N) shift from 1324 cm^{-1} to a higher frequency range of 1332-1333 cm^{-1}. The υ(C=O), υ(C-O) and δ(O-H) absorptions of the NA ligand of the complexes remained unperturbed. Aside from NA, other ligands coordinated with the central Cu atom *via* bidentate carboxylates. With regards to complex **1**, Ph is the bidentate ligand using two hydroxyls of dicarboxylic acid to coordinate with the Cu atom. This is observed by the disappearance of C-O stretching at 1282 cm^{-1} and O-H bending at 1404 cm^{-1}. As for complex **2**, stretching at 1662 and 1655 cm^{-1} (C=O) and at 3471 and 3240 cm^{-1} (O-H) disappeared with a shift of C-O stretching from 1250, 1211 and 1,156 cm^{-1} to lower frequencies. This suggested that the Cu atom formed a complex by means of a bidentate phenolic carboxylate. Similarly, the Cu atom of complex **3** was found to be coordinated with the amino carboxylate of Ant ligand, which is due to the disappearance of C=O and NH_2 stretching absorptions of Ant.

High resolution mass spectra (HRMS) measurements for complexes **1-3** were performed, but their molecular ions were not detected. Fragmented ions were observed at m/z of 124.0399 corresponding to free nicotinic acid as calculated for $C_6H_5NO_2$ $[M+H]^+$. Additionally, m/z of 124.0399 was quantified for complexes **1** and **2** while 124.0396 was detected for complex **3**.

Complexes **1-3** were paramagnetic, with magnetic moments (μ_{eff}) of 1.69, 1.68 and 1.80 B.M., respectively. The μ_{eff} value indicates that the complexes were of tetrahedral conformation with the Cu(II) center. Therefore, on the basis of both IR spectra and μ_{eff}, we can confirm that complexes **1-3** were of tetrahedral geometry with the Cu(II) center.

4.4.2 Superoxide scavenging activity

The copper complexes were assayed for SOD-like activity using the modified method by measuring the inhibition of the photoreduction of nitro blue tetrazolium (NBT). The results showed that all the tested complexes exhibited SOD activities with IC_{50} in the range of 34.42-47.49 μM as presented in Table 4.4.

Complex **1** was the most potent SOD mimic with an IC_{50} of 34.42 μM. Moreover, the SOD activity of the free ligand, NA and Ph, was very low to the point that the IC_{50} could not be obtained. The SOD activity of the uncoordinated salicylic and anthranilic acids was assayed and their IC_{50} was determined to be 594 and 236.25 μM, respectively. It was observed that complex **2** was approximately 14 times more potent than the uncoordinated Sal. Similarly, complex **3** was five times more potent than the free Ant. The results support the notion that the copper atom is essential for SOD activity and that the incorporation of copper into the structure of the ligands tremendously increased the SOD activity. We attribute this to the change in oxidation state of the copper atom modulated through its coordination with the metal-chelating ligands. It is noteworthy that the coordination complexes are much smaller than the native enzymes. Moreover, an added benefit is that the compounds can be easily synthesized from simple bioactive compounds. Some of the potent SOD mimics developed thus far were based on Mn and Cu coordination compounds. Example of such SOD mimics are the Cu-drug complexes which included Cu (aspirin), Cu $(aspirin)_4$ and Cu (ibuprofenate).

4.4.3 Antimicrobial activity

Nicotinic acid is a widely used drug for the treatment of hyperlipidemia (105). In addition, salicylic and anthranilic acids are bioactive aromatic carboxylic acids. The antimicrobial activity of complexes **1-3** has not been reported before. As the objective of this study is to develop value-added metallovitamins for therapeutic applications, therefore it is worthy to observe whether the compounds could also be used as antimicrobials, aside from being superoxide radical scavengers. Our results revealed that the tested complexes **1-3** could selectively inhibit the growth of *B. subtilis* ATCC 6633 with a MIC of 256 μg/mL (Table 4.5).

It should be noted that salicylic acid was the only free ligand that could completely inhibit the growth of *B. subtilis* ATCC 6633 (MIC of 256 μg/mL) and that the antimicrobial activity of salicylic acid and its derivatives against *E. coli*, *B. subtilis* and *S. aureus* has been previously reported (137). Aside from this, the other free ligands (e.g. nicotinic, phthalic and anthranilic acids) were inactive against all of the tested microorganisms. A plausible explanation for the antimicrobial activity of the copper complexes is that they may enhance bacterial killing by synergistically converting superoxide radical to hydrogen peroxide in which accumulation of hydrogen peroxide exerted harmful effect to the bacterial cells as well as participated in the subsequent formation of hydroxyl radical via the Fenton's reaction.

4.4.4 Molecular modeling of SOD mimics

To elucidate the mechanisms of radical scavenging activities of the copper complexes, density functional theory calculations at the B3LYP/LANL2DZ level was employed. Previous efforts have indicated that the calculation of theoretical parameters, binding energies and electron affinities, at such theoretical levels are suitable for characterizing the superoxide radical scavenging activity (138-141). The molecular structures were constructed on the basis of IR and magnetic moment data which indicated that the coordination complex was of distorted tetrahedral conformation. Geometrically optimized structure of complexes **1-3** is presented in Figure 4.1.

Electron affinity, in particular, is an appropriate theoretical parameter accounting for the electron transfer rate from superoxide anion to copper atom (139-141). The lower the EA becomes the higher the electron transfer rate is, which correspondingly leads to higher superoxide radical scavenging activity. EA was calculated according to equation (1) by taking the difference of the total energy of Cu(II) and Cu(I) coordination complexes. The EA for complexes **1-3** as presented in Table 4.6 were calculated to be -125.502, -139.283 and -212.679 kcal/mol, respectively.

The experimental SOD activities of complexes **1-3** had an IC_{50} of 34.42, 42.79 and 47.49 μM, respectively. The results indicated that there exists a positive correlation between EA and SOD activity where high EA gives rise to high SOD

activity, which is inversely correlated in previous reports (139, 140). This is presumably due to differences in the coordination geometry of the copper complexes used in this study (tetragonally distorted) and the copper complexes (distorted square-planar and square-pyramidal) reported previously (139, 140). Similar observation was deduced by Branco *et al*. in their studies on active site distortion of CuZnSOD (142, 143).

Additionally, the usefulness of quantum chemical descriptors such as energy of the highest occupied molecular orbital and energy of the lowest unoccupied molecular orbital in elucidating the radical scavenging activity were also investigated. Examples on the usage of HOMO and LUMO energies in accounting for chemical reactivities of molecules and their relevance to electron transfer complexes can be found in an excellent review by Karelson and Lobanov (144). The HOMO energies of the ligands were calculated to be -5.818, -6.729 and -7.644 eV, respectively with the following order: Ant > Sal > Ph (Table 4.7).

Likewise, the calculated value of HOMO for the complexes exhibited similar trend: **3** > **2** > **1** with the corresponding values of -5.829, -6.293 and -7.302 eV, respectively. It is well established that HOMO accounts for the electron donating ability while LUMO characterizes the ability to accept electron (145). From the frontier molecular orbital approximation, high HOMO energy value infers that the molecule or ligand can easily release electrons to the unoccupied orbital of the metal ion, indicating strong binding affinity (146). Thus, Ant possesses the strongest interaction with copper leading to the best binding capacity. Such degree of binding capacity is found to be Ant > Sal > Ph.

In addition, the selected bond lengths and angles of the geometrically optimized structures are given in Table 4.8. The average bond distance at axial position for Cu-N1 of complexes **1-3** was 2.029 Å. The longest axial bond length for Cu-O1 and Cu-O2 were observed for complex **1** with values of 1.872 and 1.870 Å, respectively. The axial bond lengths of Cu-O1 and Cu-O2 for complex **2** were found to be shorter than that of complex **1** with values of 1.838 and 1.857 Å, respectively. This is explained by the inductive effect of the two carbonyl groups of complex **1** withdraws electrons from the Cu atom giving rise to low electron donating ability of the ligand as also indicated by the lower HOMO energy. Therefore, complex **1**

exhibited the highest SOD activity. Finally, the shortest axial bond lengths for Cu-N2 and Cu-O1 were found in complex **3** to be 1.809 and 1.830 Å, respectively. This can be attributed to the greater electron donating ability of the amino group of anthranilic acid than the phenolic group of salicylic acid. This results in the lower HOMO energy of **2** than **3**. It was previously reported by Li *et al* (147) that axial bond lengths were crucial for SOD activity where long bond lengths being advantageous for the dismutation of superoxide anion. In addition, correlation between the binding capacity and the SOD activity of metal complexes was previously studied using molecular modeling and quantum chemical calculation (109, 148). It was found that molecules exhibiting higher metal binding affinity displayed lower SOD activity. This was observed for complex **3**, which possessed the lowest SOD activity and the highest calculated HOMO value. On the other hand, complex **1** exhibited the highest SOD activity with the lowest calculated HOMO value (Tables 4.4 and 4.7). Furthermore, the calculated energies of HOMO and LUMO were well correlated with the SOD activity as observed from $r = 0.999$ and 0.953, respectively. Such results demonstrate the practical usage of HOMO and LUMO as theoretical parameters for the characterization of SOD activity in terms of charge- or electron-transfer of the complex.

In summary, the novel copper complexes with nicotinic acid and carboxylic acids were synthesized in excellent yields. The coordination compounds were characterized to be tetragonally distorted structures formed by monodentate coordination of ring N-atom of NA as well as bidentate carboxylate ligands using amino carbonyl (Ant), phenolic carbonyl (Sal) and two hydroxyls (Ph). It should be noted that from the chemical and biological point of view, these copper complexes could easily be formed through the coordination of metal ions with simple dietary intake of vitamins or endogenous carboxylic acids and related compounds. All of the copper complexes were shown to exhibit superoxide scavenging activity as well as antimicrobial activities against *B. subtilis* ATCC 6633 with MIC 256 μg/mL. Complex **1** was the most potent SOD activity with an IC_{50} of 34.42 μM. Theoretical parameters as calculated by DFT methods were used to elucidate the mechanisms of SOD activity. Interestingly, copper complexes with higher SOD activity such as complex **1** were found to have higher EA value. Furthermore, calculated HOMO and LUMO energies

displayed good correlation with the SOD activities with *r* of 0.999 and 0.953, respectively. Such results corroborate the usefulness of HOMO and LUMO energies in relation to the SOD activity as it could account for the charge- or electron-transfer of the complex. These findings suggest great potential for the development of metallovitamin-based therapeutics.

Table 4.1. Organisms subjected to growth inhibition assays.

Microorganism	Reference strain	Clinical isolate
Gram-positive bacteria	*Staphylococcus aureus* ATCC 29213	*Streptococcus pyogenes* II
	Staphylococcus aureus ATCC 25923	*Bacillus cereus*
	Staphylococcus epidermidis ATCC 12228	*Listeria monocytogenes*
	Enterococcus faecalis ATCC 29212	
	Enterococcus faecalis ATCC 33186	
	Micrococcus lutens ATCC 10240	
	Bacillus subtilis ATCC 6633	
	Corynebacterium diphtheriae NCTC 10356	
Gram-negative bacteria	*Escherichia coli* ATCC 25922	*Shigella dysenteriae*
	Klebsiella pneumoniae ATCC 700603	*Salmonella enteritidis* type C
	Serratia marcescens ATCC 8100	*Morganella morganii*
	Salmonella typhimurium ATCC 13311	*Aeromonas hydrophila*
	Shewanella putrefaciens ATCC 8671	*Citrobacter freundii*
	Achromobacter xylosoxidans ATCC 2706	*Plesiomonas shigelloides*
	Pseudomonas aeruginosa ATCC 15442	
	Pseudomonas stutzeri ATCC 17587	
Yeasts	*Saccharomycess cereviseas* ATCC 2601	
	Candida albicans ATCC 90028	

Table 4.2. Physiochemical parameters of nicotinic acid-copper complexes and ligands.

Compound	Chemical Formula	Formula Weight ($g \cdot mol^{-1}$)	Color	Melting Point (°C)	Yield (%)	μ_{eff} (B.M.)
NA	$C_6H_5NO_2$	123.11	white	236-239	–	–
Ph	$C_8H_6O_4$	166.13	white	210	–	–
CuNA/Ph (**1**)	$C_{14}H_{10}CuNO_7$	367.78	aquamarine	>300	82	1.6944
Sal	$C_7H_6O_3$	138.12	white	158-160	–	–
CuNA/Sal (**2**)	$C_{13}H_{10}CuNO_6$	339.77	aquamarine	>300	85	1.6802
Ant	$C_7H_7NO_2$	137.14	yellow	144-148	–	–
CuNA/Ant **(3)**	$C_{13}H_{13}CuN_2O_5$	338.78	aquamarine	>300	91	1.8038

Table 4.3. IR spectra of the free ligands and the copper coordination complexes.

Cpd	υC=O	υC-O	υC-N	υO-H	δO-H	υNH	δNH
NA	1,718 (s) 1,700 (s)	1,299 (s)	1,324 (s)	3,072-2,449 (w)	1,418 (s)	–	–
Ph	1,700 (s) 1,685 (s)	1,282 (s)	–	3,072-2,524 (br)	1,404 (s)	–	–
1	1,718 (s) 1,701 (s) 1,685 (s)	1,298 (m)	1,333 (w)	3,080-2,565 (w)	1,418 (m)	–	–
Sal	1,662 (s) 1,655 (s)	1,296 (s) 1,250 (s) 1,211 (s) 1,156 (s)	–	3,471 (br) 3,240 (sh)	1,446 (s) 1,484 (s)	–	–
2	1,717 (s) 1,700 (s) 1,685 (s)	1,298 (s) 1,201 (w) 1,144 (w) 1,126 (w)	1,332 (m)	2,682 (sh, w) 2,567 (sh, w)	1,454 (m) 1,420 (m)	–	–
Ant	1,679 (m) 1,654 (sh, m)	1,277 (m) 1,238 (m)	1,371 (s) 1,319 (s)	2,869 (br) 2,580 (br) 2,362 (sh, w) 3,449 (br)	1,458 (m)	3,325 (sh, s) 3,239 (sh, s)	754 (vs)
3	1,718 (s) 1,700 (s)	1,298 (s)	1,386 (s) 1,332 (m)	3,400 (br) 2,681 (w) 2,565 (w)	1,458 (m) 1,420 (m)	3,275 (m)	756 (s)

Note: vs = very strong, s = strong, m = medium, w = weak, br = broad, sh = sharp

Table 4.4. Superoxide dismutase activity of the free ligands and copper complexes.

Compound *	*IC_{50} (μM)*[a]
Sal	>594.00
Ant	>236.25
1	34.42
2	42.79
3	47.49
SOD[b]	0.0026

[a] IC_{50} was defined as fifty percent inhibition concentration of NBT reduction.

[b] Superoxide dismutase derived from bovine erythrocytes was a homodimeric protein.

* Nicotinic acid and phthalic acid possessed very low activity, to the point that the IC_{50} cannot be obtained.

Table 4.5. Antimicrobial activity of the free ligands and nicotinic acid-copper complexes.

Compound	Concentration (μg/mL)	Activity
Ampicillin	25	Active[a]
NA	256	Not Active
$CuCl_2$	64*	Not Active
	32*	Not Active
Ph	256	Not Active
1	256	Active[b]
	128	Active[c]
	64	Not Active
Sal	256	Active[b]
2	256	Active[b]
	128	Active[d]
	64	Not Active
Ant	256	Not Active
3	256	Active[b]
	128	Active[c]
	64	Not Active

[a] Active (100% antigrowth) against *P. aeruginosa* ATCC 15442, *S. putrefaciens* ATCC 8671, *A. xylosoxidans* ATCC 2706, *S. aureus* ATCC 25923, *S. epidermidis* ATCC 12228, *E. faecalis* ATCC 29212, *B. subtilis* ATCC 6633, *S. cereviseae* ATCC 2601, *S. pyrogenes* II, *S. enteritidis* type C, *P. shigelloides*, *L. monocytogenes*. Active against *B. subtilis* ATCC 6633 with [b] 100%, [c] 50%, [d] 25% antimicrobial activity. * $CuCl_2$ was tested against *B. subtilis* ATCC 6633.

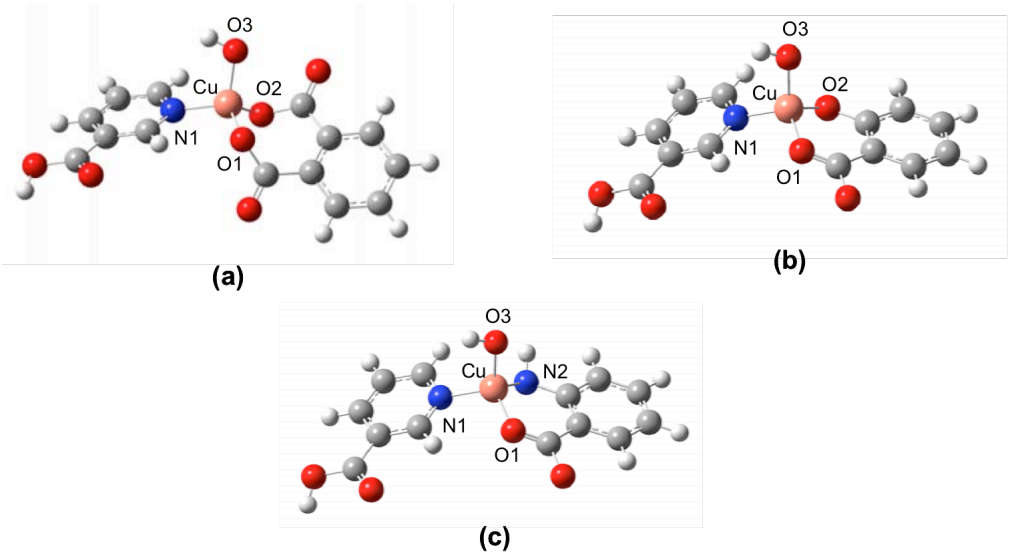

Figure 4.1. Molecular structures of copper coordination complexes **1** (a), **2** (b) and **3** (c).

Table 4.6. Theoretical parameters of the copper complexes.

Complex	$TE_{Cu(II)}$[a] (hartree)	$TE_{Cu(I)}$[b] (hartree)	EA* (kcal/mol)
1	-1316.673	-1316.873	-125.502
2	-1203.223	-1203.445	-139.283
3	-1183.292	-1183.631	-212.679

[a] Total energy of the Cu(II) coordination complexes

[b] Total energy of Cu(I) coordination complexes

* EA was calculated according to equation.

Table 4.7. HOMO and LUMO energies of the free ligands and copper complexes.

Compound	HOMO (eV)	LUMO (eV)
Ph	-7.644	-2.252
Sal	-6.729	-1.749
Ant	-5.818	-1.553
1	-7.302	-4.898
2	-6.293	-4.595
3	-5.829	-4.086

Table 4.8. Selected bond distances (Å) and angle (°) of complexes **1-3**.

Complex	Bond Lengths (Å)		Angles (°)	
1	Cu-N1	2.035	N1-Cu-O1	111.475
	Cu-O1	1.872	N1-Cu-O2	111.235
	Cu-O2	1.870	N1-Cu-O3	107.711
	Cu-O3	1.829	O1-Cu-O2	105.661
			O1-Cu-O3	110.275
			O2-Cu-O3	110.513
2	Cu-N1	2.035	N(1)-Cu-O1	109.012
	Cu-O1	1.838	N(1)-Cu-O2	111.596
	Cu-O2	1.857	N(1)-Cu-O3	109.467
	Cu-O3	1.836	O(1)-Cu-O2	107.727
			O(1)-Cu-O3	109.929
			O(2)-Cu-O3	109.355
3	Cu-N1	2.016	N1-Cu-O1	109.926
	Cu-N2	1.809	N1-Cu-O2	109.365
	Cu-O1	1.830	N1-Cu-N2	110.023
	Cu-O2	1.835	N2-Cu-O2	109.091
			N2-Cu-O1	108.241
			O1-Cu-O2	109.581

CHAPTER V
COPPER COMPLEXES OF PYRIDINE DERIVATIVES WITH SUPEROXIDE SCAVENGING AND ANTIMICROBIAL ACTIVITIES

5.1 Abstract

Superoxide anions are reactive oxygen species that can attack biomolecules such as DNA, lipids and proteins to cause many serious diseases. This study reports the synthesis of copper complexes of nicotinic acid with related pyridine derivatives. The copper complexes were shown to possess superoxide dismutase (SOD) and antimicrobial activities. The copper complexes exerted SOD activity in range of 49.07-130.23 μM. Particularly, copper complex of nicotinic acid with 2-hydroxypyridine was the most potent SOD mimic with an IC_{50} of 49.07 μM. In addition, the complexes exhibited antimicrobial activity against *Bacillus subtilis* ATCC 6633 and *Candida albicans* ATCC 90028 with MIC range of 128-256 μg/mL. The SOD activities were well correlated with the theoretical parameters as calculated by density functional theory at the B3LYP/LANL2DZ level of theory. Interestingly, the SOD activity of the copper complexes was demonstrated to be inversely correlated with the electron affinity, but was well correlated with both HOMO and LUMO energies. The vitamin–metal complexes described in this report are great examples of the value-added benefits of vitamins for medicinal applications.

5.2 Introduction

Free radicals such as superoxide anions ($O_2^{\bullet -}$) are very reactive oxygen species (ROS), which are primarily produced in the human body and has been involved in many cellular processes, which causes various diseases (149). The deleterious effects of ROS are counterbalanced by antioxidant enzymes such as superoxide dismutase (SOD), catalase and glutathione peroxidase as well as by small molecular antioxidants. Under oxidative stress conditions, ROS can induce molecular and cellular damages to DNA, lipids and proteins. Such events lead to the development of many serious diseases (2, 5), e.g. cancer (150), atherosclerosis (151), asthma (152) and neurodegenerative disorders (153). SOD, in particular, is the antioxidant enzyme, which can convert superoxide anion to a less-reactive form, e.g. H_2O_2 (154). The utilization of SOD as a therapeutic agent has been reported, however there are many limitations, which hinders its application, such as its high molecular weight (155). Therefore, small molecular weight SOD mimics as afforded by transition metal complexes are more lucrative alternatives. Some examples include metalloporphyrins (32), metal–drug complexes (109) and metallopyridine complexes (156).

Pyridine derivatives possess a diverse array of bioactivities as well as playing crucial roles for physiological functions. They have been extensively used as ligands in the formation of coordination compounds as medicinal agents. The most striking one to our interest is nicotinic acid (NA) or pyridine-3-carboxylic acid, also known as vitamin B3 (niacin), which acts as an antihyperlipidemic drug and as effective HDL cholesterol raising agent for reduction of cardiovascular risks (157, 158). Complexation of NA with various metals, e.g. manganese, cobalt, nickel, copper and zinc, had previously been reported (110), where nicotinic acid–copper complex has particularly been shown to stimulate blood flow and prevent gastric congestion (111), reduce total lipids in sera hepatic tissue as well as reducing the levels of ALT, AST, ALP, GGT and oxidative markers, e.g. nitric oxide (NO) and lipid peroxidation. Such complex was also demonstrated to exhibit SOD activity for treatment of patients with hepatocellular carcinoma (112). Recently, we have reported promising SOD mimic activity for copper complexes of nicotinic-carboxylic acids (156). Such copper complexes were formed by coordination of NA *via* the ring N-

atom with bidentate carbonyl and oxy/amino groups of carboxylic acids as electron donors. Aside from NA, other interesting ligands used in this study bearing suitable N- and/or O-electron donors are bioactive pyridine derivatives and related compounds such as hydroxypyridines, aminopyridines and picolinic acid (pyridine-2-carboxylic acid). Picolinic acid, an isomeric form of NA, is a metabolite derived from tryptophan of humans and animals. The picolinic acid plays an important role in zinc transport (159, 160). Its complexes have been demonstrated to possess antiviral (161), antifungal (162) and antibacterial (163) activities as well as being involved in the induction of apoptosis (164) and immune responses (165).2-Hydroxypyridines (2-pyridone) have been reported to form complex with metals (166). The complex of hydroxypyridine bases, such as 2-, 3- and 4-hydroxypyridines, with platinum or palladium was shown to possess promising anticancer activity against human ovarian cancer cells (167-169). Moreover, 4-aminopyridines and their derivatives were reported to be involved in the inactivation of voltage-dependent K^+ channels (170, 171) as well as implicated in reversing anesthesia and relaxing muscles (172, 173). The copper ion is an essential element, which possesses interesting anti-inflammatory and anti-ulcer activities (174). As a metal cofactor in the copper–zinc superoxide dismutase, copper exerts important catalytic function in the dismutation of superoxide anions (121, 122). It is known that copper deficiency is responsible for hematological disorders, hypopigmentation, defective connective tissue cross-linking and ataxia (123, 124).

The aforementioned statements have motivated us, as part of a continuous study, to synthesize low molecular weight copper complexes of biologically important pyridines as SOD mimics. The nicotinic acid was used as a primary ligand for such synthesis. Therefore, novel copper complexes of nicotinic acid with 2-substituted pyridines containing bidentate N, O and/or N, N electron donors were synthesized as SOD mimic activity. The 2-substituted pyridines are 2-hydroxypyridine, 2-aminopyridine and pyridine-2-carboxylic acid. To give insight into the cardinal mechanisms of SOD activities, quantum chemical parameters calculated at density functional theory (DFT) level were used as physicochemical description of the compounds. DFT has wide applications in the life sciences particularly in the development of quantitative structure–activity/property relationship (QSAR/QSPR)

models, for the elucidation of enzymatic reactions as well as in clarification of the superoxide radical scavenging activity. Results indicated that the calculated physicochemical parameters were well correlated with the experimental SOD activities (156). The theoretical parameters used are comprised of energies of the highest occupied molecular orbital (HOMO), energies of the lowest unoccupied molecular orbital (LUMO) and electron affinity (EA). Moreover, the antimicrobial activity of the novel complexes was also explored.

5.3 Materials and methods

5.3.1 Materials

All chemicals were of analytical reagent grade and were purchased from Sigma–Aldrich. Bovine erythrocyte superoxide dismutase was supplied from the same source. Melting points of the complexes were determined on the Griffin capillary melting point apparatus and are reported without correction. Infrared (IR) spectra were obtained on Perkin Elmer System 2000 FTIR as a potassium bromide (KBr) pellet. Magnetic moment was performed by Magnetic Susceptibility Balance, Mark 1, Serial 15257, Sherwood Scientific, Cambridge, UK.

5.3.2 Synthesis of copper complexes of pyridine derivatives

5.3.2.1 Copper complex of nicotinic acid-2-hydroxypyridine

Nicotinic acid (NA, 0.123 g, 1 mmol) dissolved in methanol (30 mL) was heated (70°C) and stirred under reflux until the solution was clear. Cupric chloride dihydrate (0.170 g, 1 mmol) was dissolved in methanol (2 mL) and added dropwise to the prepared NA solution. After heating for 45 min, a solution of 2-hydroxypyridine (2Hy, 1 mmol, 0.138 g) in methanol (2 mL) was added drop- wise to the reaction mixture. The mixture was then heated for 1 h at the same condition. The precipitated solid was collected by filtration, washed with cold methanol and dried in vacuo over silica gel at room temperature to yield cyan powder of complex **1**, m.p. >300°C; IR (KBr, cm^{-1}): 1389 (m, C–N), 1375 (m, C–N), 1191 (w, C– O), 1093 (w, C–O), 1053 (w, C–O); μ_{eff}: 1.5545 BM.

5.3.2.2 Copper complex of nicotinic acid-2-aminopyridine

Complex **2** was prepared in the same method as complex **1** using NA (0.123 g, 1 mmol), cupric chloride (0.170 g, 1 mmol) and 1 mmol (0.137 g) of 2-aminopyridine (2Am). As aquamarine powder, product **2** was obtained by filtration, washed with cold methanol and dried over silica gel, m.p. >300°C; IR (KBr, cm^{-1}): 1386 (s, C–N), 1375 (s, C–N), 1191 (s, C–O), 1155 (w, C–O), 1093 (m, C–O), 1050 (m, C–O); μ_{eff}: 1.9381 BM.

5.3.2.3 Copper complex of nicotinic acid–picolinic acid

Copper complex of the nicotinic–picolinic acids (**3**) was prepared in an analogous fashion using 1 mmol of NA, cupric chloride and picolinic acid (Pi; 1 mmol, 0.166 g). The precipitated complex was obtained as blue powder after filtration, washing with cold meth- anol and dried over silica gel. m.p. >300°C; IR (KBr, cm^{-1}): 1475 (w, O–H), 1348 (vs, C–N), 1286 (s, C–O), 1152 (w, C–O), 1049 (s, C–O); μ_{eff}: 1.7014 BM.

5.3.3 Determination of superoxide dismutase activity

The complexes were tested for SOD activity using the previously described method (109, 175). The SOD activity of copper complexes was assayed in the pH range of 6.9-7.4 by measuring the inhibition of the photoreduction of nitro blue tetrazolium (NBT). This indirect assay is comprised of several reactions: the photochemically excited riboflavin was first reduced by methionine into a semiquinone, which donated an electron to oxygen to form a superoxide source. The superoxide readily converted NBT into a purple formazan product, being spectrophotometrically detected at 550 nm. In this regard, the SOD activity was inversely related to the amount of formazan formed and expressed in terms of 50% inhibition concentration (IC_{50}) of NBT reduction.

5.3.4 Antimicrobial activity

The antimicrobial activity of the complexes was investigated against representative microorganisms using the method previously reported (129, 175). Briefly, the tested complexes dissolved in dimethyl sulfoxide (DMSO) were mixed

with Müller Hinton (MH) broth to receive a final volume of 1 mL. Two-fold dilution was prepared and the MH broth of the tested sample then was transferred to MH agar solution to yield the final concentrations ranging from 64 to 256 μg/mL. The solutions were placed onto the plates. Twenty-seven strains of microorganisms (Table 5.1), cultured in the MH broth at 37°C for 24 h, were diluted with 0.9% normal saline solution to $3x10^8$ cells/mL. The organisms were inoculated onto each plate and incubated at 37°C for 18-48 h. The complexes found to be effective against the tested strains were selected. The inhibition of microbial cell growth was determined.

5.3.5 Molecular model of superoxide dismutase mimics

The copper complexes were drawn with GaussView 3.09 (130) and calculated by Gaussian 03 (135). Fullyoptimized geometry without symmetry constraints of the copper complexes was performed in vacuo using density functional theory (DFT) at B3LYP/ LANL2DZ level (141).

5.4 Results and discussions

Copper-based pyridine complexes **1**–**3** were synthesized by the reaction of cupric chloride with nicotinic acid and pyridine derivatives (2-hydroxypyridine, 2-aminopyridine and picolinic acid) in a molar ratio of 1:1:1. The complexes were obtained in good yields (75-87%) as cyan, aquamarine and blue powder, respectively. They are highly polar compounds, insoluble in methanol and water, but soluble in DMSO. Their melting points and magnetic moment are shown in Table 5.2. IR spectral data are outlined in Table 5.3.

5.4.1 Infrared spectra

From the IR spectral data, it can be seen that the C–N stretching vibration of complex **1** showed at 1389 and 1375 cm^{-1} whereas the C–N absorption of free NA and free 2Hy appeared at 1324 and 1243 cm^{-1}, respectively. It was observed that the hydroxyl absorption of NA at 1418 cm^{-1} δ(O–H) disappeared. In addition, strong absorptions at 1575 and 781 cm^{-1} δ(N–H) for 2Hy were not observed. The C–O stretching vibration of complex **1** displayed weak bands at 1191, 1093 and 1053 cm^{-1},

whereas the C–O absorptions of free NA appeared at 1299 cm^{-1} and for 2Hy at 1156 and 1098 cm^{-1}. Based on the IR spectra, the carbonyl absorption of complex **1** could not be observed. It is suggested that complex **1** was formed by coordination of copper atom with the two carbonyl groups (carboxylic of NA and 2-pyridone) and the two nitrogen atoms of pyridine ring of both NA and 2Hy.

The IR spectra of complex **2** pointed out the disappearance of carbonyl absorption, while the free NA exhibited absorption at 1718 and 1700 cm^{-1}. The amino (NH_2) absorption of 2Am appeared at 3448 and 3315 cm^{-1}, while the NH absorption of **2** was shown at 3116 cm^{-1}. Strong C–N stretching vibration of complex **2** was observed at 1386 and 1375 cm^{-1}. Such C–N absorption of NA appeared at 1324 cm^{-1} and at 1492, 1442 and 1326 cm^{-1} for 2Am. The strong C–O stretching of free NA was observed at 1299 cm^{-1}, weak hydroxyl (O–H) stretching was noted at 3072–2449 cm^{-1} and strong OH bending displayed at 1418 cm^{-1}. The C–O absorption of complex **2** was observed at 1191, 1155, 1093 and 1050 cm^{-1}. As evidence by the IR spectra, complex **2** was formed by coordination of the carbonyl group and the pyridine ring nitrogen atom of NA with the amino group and nitrogen ring atom of 2Am.

Similarly, the IR spectra of complex **3** were determined by comparing with the free ligands. It can be seen that the frequency of C–O stretching vibration was presented at 1286 cm^{-1} ν(C–O), while the absorption of free NA and Pi appeared at 1299 and 1294 cm^{-1}, respectively. Furthermore, disappearances of the stretching vibration at 1718 and 1700 cm^{-1} of the carbonyl groups ν(C≡O) of both NA and Pi were observed. The weak band at 1475 cm^{-1} could be attributed to the O–H bending vibration of complex **3** when compared with the spectra of both NA and Pi, which showed strong bands at 1418 and 1454 cm^{-1}, respectively. The C–N stretching vibration of complex **3** exhibited very strong band at 1348 cm^{-1}, while the absorption of free NA and Pi showed ν(C–N) at 1324 and 1342 cm^{-1}, respectively. Hence, complex **3** was formed using carbonyl groups and nitrogen atoms of pyridine ring of NA and Pi as bidentate ligands to coordinate with copper atom.

It is observed that the copper complexes were formed by the coordination of NA as a primary bidentate ligand with 2-substituted pyridines (2Hy, 2Am and Pi). The bidentate NA used carbonyl moiety and ring nitrogen atom as electron donating group, which caused the C–N shift from 1324 cm^{-1} to higher frequency range of

1348–1389 cm^{-1}. Apparently, the carbonyl absorptions of complexes **1-3** were not observed. Likewise, the 2-substituted pyridine was coordinated to the central copper atom as bidentate ligands. In this regard N–H bending of **1** at 781 and 1575 cm^{-1} disappeared with a shift of C–O stretching from 1156 cm^{-1} to higher frequency. This suggested that the copper atom of complex **1** formed a complex by means of the bidentate amino ketone (2-pyridone). Similarly, the coordination of the copper atom from complex **2** is made possible via the amino- pyridine (2Am) ligand, which is evident by the disappearance of NH_2 stretching absorptions and the shift of C–N stretching. As for complex **3**, Pi is also a bidentate ligand, which uses the ring nitrogen atom and the carbonyl group to coordinate with the copper atom.

Magnetic susceptibility determination showed that complexes **1-3** were paramagnetic with a magnetic moment (μ_{eff}) of 1.55, 1.94 and 1.70 BM, respectively. The μ_{eff} value indicates that the complexes were of tetrahedral geometry with a copper center. Based on the IR spectra and μ_{eff}, we can confirm that complexes **1-3** were of copper tetrahedral geometry.

5.4.2 Superoxide scavenging activity

Complexes **1-3** were assayed for SOD activity using the modified approach (109, 175), which involved measuring the inhibition of NBT reduction. The results as shown in Table 5.4 revealed that all of the tested complexes exhibited SOD activity with IC_{50} in the range of 49.07–130.23 μM. Complex **1** was the most powerful superoxide scavenger with an IC_{50} value of 49.07 μM. In addition, the SOD activity of complex **2** was higher than that of complex **3** with IC_{50} values of 50.32 and 130.23 μM, respectively. The SOD activity of these complexes are shown to be in the order of **1** > **2** > **3**. It should be noted that the activity of complex **2** was comparable to that of **1** as observed from the IC_{50} values of 49.07 and 50.32 μM, respectively. Furthermore, the SOD activity of the free ligands NA, 2Hy, 2Am and Pi were elucidated and was found to be very low to the point that the IC_{50} value could not be obtained. The result strongly suggests that the copper atom is of prime importance for the SOD activity as its coordination to the ligands profoundly increased the SOD activity. Such phenomenon can be attributed to the change in oxidation state of the

copper atom upon coordination with the ligands. Fascinatingly, these copper complexes were significantly small in molecular weight than the native enzyme. Moreover, these copper coordination compounds are easily formed from bioactive molecules such as nicotinic acid.

5.4.3 Antimicrobial activities

Nicotinic acid has been widely used for hyperlipidemic treatment. The biological activities of 2-hydroxypyridine, 2-aminopyridine and picolinic acid have previously been reported (160, 168, 171). The exploration of antimicrobial activities for the complexes of nicotinic acid and its derivatives is a relatively new endeavor. Results (Table 5.5) demonstrated that complexes **1-3** could completely inhibit the growth of *Bacillus subtilis* ATCC 6633 with MIC of 256 μg/mL. In addition, the tested complexes **1-3** could partially inhibit the growth of *Candida albicans* ATCC 90028 with MIC in the range of 128-256 μg/mL. Such augmentation in the observed antimicrobial activity of the metal complexes over those of the free ligands could be attributed to the chelation effect (176). As a result, this alters the lipophilic property of the central metal ion thereby allowing its permeation through the cell membrane to exert its antimicrobial activity. In parallel with our results, previous studies have found that the free ligands used in this study, comprising of 2-hydroxypyridine (177), 2-aminopyridine (178) and picolinic acid (165), possessed antibacterial, antifungal and antiviral activities. To discern whether the observed antimicrobial activities arose from the ligand themselves or as a result of coordinating with the metal ions, the biological activities of the uncomplexed ligands were examined. Antimicrobial activities were observable only in the metal complexes and not in the uncomplexed ligands, therefore confirming the participating role of the metal ion in the biological activities.

5.4.4 Theoretical studies of SOD mimics by computational chemistry

Quantum chemical parameters of the metal complexes were calculated using the minimum energy conformers in order to deduce quantitative relationships of the theoretical descriptors with the superoxide scavenging activity by performing Density Functional Theory calculations at B3LYP/LANL2DZ level. The fully optimized structures of complexes **1**–**3** were of tetragonally distorted geometry as

demonstrated in Figure 5.1. The calculated theoretical parameters, including binding energy (BE) and electron affinity (EA), has previously been reported to be good descriptors for characterizing superoxide radical scavenging activity (138-141). It is well established that EA is a suitable parameter in accounting for the rate of electron transfer from superoxide anion to copper ion. Ji and Zhang previously reported that compounds with the lowest EA possessed the highest electron transfer rate, thereby conferring the highest SOD activity (139). The calculated results for EA as shown in Table 5.5 were in the following order **1** > **2** > **3** and their respective values are -100.40, -109.39 and -162.71 kcal/mol, respectively. The observed trend is positively correlated with the SOD activity where complex **1** had the highest SOD activity as well as the highest calculated EA. Such findings contradict with those previously reported by Branco *et al* (142, 143) where an inverse relationship was observed for the calculated EA and the SOD activity. A plausible explanation for such discrepancy can be made on the basis of differences in the coordination geometry of the copper coordination complexes used in this study (tetrahedral) and those previously reported by Ji *et al*. (square planar and square pyramidal). Such observation is further corroborated by previous studies on active site distortion of CuZnSOD (142, 143).

Examination of the energy level of HOMO revealed that complex **3** possessed the highest HOMO energy with a value of -3.32 eV while coordination compounds **2** and **1** gave HOMO energies of -4.65 and -5.09 eV, respectively (Table 5.6). Higher HOMO energy as deduced from the frontier molecular orbital indicates that the molecule can readily transfer electron to the unoccupied orbital of the metal ion thereby indicating strong binding capacity (146). Such molecules displaying high binding capacity was demonstrated to also exhibit lower SOD activity (148, 179). This coincides with our findings that complex **1** possessed the highest SOD activity as well as having the lowest HOMO energy and vice versa for complex **3** which exhibited the lowest SOD activity while having the highest HOMO energy. An analysis of the calculated energy level for the LUMO indicates the order of **3** > **2** > **1** for the coordination compounds bearing values of -2.61, -2.96 and -2.99 eV, respectively. It was previously reported by Schepetkin *et al* (179)that low LUMO energy was important for superoxide dismutation. Moreover, the calculated energies of HOMO and LUMO were significantly correlated with the SOD activity which was

represented as $\log(1/IC_{50})$, yielding *r* of 0.97 and 0.99, respectively. The results clearly suggest that the energies of HOMO and LUMO are potentially useful theoretical parameters for elucidating superoxide scavenging activity, a phenomenon involving charge- or electron-transfer.

In characterizing the physicochemical properties of the metal complexes, it is worthy to consider the tendency for nicotinic acids to dissociate a proton from the carboxylic acid moiety to form a carboxylate anion. Such notion is valid when nicotinic acids are present as free ligands. However such situation may not apply in our case since the ligand is coordinated to a metal ion. Such finding coincides with previous observation that metal coordination exerts direct effect on the ligand's acidity (180). Correspondingly, Bóka *et al*. had observed in their efforts to mimic the SOD activity that strong electron donating ability of ligands is detrimental towards SOD activity (181). The coordination complexes was shown to possess good SOD activity which implied that the coordinated nicotinic acids should be in the neutral form whereas the anionic form are expected to possess greater electron donating properties, which would consequently hinder its reactivity with superoxide anions. Similar findings were also observed in our previous investigation on mixed ligand complexes of copper with nicotinic and other selective carboxylic acids (phthalic, salicylic and anthranilic acids) (156). It was shown that the complex constituting stronger electron withdrawing group exhibited better SOD activity.

The contributions of metal–ligand binding affinity on the observed SOD activity was investigated using information such as bond lengths and angles as derived from geometrically optimized structures at B3LYP/LANL2DZ level (Table 5.7). It was observed that the mean bond distances at the axial position for Cu–N(1) and Cu–O(1) of complexes **1**–**3** were 1.801 and 2.008 Å, respectively. The longest axial distance for Cu–N(2) and Cu–O(2) bonds corresponds to that of complex **1** with 1.908 and 1.856 Å, respectively. The bond lengths for Cu–N(2) and Cu–N(3) at axial position for complex **2** were observed to be 1.834 and 1.854 Å, respectively, which was shorter than that of complex **1**. This is attributed to the fact that the amino group of 2-aminopyridine from complex **2** possessed greater electron donating capability than the hydroxyl group of 2-hydroxypyridine from complex **1** as indicated by the higher HOMO energy of **2** (Table 5.6). The shortest axial bond lengths for Cu–N(2)

and Cu–O(2) were observed in complex **3** which gave values of 1.826 and 1.822 Å, respectively. This result coincides with the fact that complex **3** possessed the lowest SOD activity, which could be attributed to the higher metal binding affinity. Previous study by Li *et al*. has reported that long axial bond lengths were critical for the dismutation of superoxide anion (147). Interestingly, complex **1**, which had the longest axial bond length was also shown to possess the highest SOD activity. The calculated bond angles for the three coordination complexes further corroborate a distorted tetragonal geometry with bond angles in the range of 73.35°–126.73°.

In summary, we report the synthesis of novel copper complexes **1-3** with nicotinic acid as the primary ligand along with 2-substituted pyridines: 2-hydroxypyridine, 2-aminopyridine and picolinic acid. The experimentally derived magnetic moments and the calculated bond angle suggest a tetragonally distorted geometry for the coordination complexes. Nicotinic acid is a bidentate ligand, which utilizes the ring N-atom of pyridine and the carbonyl group of carboxylic acid. Likewise, the 2-substituted pyridines are also bidentate ligands making use of the following functional groups: amino ketone of 2-pyridone (2Hy), aminopyridine (2Am) and carbonyl pyridine (Pi), respectively. All of the coordination compounds used in this study displayed promising superoxide radical scavenging properties as well as antimicrobial activities against *B. subtilis* ATCC 6633 and *C. albicans* ATCC 90028. Of these compounds, complex **1** displayed the greatest superoxide scavenging activity with IC_{50} of 49.07 μM, while complex **1** possessed the highest antimicrobial activity with IC_{50} of 256 μg/mL. The physicochemical parameters as derived from low energy conformer calculated at B3LYP/LANL2DZ level were well correlated with the observed superoxide scavenging properties. In particular, it has been shown that HOMO and LUMO energies are useful theoretical parameters for elucidating the superoxide scavenging activity as observed from the correlation coefficient of 0.97 and 0.99, respectively. Such coordination complexes described herein demonstrate great potential for the development of value-added metallovitamins for therapeutic applications.

Table 5.1. Microorganisms for antimicrobial assays.

Microorganism	Reference strain	Clinical isolates
Gram-positive bacteria	*Staphylococcus aureus* ATCC 29213	*Streptococcus pyrogenes* II
	Staphylococcus aureus ATCC 25923	*Bacillus cereus*
	Staphylococcus epidermidis ATCC 12228	*Listeria monocytogenes*
	Enterococcus faecalis ATCC 29212	
	Enterococcus faecalis ATCC 33186	
	Micrococcus lutens ATCC 10240	
	Bacillus subtilis ATCC 6633	
	Corynebacterium diphtheriae NCTC 10356	
Gram-negative bacteria	*Escherichia coli* ATCC 25922	*Shigella dysenteriae*
	Klebsiella pneumoniae ATCC 700603	*Salmonella enteritidis* type C
	Serratia marcescens ATCC 8100	*Morganella morganii*
	Salmonella typhimurium ATCC 13311	*Aeromonas hydrophila*
	Shewanella putrefaciens ATCC 8671	*Citrobacter freundii*
	Achromobacter xylosoxidans ATCC 2706	*Plesiomonas shigelloides*
	Pseudomonas aeruginosa ATCC 15442	
	Pseudomonas stutzeri ATCC 17587	
Yeasts	*Saccharomyces cerevisiae* ATCC 2601	
	Candida albicans ATCC 90028	

Table 5.2. Physiochemical parameters of pyridine-copper complexes and its ligands.

Compound	Chemical formulae	Formula weight (g/mol)	Color	Melting point (°C)	Yield (%)	μ_{eff} (BM)
NA	$C_6H_5NO_2$	123.11	White	236–239	–	–
2Hy	C_5H_5NO	95.10	White	105–107	–	–
1	$C_{11}H_{10}CuN_2O_4$	297.75	Cyan	>300	84	1.5545
2Am	$C_5H_6N_2$	94.11	White	54–58	–	–
2	$C_{11}H_{11}CuN_3O_3$	279.76	Aquamarine	>300	87	1.9381
Pi	$C_6H_5NO_2$	123.11	White	139–142	–	–
3	$C_{12}H_{10}CuN_2O_4$	309.76	Blue	>300	75	1.7014

μ_{eff} Magnetic moment; B.M., Bohr magnetron.

Table 5.3. IR spectra of pyridine-copper complexes and its ligands.

Cpd	νC=O	νC-O	νC-N	νO-H	δO-H	νN-H	δN-H
NA	1718(s), 1700(s)	1299(s)	1324(s)	3072-2449(w)	1418(s)	-	-
2Hy	1690(s), 1652(vs)	1156(s), 1098(m)	1243(s)	-	-	-	1575(br, s), 781(vs)
1	-	1191(w), 1093(w), 1053(w)	1389)m), 1375(m)	3400(br, w)	1458(m)	-	-
2Am	-	-	1492(s), 1442(s), 1326(m)	-	-	3448(sh, s), 3315(sh, w)	772.84(s)
2	-	1191(s), 1155(w), 1093(m), 1050(m)	1386(s), 1375(s)	2609(br, w)	1426(m)	3116(sh, w)	760.72(s)
Pi	1718(w), 1700(w)	1294(s), 1165(w), 1086(w)	1342(m)	2362(m), 2341(m)	1454(s)	-	-
3	-	1286(s), 1152(w), 1049(s)	1348(vs)	3400(br, w)	1475(w)	-	-

Note: vs = very strong, s = strong, m = medium, w = weak, br = broad, sh = shape.

Table 5.4. Superoxide dismutase activity of copper complexes.

Compound[c]	IC_{50} (μM)[a]
1	49.07
2	50.32
3	130.23
SOD[b]	0.0026

[a] IC_{50} was defined as fifty percent inhibition concentration of NBT reduction.

[b] Superoxide dismutase derived from bovine erythrocytes was a homodimeric protein.

[c] Substituted pyridines (ligands) mimic very low activity that the IC_{50} cannot be obtained.

Table 5.5. Antimicrobial activity of pyridine-copper complexes.

Compound	Concentration (μg/mL)	Activity
Ampicillin	25	Active[a]
NA	256	Not active
$CuCl_2$	64	Not active[h]
	32	Not active[h]
2Hy	256	Not active
1	256	Active[b,e]
	128	Active[c, f]
	64	Not active
2Am	256	Not active
2	256	Active[b, f]
	128	Active[d, g]
	64	Not active
Pi	256	Not active
3	256	Active[b, f]
	128	Active[d, g]
	64	Not active

[a] Active (100% antigrowth) against *P. aeruginosa* ATCC 15442, *S. putrefaciens* ATCC 8671, *A. xylosoxidans* ATCC 2706, *S. aureus* ATCC 25923, *S. epidermidis* ATCC 12228, *E. faecalis* ATCC 29212, *B. subtilis* ATCC 6633, *S. cerevisiae* ATCC 2601, *S. pyrogenes* II, *S. enteridis* type C, *P. shigelloides*, *L. monocytogenes*.

[b] Active against *B. subtilis* ATCC 6633 with 100% antimicrobial activity.

[c] Active against *B. subtilis* ATCC 6633 with 75% antimicrobial activity.

[d] Active against *B. subtilis* ATCC 6633 with 50% antimicrobial activity.

[e] Active against *C. albicans* ATCC 90028 with 75% antimicrobial activity.

[f] Active against *C. albicans* ATCC 90028 with 50% antimicrobial activity.

[g] Active against *C. albicans* ATCC 90028 with 25% antimicrobial activity.

[h] $CuCl_2$ was tested against *B. subtilis* ATCC 6633 and *C. albicans* ATCC 90028.

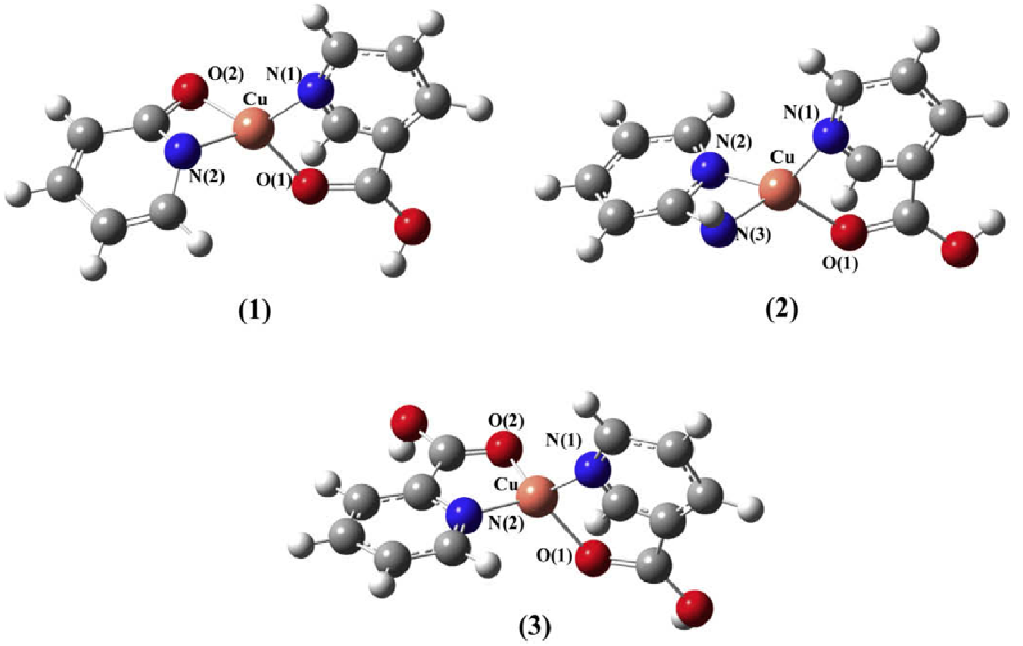

Figure 5.1. Geometrically optimized structures of complexes **1-3** calculated at B3LYP/LANL2DZ level.

Table 5.6. Quantum chemical parameters of copper complexes calculated at B3LYP/LANL2DZ level.

Complex	TE_{CuII} (hartree)	TE_{CuI} (hartree)	EA[a] (kcal/mol)	HOMO (eV)	LUMO (eV)
1	−955.7254	−955.8854	−100.40	−5.09	−2.99
2	−935.8071	−935.9814	−109.39	−4.65	−2.96
3	−1069.5318	−1069.7911	−162.71	−3.32	−2.61

[a] $EA = TE_{Cu(I)} - TE_{Cu(II)}$.

Table 5.7. Selected bond lengths and angles of complexes **1**-**3**.

Complex	Bond length (Å)		Angle (°)	
1	Cu–N(1)	1.8013	N(1)–Cu–N(2)	124.420
	Cu–O(1)	2.0100	N(1)–Cu–O(1)	90.624
	Cu–N(2)	1.9076	N(1)–Cu–O(2)	124.119
	Cu–O(2)	1.8561	N(2)–Cu–O(1)	123.331
			N(2)–Cu–O(2)	74.389
			O(1)–Cu–O(2)	124.407
2	Cu–N(1)	1.8014	N(1)–Cu–N(2)	124.390
	Cu–O(1)	2.0105	N(1)–Cu–N(3)	126.729
	Cu–N(2)	1.8336	N(1)–Cu–O(1)	89.214
	Cu–N(3)	1.8542	N(2)–Cu–N(3)	73.359
			N(2)–Cu–O(1)	125.380
			N(3)–Cu–O(1)	122.785
3	Cu–N(1)	1.7990	N(1)–Cu–N(2)	116.156
	Cu–O(1)	2.0031	N(1)–Cu–O(1)	92.119
	Cu–N(2)	1.8255	N(1)–Cu–O(2)	122.541
	Cu–O(2)	1.8221	N(2)–Cu–O(1)	122.623
			N(2)–Cu–O(2)	91.883
			O(1)–Cu–O(2)	114.330

CHAPTER VI
SYNTHESIS AND THEORETICAL STUDY OF MOLECULARLY IMPRINTED NANOSPHERES FOR RECOGNITION OF TOCOPHEROLS

6.1 Abstract

Molecular imprinting is a technology that facilitates the production of artificial receptors toward compounds of interest. The molecularly imprinted polymers act as artificial antibodies, artificial receptors, or artificial enzymes with the added benefit over their biological counterparts of being highly durable. In this study, we prepared molecularly imprinted polymers for the purpose of binding specifically to tocopherol (vitamin E) and its derivative, tocopherol acetate. Binding of the imprinted polymers to the template was found to be two times greater than that of the control, non-imprinted polymers, when using only 10 mg of polymers. Optimization of the rebinding solvent indicated that ethanol-water at a molar ratio of 6:4 (v/v) was the best solvent system as it enhanced the rebinding performance of the imprinted polymers toward both tocopherol and tocopherol acetate with a binding capacity of approximately 2 mg/g of polymer. Furthermore, imprinted nanospheres against tocopherol was successfully prepared by precipitation polymerization with ethanol-water at a molar ratio of 8:2 (v/v) as the optimal rebinding solvent. Computer simulation was also performed to provide mechanistic insights on the binding mode of template-monomer complexes. Such polymers show high potential for industrial and medical applications, particularly for selective separation of tocopherol and derivatives.

6.2 Introduction

Reactive oxygen species are produced during normal aerobic metabolism and are eliminated by antioxidative enzymes and compounds. Perturbation to this equilibrium triggers a condition known as oxidative stress that has been associated with a wide range of diseases. Vitamin E, commonly known as α-tocopherol (TP), has attracted much interest in recent years due to its multifaceted therapeutic potential. Many reports have suggested that supplementation with vitamin E may help reduce the risk of cardiovascular diseases (182), cancer (183) and neurodegenerative diseases such as Alzheimer's disease. Mechanistically, tocopherol functions in vivo as a potent peroxyl radical scavenger which displays an ability to competitively bind to peroxyl radical a thousand-fold greater than that of polyunsaturated fatty acids (184) by donating its electrons to stabilize the radicals.

Tocopherol is found abundantly in vegetables and fruits (185, 186). Because of its high medical importance, it is desirable to develop ways to rapidly and accurately assess the concentrations of vitamin E in foodstuffs. The gold standard approach for determination of vitamin E relies on chromatographic methods such as high performance liquid chromatography, supercritical fluid chromatography, capillary gas chromatography and thin layer chromatography. The drawback of such approaches is that they are labor-intensive and require tedious sample pre-treatment such as saponification (187), transesterification (188), distillation, solvent extraction, membrane separation (189), crystallization and supercritical CO_2 extraction (190).

Molecular imprinting is a simple technique for preparing tailor-made affinity adsorbents possessing specific binding sites within polymer matrices (75). The molecular imprinting process, as shown in Figure 6.1, essentially involves three main steps: (i) self-assembly of template and functional monomer molecules, (ii) polymerization of template-monomer complex with cross-linking monomers and (iii) template removal to unveil binding cavity that is specific to the imprint molecule.

The molecularly imprinted polymers (MIPs) have been demonstrated to possess excellent properties for separation of many interesting compounds, ranging from small molecules to macromolecules (191-193). Moreover, MIPs can bind specifically to their original and related templates and possess tolerance to mechanical stress, temperature, pH, acid-base, etc. Owing to their robust properties, MIPs are

suitable for broad range of applications as separation media for chromatography (194) and solid phase extraction (195), nanoreactors for combinatorial synthesis of novel enzyme inhibitors (196), recognition elements for biosensors (193, 197), artificial receptors for drug assays (198), synthetic receptors for peptides (199) and biological molecules (200, 201), biological receptor mimics (202), drug delivery (203) and enzyme mimetics (204-206).

In this study, we explore the utilization of MIPs as recognition unit for tocopherol and its derivative tocopherol acetate (TPA) using methacrylic acid as functional monomer, dicholoromethane and acetonitrile as porogenic solvents. The first part of the study focused on improving upon the binding performance of bulk polymers prepared by thermal polymerization. The second portion of the study discusses for the first time the preparation of nanospheres molecularly imprinted toward tocopherols via precipitation polymerization. Molecular modeling was then used to analyze and discern the relative strength of molecular interaction between the template molecules and functional monomers. The produced polymers exhibited good prospects for future application as robust separation matrices for the purification of tocopherols and derivatives.

6.3 Materials and methods

6.3.1 Materials

Tocopherol (TP) and tocopherol acetate (TPA), methacrylic acid (MAA), ethylene glycol dimethacrylate (EDMA), 2,2'-azoisobutyronitrile (AIBN) were purchased from Sigma-Aldrich. Dicholoromethane (DCM) and acetonitrile was purchased from Merck. All solvents were of analytical or HPLC grade.

6.3.2 Preparation of molecularly imprinted polymers

Molecularly imprinted polymers were prepared in DCM using TP or TPA as template molecule and MAA as functional monomer. TP or TPA (0.5 mmol) was dissolved in DCM (10 mL) containing MAA (8 mmol). To the solution was then added the crosslinker, EDMA (50 mmol) and the initiator, AIBN (202 mg). The obtained solution was transferred into a 20 mL screw-capped borosilicate tube and purged with argon for 10 min. The tube was then submerged in a 60°C water bath for

18 h. The solid polymer was smashed and ground with a mechanical mortar. Particles with apparent diameter of 10-25 μm were collected by repetitive sieving and sedimentation in acetone. To remove the template, methanol containing 15% acetic acid (v/v) was used for extraction. Quantitative removal of the template was ensured by monitoring the amount of template remaining in the extraction solvent by UV spectrophotometry. The non-imprinted control polymers were prepared in a similar manner as used for the corresponding imprinted polymers except for omission of the template molecule during polymerization.

6.3.3 Preparation of molecularly imprinted nanospheres

Molecularly imprinted nanosphere was prepared *via* precipitation polymerization (207) in acetonitrile using tocopherol as template molecule. The contents of template and monomer were the same as those prepared by bulk polymerization except for the use of excess solvent which was increased by 20-fold. The template molecules were directly removed from the produced nanospheres by Soxhlet extraction using methanol containing 15% acetic acid (v/v). The non-imprinted control nanospheres were prepared in the same way as that of the corresponding imprinted nanospheres, except for the omission of the template molecule during polymerization.

6.3.4 Scanning Electron Microscopy (SEM)

The particle sizes of the imprinted and non-imprinted nanospheres were determined by scanning electron microscope (HITACHI S-3400). Briefly, the nanospheres were mounted on metallic studs *via* double sided conductive tape and subsequently applied gold ion coating using sputter coater (Baltec SCD 050) for 90 s under vacuum at current intensity of 60 mA and scanning accelerating voltage of 15 kV.

6.3.5 Binding analysis

Binding analysis was carried out by incubating varying amounts of polymer in 1 mL volume of analyte solution (0.1 mg/mL) on a rocking table for 12 h at room temperature. After incubation, the samples were centrifuged at 12,000 rpm for

10 min, from which 0.75 mL supernatant was collected for determination of the free analyte by spectrophotometry at wavelengths of 292 and 283 nm for TP and TPA, respectively.

6.3.6 Molecular modeling analysis

The molecular models of the template molecules, functional monomer and their complexations were drawn using GaussView, version 3.09 and subjected to full geometry optimization without symmetry constraints under Gaussian 03W at the Hartree-Fock level of theory in combination with the 3-21g(d) basis set. The possible modes of interaction between template molecules and functional monomers at molar ratio of 1:1 were sampled by manually docking the functional monomer to each functional group of the template molecule in a systematic manner. The interaction energy of the template-monomer complex as derived at the B3LYP/6-31g(d) level was calculated according to the following equation:

$$\Delta E = \left| E_{template-monomer} - E_{template} - E_{monomer} \right|$$

where ΔE represents the interaction energy, $E_{template-monomer}$ represents the energy of template-monomer complex, $E_{template}$ represents the energy of template molecule and $E_{monomer}$ is the energy of functional monomer molecule.

6.4 Results and discussions

6.4.1 Preparation of tocopherol-imprinted polymers

The first report of TP-imprinted polymers utilized the traditional bulk polymerization method, which had yielded imprinted polymers with rather high non-specificity when compared to the non-imprinted polymers (208). In light of this, a series of works have been published on the molecular imprinting of TP in efforts to enhance its binding performance. Such approaches utilize supramolecules such as calixarenes as functional monomer (209) or by the semi-covalent approach where the functional monomers are covalently linked to the template molecule in the pre-polymerization step subsequently followed by base hydrolysis to remove the

template molecule (210). Novel applications of MIPs as drug delivering materials have also been demonstrated by Puoci and co-workers (211). This study reports the preparation of TP-imprinted polymers using higher cross-linking density and more polar porogenic solvent via thermal-induced bulk polymerization method as well as the preparation of TP-imprinted nanospheres via precipitation polymerization. The pre-polymerization mixture was prepared using methacrylic acid as functional monomer and ethylene glycol dimethacrylate as cross-linking monomer. These components were solubilized in dichloromethane and acetonitrile for preparation of monolithic bulk polymers and nanospheres, respectively. The molecular structures of the imprint molecules and functional monomer are shown in Figure 6.2 as ball-and-stick model.

6.4.2 Recognition properties of tocopherol-imprinted polymers

Preliminary rebinding analysis was performed in the porogenic solvent dichloromethane in which the polymer was formed. It was observed (data not shown) that the solvent could not provide distinctive differences in the binding performance of imprinted and non-imprinted polymer. This is in agreement with the previous report that the solvent used for polymerization did not afford good rebinding performance (208). Owing to the amphipathic properties of tocopherol in that it is comprised of both hydrophobic and hydrophilic moieties, the desired rebinding solvent should be able to solubilize the tocopherols, while at the same time minimize interaction with the polar aqueous solution which competes with the functional monomers in binding to the template molecules. To meet such requirements, the selected solvents used for rebinding are binary mixtures of ethanol with water at a molar ratio of 6:4 v/v. As shown in Figure 6.3, both TP- and TPA-imprinted polymers displayed selective recognition towards the template molecules TP and TPA as compared to the respective non-imprinted polymers. It is observed that at 10 mg of polymer, both TP and TPA imprinted polymers displayed two-fold greater binding capacity towards the template than the corresponding non-imprinted polymers. The calculated binding capacity of all imprinted polymers was approximately 2 mg/g of polymer. Upon increasing the polymer concentration, both of the imprinted polymers exhibited higher binding capacities with high non-specific binding afforded by the TP imprinted polymers. On

the other hand, the non-imprinted polymers displayed quite low non-specificity towards the template molecule. The better selectivity afforded by the TPA imprinted polymer can be ascribed to the differences in the binding capacity between imprinted and non-imprinted polymers which were significantly greater for TPA imprinted polymer. Possible explanation for such observation can be attributed to the fact that TPA can act as only a hydrogen bond acceptor whereas the dual properties of TP allows it to act as both hydrogen bond donor and acceptor, which therefore predisposes it to higher non-specific binding with the non-imprinted polymers.

In this study, the monolithic polymers were prepared by thermal-induced polymerization which was similar to the initial efforts of Puoci *et al* (208). The bulk polymers developed herein had the following notable differences with the previous report: higher cross-linking density and more polar porogenic solvent. Comparison in the binding performance of the polymers prepared in this study and that reported previously, has an imprinting effect of 2 for the former, while for the latter no imprinting effect was observed for thermal-induced polymerization and imprinting effect of 1.47 was observed for photo-induced polymerization of the imprinted polymers in relation to the non-imprinted polymers as demonstrated in this paper. Discrepancies in the binding performances of the MIPs reported in this study and that previously reported could be attributed to differences in the degree of cross-linking density as the molar ratio of template:monomer:cross-linker used in this study was 0.5:8:50 whereas the previously reported ratio was in the range of 1:8:25 to 1:16:25. Such variation in the cross-linking density may give rise to different degree of rigidity of the polymers suggesting that polymers with more rigidity would exert better binding performance. Another possible explanation for the higher imprinting effect of polymers described in this paper may also be attributed to differences in the chemical properties of the porogenic solvents used in this study and that previously reported. In this regard, the polymers described herein were prepared in dichloromethane (dielectric constant of 8.93) while those previous reported were made in chloroform (dielectric constant of 4.8069). On the basis of the dielectric constant, dichloromethane is clearly a more polar solvent than chloroform, which is also more favorable for subsequent rebinding in the polar binary mixture of ethanol (dielectric constant of 25.3) and water (dielectric constant of 80.1). An added benefit of the use of more polar

porogenic solvent is that it helps reduce the polarity gap of solvent used for polymer preparation and solvent used for rebinding experiments. Such reduction in the polarity gap helps reduce the degree of polymer swelling, which may perturb the binding cavity and adversely affect the binding performance.

To determine the cross-selectivity of the prepared polymers, both imprinted polymers were cross-bound with the two template molecules using 40 mg of polymer that was incubated in 1 mL of each template (50 $\mu g \cdot mL^{-1}$) solubilized in a solution of ethanol:water (6:4, v/v). The cross-selectivity results as represented in Figure 6.4 show that the TP imprinted polymer can bind to the TP molecules (37.2%) significantly greater than the competing TPA molecules (6.5%). However, the TPA imprinted polymer can bind to the TPA molecules (28.6%) at approximately half of the competing TP molecules (53.8%). A plausible explanation for such observation is attributed to differences in the molecular structures of TP and TPA where the former is smaller than the latter, particularly, the former has a hydroxyl moiety whereas the latter possesses a more bulky acetate ester group. Consequently, the imprinted cavity for TPA imprinted polymers would likewise be larger than that of the TP imprinted polymers, which would allow the smaller TP molecules to easily occupy the binding cavity within the macromolecular matrices of TPA imprinted polymers. On the other hand, the smaller imprinted cavity of TP imprinted polymers would not accommodate the much larger TPA molecules.

Aside from the preparation of imprinted bulk monoliths, we had also molecularly imprinted nanospheres towards tocopherol (MIN-TP) via the precipitation polymerization approach. The morphology of the molecularly imprinted nanospheres was characterized by scanning electron microscope (SEM) as shown in Figure 6.5 to be uniform in size and shape. The nanospheres were spherical and the particle size was estimated to be in the range of 200-400 nm.

Rebinding analysis of the imprinted nanospheres was determined by batch mode analysis and its binding performance is indicated in Figure 6.6. Results indicated that the imprinted nanospheres were able to bind selectively to TP as observed from the imprinting effect, which can be inferred from differences in the binding capacity of imprinted and non-imprinted nanospheres in the range of 1.22-1.57-fold for polymers with concentrations of 10-80 $mg \cdot mL^{-1}$. Polymer concentrations of 40 and 80 $mg \cdot mL^{-1}$

had the highest differences at 1.51 and 1.57 fold, respectively, with binding capacity of 25.55 and 16.94 % for imprinted and non-imprinted polymers at 40 $mg \cdot mL^{-1}$ and binding capacity of 34.84 and 22.24 % at 80 $mg \cdot mL^{-1}$.

To maximize the binding capacity of the prepared nanospheres, the optimal rebinding solvent was empirically determined using binary mixtures of either acetonitrile with water or ethanol with water (212). Fixed amount (40 mg) of MIN or NIN was tested with 0.1 $mg \cdot mL^{-1}$ of TP in different types of solvent, which included acetonitrile:water (1:1, v/v), ethanol:water (8:2, v/v) and ethanol:water (6:4, v/v). The result of this solvent optimization is shown in Figure 6.7 where the appropriate solvent was identified to be ethanol:water (8:2,v/v) as it afforded the highest imprinting effect of 1.85 with a binding capacity of 39 and 21%, respectively, for imprinted and non-imprinted nanospheres.

It is observed that the binding performances of both molecularly imprinted bulk polymers and nanospheres are discretely different in that the former gave higher binding capacity. In spite of this, the imprinting effect of the nanospheres was comparable to that of the bulk polymers. Nevertheless, the potential advantages of the imprinted nanospheres far outweight its binding capacity shortcoming in the following respect when compared to bulk polymers: (i) monodisperse particles (213), (ii) precise control over the polymerization process (214), (iii) colloidal stability, (iv) larger surface area (214), (v) homogeneous binding sites (213), (vi) higher association constants (215), (vii) faster mass transfer kinetics (216) and (viii) faster binding kinetics (217). In practical terms, the monodisperse nanospheres are more suited for applications in separation as they are known to pack efficiently in chromatograhic columns by providing good flow properties, low back pressure and good column efficiency. In regards to the traditional approach of MIP preparation by bulk polymerization, the synthesized monolithic polymer possess the following undesirable properties which limit its scope of application: (i) irregular particles, (ii) limited control over the polymerization process (218), (iii) low yield and time-consuming (219), (iv) heterogeneous binding sites (215) and (v) poorly accessible binding sites. Owing to the irregularity in size and shape of the bulk polymers, the irregular particles have poor chromatography efficiency and are therefore unsuited to serve as

biorecognition elements in novel applications as MIP- based assays or MIP-based sensor arrays (214).

6.4.3 Molecular modeling of template-monomer complex

Nicholls and colleagues (220) previously pointed out in their thermodynamics study that one of the major factors governing the binding performance of MIPs lies in the relative strengths of the template-monomer complexes. Therefore, to gain mechanistic insight into the binding performance of the imprinted polymers, computer simulation was performed to discern the relative strengths of interaction between TP or TPA with MAA. The usefulness of computational approaches for elucidating and modeling the interaction strengths of MIPs had previously been demonstrated in our previous investigations (221-224) on MIP systems. These included the neural network method pioneered by our group for quantitatively correlating the structures of template molecules and functional monomers with their respective imprinting factor values (222-224), an approach which had been successfully applied for modeling a wide range of molecular systems (127, 225-228). A practical overview of this quantitative structure-property relationship paradigm is provided in a recent review (229). The methodology used herein is essentially based on theoretical calculations of the interaction energy for putative template-monomer adducts. The relative strength of a given template-monomer adduct can be inferred from calculated interaction energy whereby high interaction energy implied strong association between the template and functional monomers. Such approach has previously been demonstrated to be useful in the selection of promising functional monomers from a vast library of compounds. For this study, we utilize this computational method for retrospectively analyze and elucidate the mechanistic details and mode of interaction for the TP-MAA and TPA-MAA adducts. The interaction energy is calculated by first deriving the geometrically optimized structures at the Hartree-Fock level of theory in combination with the 3-21g(d) basis sets followed by single-point calculation at the density functional theory level using the B3LYP functional in combination with 6-31g(d) basis set.

The quantum chemical calculations were performed on possible modes of interaction for the pre-polymerization complexes. It is apparent that the template-monomer complexes can exist in various combinations of conformers, therefore simplified models of the template-monomer complexes existing at 1:1 ratio were used for the computational study. The molecular models were derived by manually docking the functional monomer to each functional group of the template molecule. A summary of the molecular properties for the sampled conformations of the template-monomer complex are provided in Table 6.1.

A total of 3 possible conformers for TP–MAA complexes were obtained from the molecular simulation as shown in Figure 6.8. As observed in Figure 6.8a, the carboxylic acid moiety of MAA could interact with the hydroxyl moiety of TP in a two point interaction, which yielded the highest interaction energy of –61.042 kJ/mol. Figure 6.8b demonstrates a one-point interaction of MAA's hydroxyl oxygen with TP's hydroxyl hydrogen, which gave significantly lower interaction energy of –27.159 kJ/mol. A third possible TP–MAA conformer is shown to utilize MAA's hydroxyl hydrogen to interact with TP's ether oxygen. Such complex gave the second highest interaction energy in this set with a value of –40.222 kJ/mol.

The possible conformations for TPA–MAA complexes are illustrated in Figure 6.9. It can be seen in Figure 6.9a that MAA can act as a hydrogen bond donor by using the hydrogen atom of the hydroxyl group to engage in one point interaction with the carbonyl oxygen of the terminal ester group with interaction energy of –51.514 kJ/mol. Figure 6.9b illustrates the interaction of MAA's hydroxyl hydrogen with TPA's ester oxygen in a one point interaction with an energy of –39.900 kJ/mol. Figure 6.9c shows the interaction of MAA's hydroxyl hydrogen with TPA's central ether oxygen with an interaction energy of –38.108 kJ/mol. It should be noted that TPA can only act as a hydrogen bond acceptor due to absence of the hydrogen atom and can therefore engage in only one point of interaction with MAA. This is unlike TP which possesses both hydrogen bond acceptor and donor and can therefore interact with MAA at two points of interaction thereby affording higher strengths of interaction.

Molecular descriptors that are commonly used for elucidating the chemical properties of molecules in terms of its stability and reactivity (144) included the

energy of the highest occupied molecular orbital (HOMO), the energy of the lowest unoccupied molecular orbital (LUMO) and the energy difference of HOMO and LUMO which is also known as the HOMO–LUMO gap. The former represents the electron-donating ability while the latter represents the electron-withdrawing ability of the molecules. Furthermore, the energy differences between the HOMO and LUMO level represent the stability and chemical reactivity of a molecule, where large values indicate high molecular stability and low chemical reactivity while small values give rise to low molecular stability and high chemical reactivity. Therefore, the HOMO-LUMO gap can be used as a relative index for the degree of interaction strength between templates and monomers in which lower values indicate higher strengths of interaction. According to this notion, the molecular interaction between the template and functional monomer (in the range of 3.826-4.911 eV for TP–MAA and 4.716-5.181 eV for TPA–MAA) caused a marked decrease in the HOMO–LUMO energy gap (as shown in Table 6.2) when compared to the free forms of the template (6.299 and 5.717 eV for TP and TPA, respectively) and functional monomer (5.728 eV for MAA). Furthermore, it is observed that TP–MAA (3.826-4.911 eV) possessed lower HOMO–LUMO gap than that of TPA–MAA (4.716-5.181 eV), which in addition to the calculated interaction energies, suggests that the molecular interaction of TP–MAA complex was higher than that of TPA–MAA.

Although the experimental results may suggest that TPA-imprinted polymer provided better imprinting effects (as observed by the difference in binding performance of imprinted and non-imprinted polymers) than that of TP-imprinted polymer. However, the former did not afford good cross-selectivity as it can cross-bind to TP at significantly higher capacity than that of the imprint molecule. On the other hand, although TP-imprinted polymers may provide lower imprinting effect than the TPA-imprinted polymers, it offsets this by maintaining stellar binding performance towards only the imprint molecule while not being able to cross-bind to TPA.

Such observations could be accounted for by the mechanistic insights provided by the computer simulations. Firstly, the lower imprinting effect of TP-imprinted polymers could be explained by the fact that TP can interact more strongly with MAAs and that TP can engage in more points of interaction in that it can

act as both hydrogen bond acceptor and donor. Following this notion, TP would also be expected to interact non-specifically with the randomly oriented MAAs in the macromolecular matrices of the non-imprinted polymers. On the other hand, as TPA can act as only a hydrogen bond acceptor it can likewise engage in a weaker interaction with the MAA which also decreased its chances of interaction with the randomly oriented MAAs of the non-imprinted polymers. Secondly, the better cross-selectivity provided by TP-imprinted polymers is due to the fact that TPA is a larger molecule which would find it difficult to transfer through the somewhat smaller and restricted cavity of the macromolecular matrices of the imprinted polymers. As a result, the TP-imprinted polymers would allow only TP to enter while restricting access to TPA as a result of the difficulty in mass transfer through the polymer. The opposite applies to the TPA-imprinted polymers where TP, which has a molecular weight of 430.706 g/mol, can easily enter the macromolecular matrices of the imprinted polymers as it is significantly smaller than the TPA molecules, which has a molecular weight of 472.743 g/mol.

In summary, we have successfully prepared molecularly imprinted polymers as bulk monoliths and nanospheres for selective recognition of tocopherol and tocopherol acetate. The mechanistic insights into the binding modes of the template-monomer complexes were elucidated from computer simulation and their results were well correlated with the experimental results. The rebinding of the prepared polymers in various concentrations of ethanol-water binary mixtures was performed to discern the optimal aqueous-based rebinding solution. The MIPs described herein has great potential for future application in separation and extraction of tocopherols from biological milieu both at the academic and industrial settings.

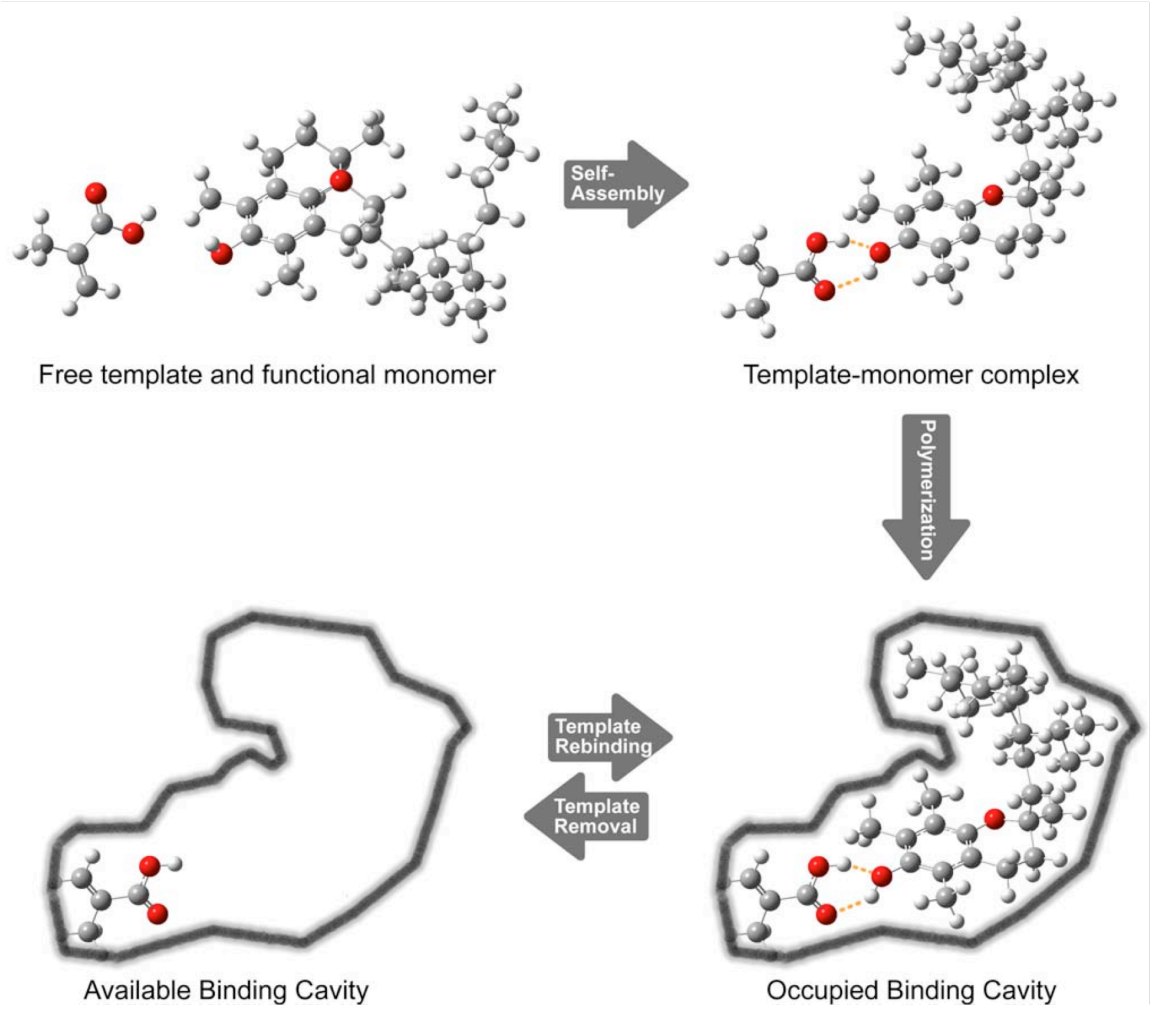

Figure 6.1. Schematic representation of the molecular imprinting process.

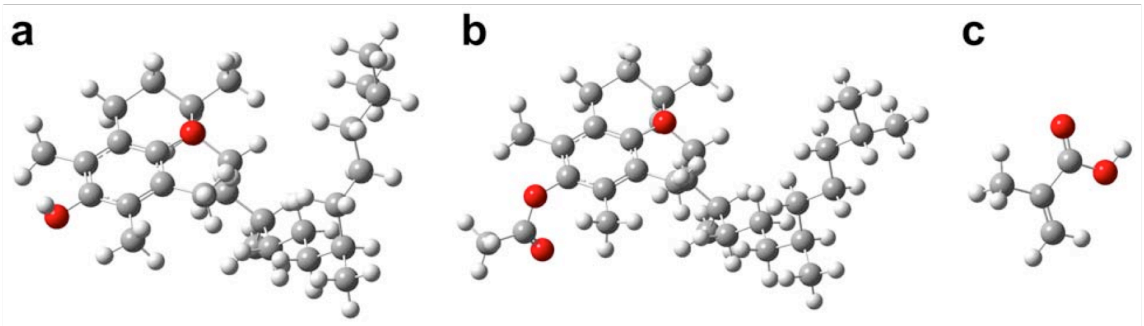

Figure 6.2. Molecular structures of tocopherol (a) and tocopherol acetate (b) and methacrylic acid (c).

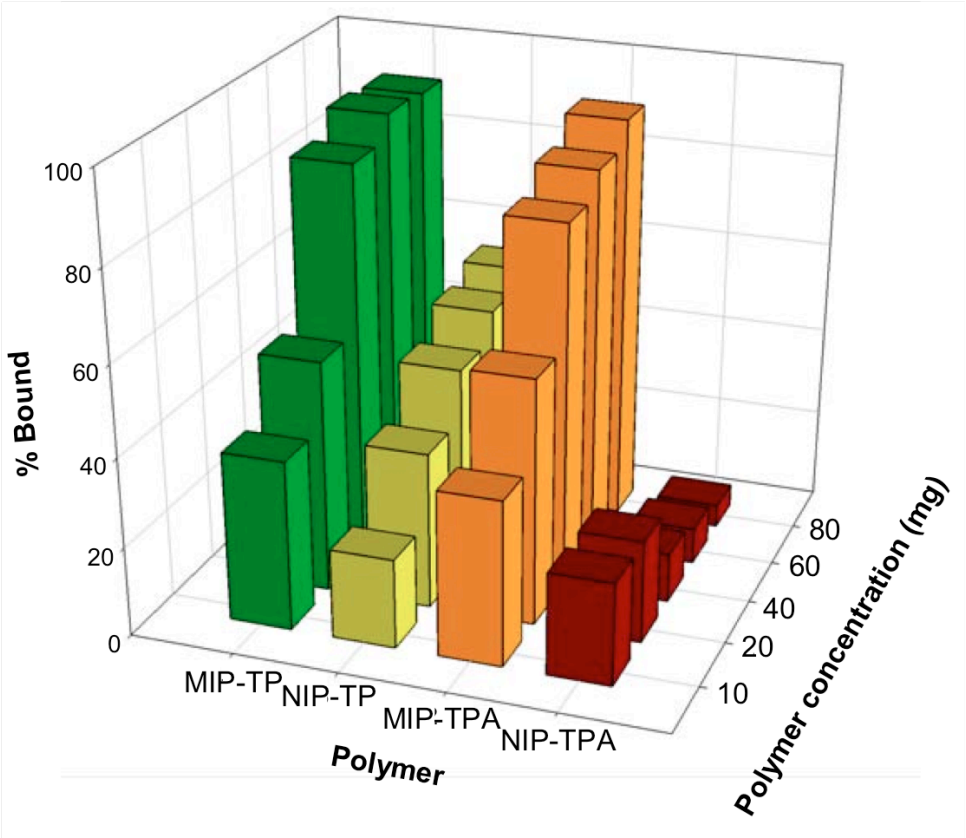

Figure 6.3. Rebinding analysis of imprinted and non-imprinted polymers towards its respective template molecule.

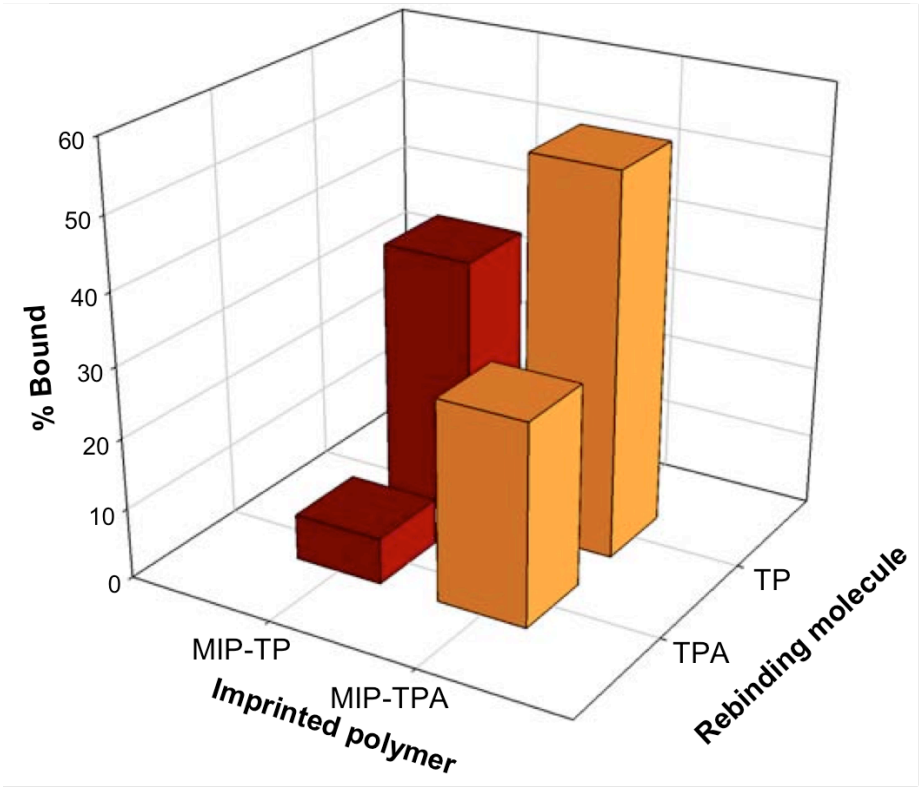

Figure 6.4 Cross-selectivity of MIP-TP and MIP-TPA with templates TP and TPA.

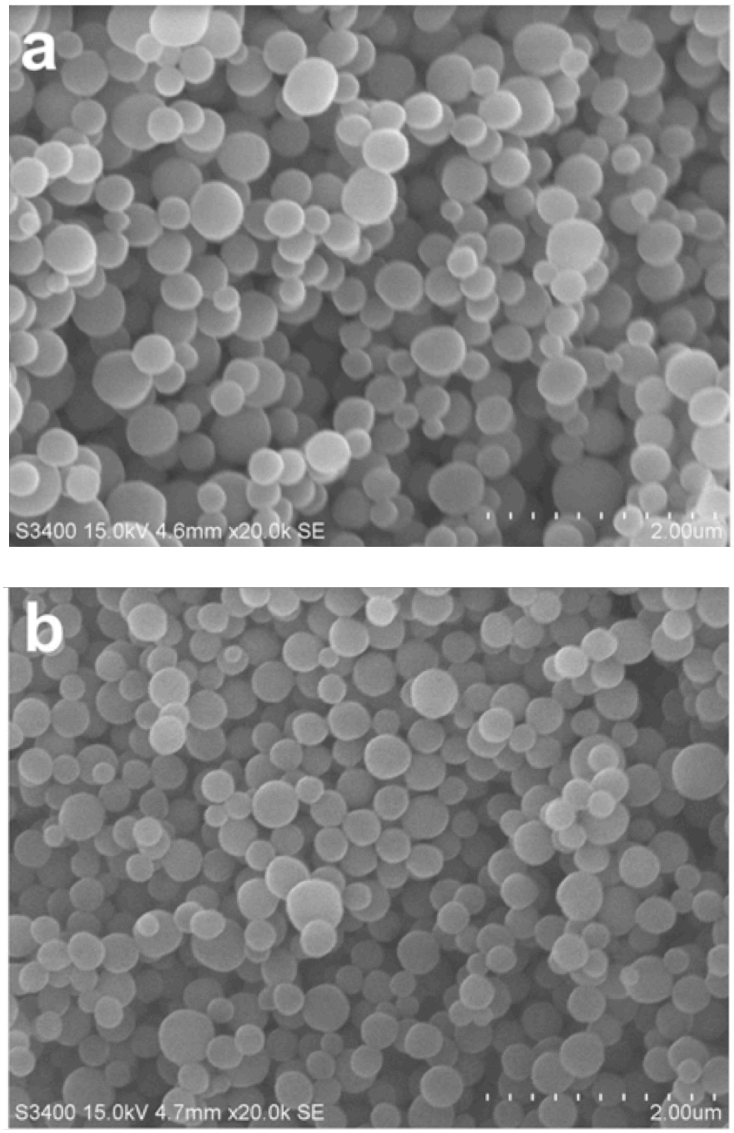

Figure 6.5. SEM micrograph of TP-imprinted nanospheres (a) and non-imprinted nanosphere (b).

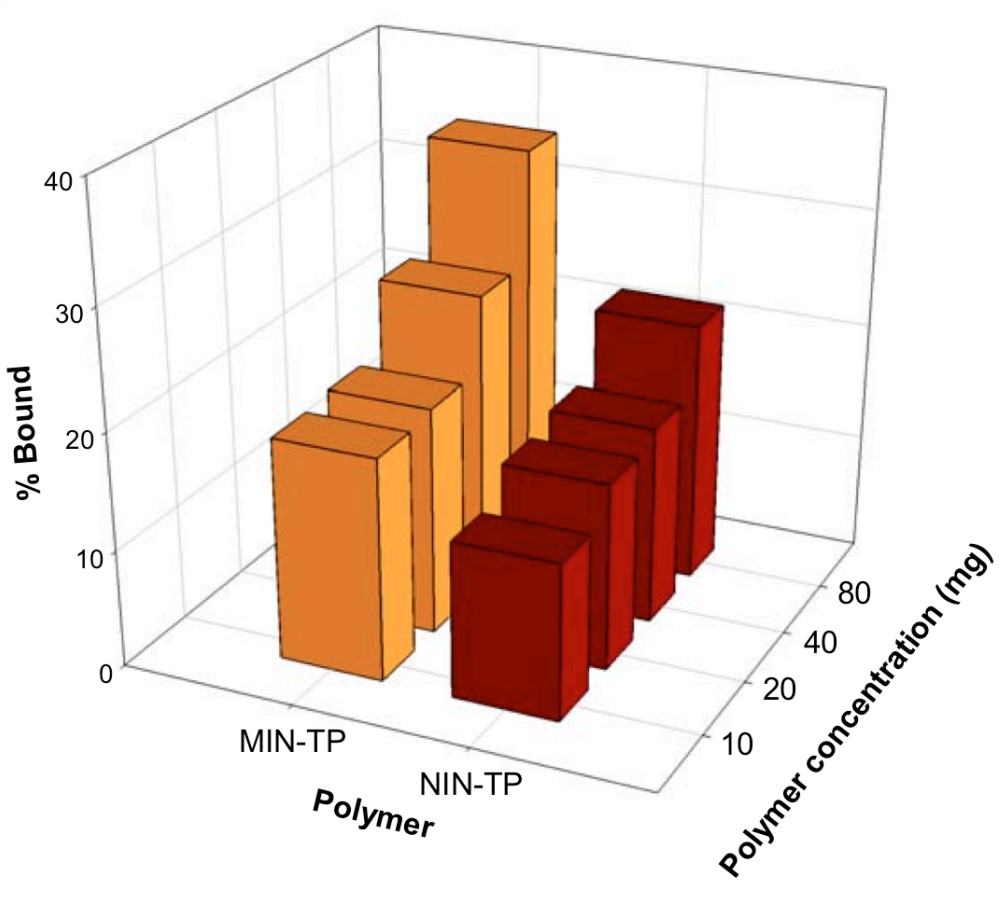

Figure 6.6. Rebinding analysis of TP-imprinted and non-imprinted nanospheres with TP.

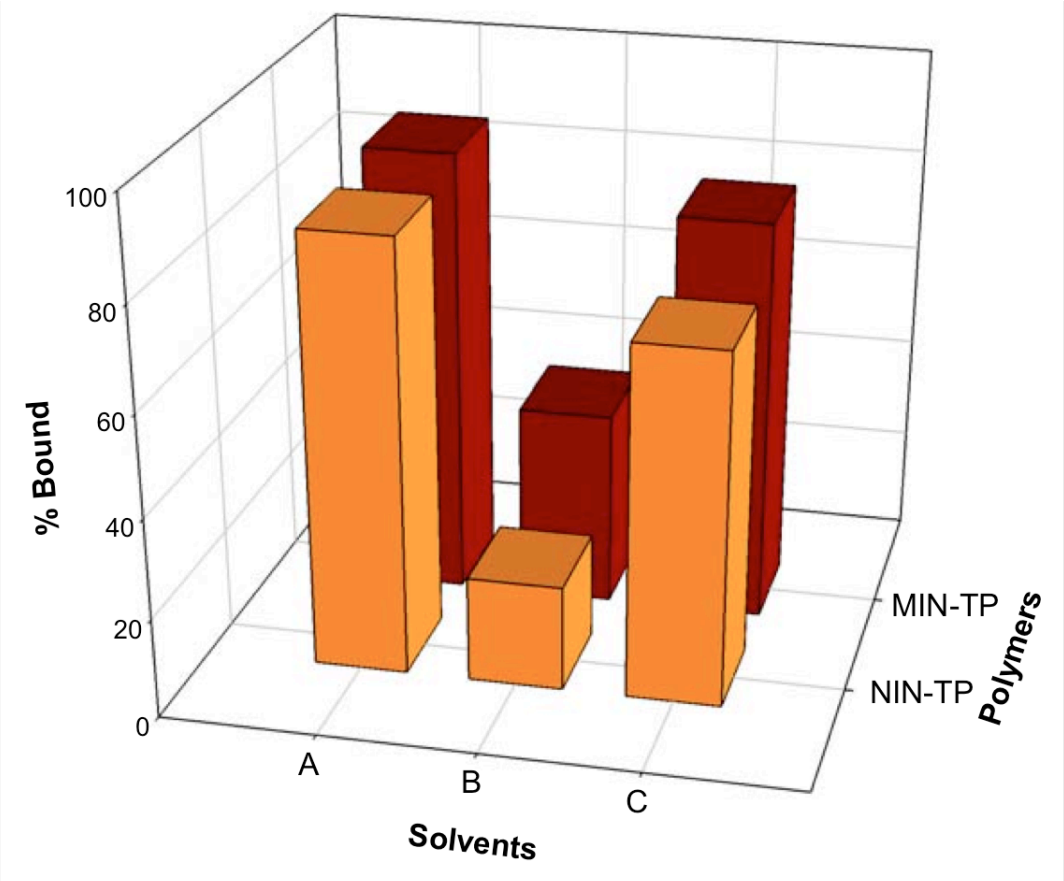

Figure 6.7. Rebinding of TP-imprinted and non-imprinted nanospheres with TP in various solvent systems: acetonitrile:water (1:1, v/v) (A), ethanol:water (8:2, v/v) (B) and ethanol:water (6:4, v/v).

Table 6.1. Summary of the interaction energies of template-monomer complexes.

	***E* (a.u.)**	**Δ*E* (a.u.)** [a]	**Δ*E* (kJ mol^{-1})** [b]
TP	–1285.682		
TPA	–1438.350		
MAA	–306.475		
TP–MAA(1)	–1592.180	–0.023	–61.042
TP–MAA(2)	–1592.167	–0.010	–27.159
TP–MAA(3)	–1592.172	–0.015	–40.222
TPA–MAA(1)	–1744.844	–0.020	–51.514
TPA–MAA(2)	–1744.840	–0.015	–39.900
TPA–MAA(3)	–1744.839	–0.015	–38.108

[a] ΔE is the interaction energy calculated from $\Delta E = E_{template\text{-}monomer} - E_{template} - E_{monomer}$

[b] ΔE is converted from a.u. to kJ·mol^{-1} using the conversion factor 2.626×10^3.

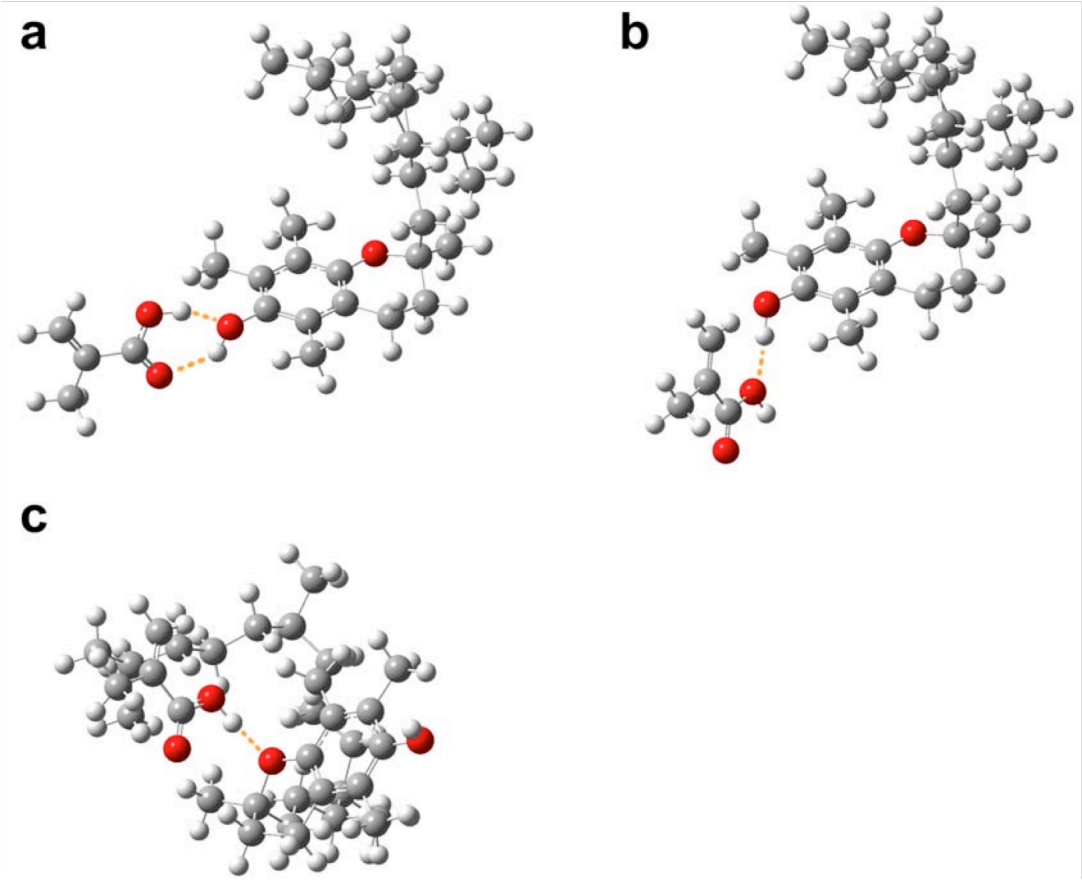

Figure 6.8. Possible modes of interaction of TP with MAA.

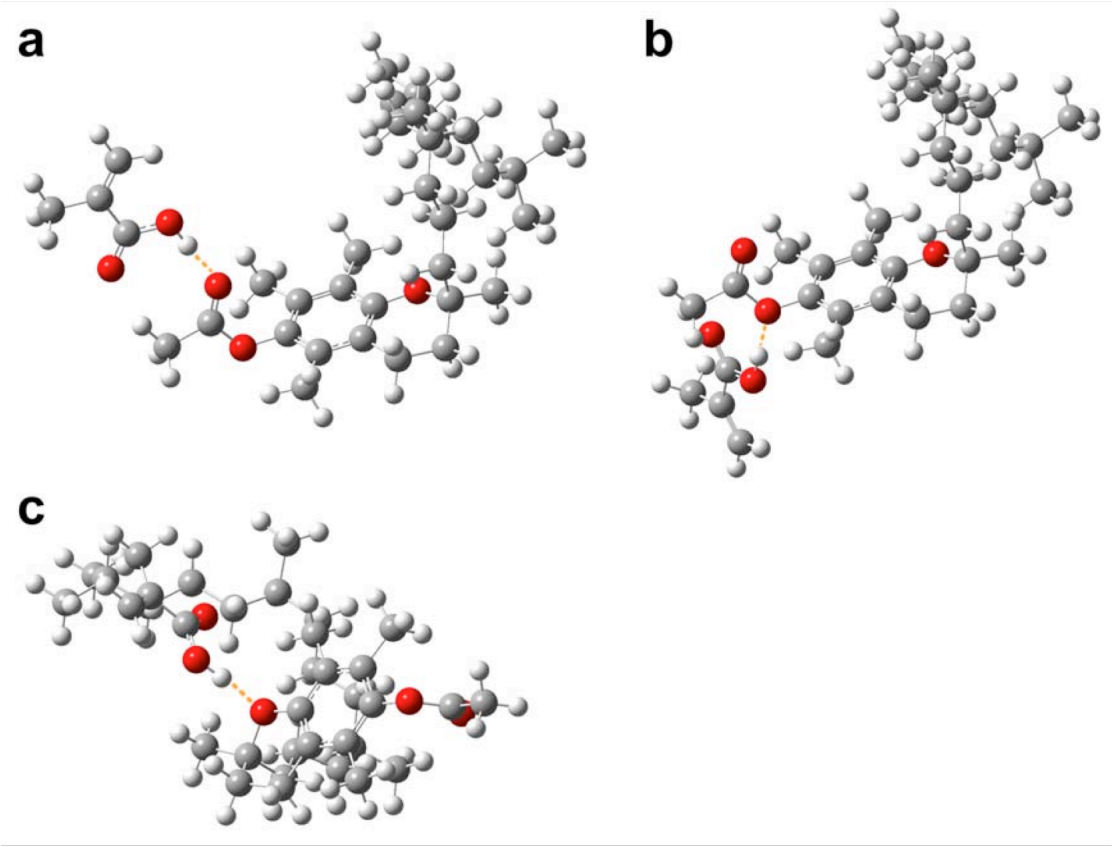

Figure 6.9. Possible modes of interaction of TPA and MAA.

Table 6.2. Summary of the quantum chemical parameters of template-monomer complexes.

	E_{HOMO}	E_{LUMO}	$E_{HOMO-LUMO}$
TP	–7.442	–1.143	6.299
TPA	–5.371	0.346	5.717
MAA	–5.492	0.236	5.728
TP–MAA(1)	–5.446	–1.032	4.414
TP–MAA(2)	–5.184	–1.359	3.826
TP–MAA(3)	–5.749	–0.839	4.911
TPA–MAA(1)	–5.664	–0.604	5.059
TPA–MAA(2)	–5.646	–0.930	4.716
TPA–MAA(3)	–5.959	–0.778	5.181

The energies of HOMO, LUMO and their gaps were converted from a.u. to eV using the conversion factor of 27.2114.

CHAPTER VII
CLICKABLE AFFINITY LIGANDS FOR EFFECTIVE SEPARATION OF GLYCOPROTEINS

7.1 Abstract

In this work, we present a new modular approach to immobilize boronic acid ligands that can offer effective separation of glycoproteins. A new "clickable" boronic acid ligand was synthesized by introducing a terminal acetylene group into commercially available 3-aminophenyl boronic acid. The clickable ligand, 3-(prop-2-ynyloxycarbonylamino)phenylboronic acid (**2**) could be easily coupled to azide-functionalized hydrophilic Sepharose using Cu(I)-catalyzed 1,3-dipolar cycloaddition reaction under mild condition. Compared to other boronic acid affinity gels, the new affinity gel displayed superior effectiveness in separating model glycoproteins (ovalbumin and RNase B) from closely related bovine serum albumin and RNase A in the presence of crude *Escherichia coli* proteins. Because of the simplicity of the immobilization through "click chemistry", the new ligand **2** is expected to not only offer improved glycoprotein separation in other formats, but also act as a useful building block to develop new chemical sensors for analysis of other glycan compounds.

7.2 Introduction

Glycosylated biomolecules, especially glycoproteins play important roles in diverse physiological and pathological processes (230). As one of the most important posttranslational modifications, protein glycosylation is one important step to construct many fully functional proteins in eukaryotic organisms. To get in-depth understanding of glycoproteins, it is required that the target glycoproteins can be efficiently separated from other cellular components before further characterization. Separation of glycoproteins can be achieved by using either lectins (sugar-binding proteins) or small organic ligands immobilized on a solid supporting material. Because of their high binding constant and chemical stability, affinity ligands based on boronic acid derivatives have been used to offer the most efficient separation of carbohydrates, nucleosides, glycolipids, RNA and glycoproteins (89, 231). The basic principle of boronate affinity chromatography is that immobilized boronic acids can form covalent ester bonds with *cis*-diols under basic condition, allowing glycosylated or glycated molecules to be easily separated (90-92, 232). The reversible boronate ester bond can be hydrolyzed under neutral or acidic condition to release the target molecules. Various boronic acid ligands have been developed in the past. The common feature of these ligands is that they contain one boronic acid moiety able to bind *cis*-diols and one functional group (e.g. amino, thiol, or polymerizable vinyl group) that can be used for immobilization on solid support (91, 92, 232-239). The chemical reactions used for immobilization often require harsh conditions (non-aqueous solvent, high temperature, etc.) and are often difficult to perform in the presence of proteins and other biological molecules due to the low selectivity of the coupling reactions. In this respect, more efficient and truly bio-orthogonal coupling reactions, for example the recently established “Click Chemistry” methodology (94), become very attractive. Besides for ligand immobilization and bio-conjugation, we believe that bio-orthogonal click chemistry will open new opportunities for protein molecular imprinting under non-denaturing conditions.

One particularly interesting click reaction is the Cu(I)-catalyzed 1,3-dipolar cycloaddition reaction between organic azide and acetylene (240, 241). This type of click reaction is normally very fast, can tolerate numerous functional groups and can be easily carried out in aqueous solution. The use of click chemistry to

achieve efficient ligand immobilization and bio-conjugation has been reviewed in several excellent Refs (242, 243). In this work, we intended to develop a modular click coupling approach for immobilization of boronic acid ligands. The key issue was to introduce a clickable terminal acetylene group into commercially available boronic acids. Since a variety of surface functional groups can be easily converted into terminal azides, we believe the new clickable boronic acids can be very versatile building blocks not only for affinity chromatography separation, but also for the development of chemosensors for detection of various glycan compounds. In this paper, we describe the synthesis of a stable phenylboronic acid bearing a terminal acetylene group and the immobilization of the ligand on azide-functionalized hydrophilic Sepharose using Cu(I)-catalyzed 1,3-dipolar cycloaddition reaction. The binding selectivity of the obtained affinity matrix was tested using ovalbumin and ribonuclease B (RNase B) as model glycoproteins. Non-glycosylated bovine serum albumin (BSA), RNase A and bacterial proteins were used as controls to simulate the complex sample conditions that can occur in real applications. The efficiency of glycoprotein separation afforded by the new affinity matrix was compared with that offered by a commercial boronic acid gel, as well as by a similar ligand immobilized through a conventional coupling reaction.

7.3 Materials and methods

7.3.1 Materials

3-Aminophenylboronic acid (APBA) hemisulfate salt (≥95%), APBA monohydrate (98%), propargyl chloroformate (96%), propargyl acrylate (98%), sodium ascorbate (≥98%), copper (II) sulfate pentahydrate (>98%), bovine serum albumin (BSA, Cohn Fraction V from bovine serum, ≥96%), ovalbumin from egg white (≥90%), ribonuclease A (RNase A, Type I-A from bovine pancreas) and ribonuclease B (RNase B, from bovine pancreas) were purchased from Sigma–Aldrich. Sodium hydrogen carbonate ($NaHCO_3$, 99%) and sodium hydroxide (NaOH, 99%) were obtained from MERCK. Sodium azide (NaN_3, 96%) was obtained from The British Drug House LTD. Sepharose 4B was purchased from GE Healthcare. All solvents were HPLC grade and were purchased from Fisher Scientific.

7.3.2 Synthesis of 3-(3-oxo-3-(prop-2-ynyloxy)propylamino)phenylboronic acid (OPAPBA, 1)

3-Aminophenylboronic acid hemisulfate salt (186 mg, 1 mmol) was dissolved in methanol/H_2O (7/3, v/v) (6 mL). The solution was cooled to 0°C and then a solution of $NaHCO_3$ (168 mg, 2 mmol) in H_2O (4 mL) was added. The reaction mixture was stirred and propagryl acrylate (110 mg, 110 μL, 1 mmol) was added dropwise. After being stirred at 0°C for 20 min, the reaction mixture was warmed up to ambient temperature and stirred overnight. The solvent was removed to give pale reddish solid. The organic compounds were recovered by dissolving in ethyl acetate (6 mL), which was subsequently removed under vacuum. The crude product was purified by silica column chromatography using dichloromethane/methanol/acetic acid (97/2/1 to 90/9/1, v/v/v) to give pale reddish oil. This product was further purified by reverse phase column chromatography (C_{18} RP-silica gel) using methanol/H_2O (5/95 to 20:80, v/v) as solvent to give a white solid. Yield: 10%. ^{1}H-NMR (CD_3OD, 400 MHz): δ/ppm=2.52 [2H, t, J = 6.47 Hz, R(CO)C***H*****$_2$**CH_2R], 2.92 [1H, t, J = 2.48 Hz, ***H***≡CR], 3.42 [2H, t, J = 6.75 Hz, R(CO)CH_2C***H*****$_2$**-R], 4.70 (2H, d, J = 2.48 Hz, H≡CC***H*****$_2$**OR), 6.70–7.20 (4H, m, phenyl-*H*). MS (ESI+) ($M+H^+$): Calc'd, 248.11; found, 249.07.

7.3.3 Synthesis of 3-(prop-2-ynyloxycarbonylamino)phenylboronic acid (PCAPBA, 2)

To a solution of 3-APBA hemisulfate (372 mg, in methanol/water (MeOH/H_2O, 1/1, 20 mL), $NaHCO_3$ 2 mmol) (504 mg, 6 mmol) was added. The suspension was cooled to 0°C before propargyl chloroformate (210 μL, 2 mmol) was added dropwise over a period of 15 min. The reaction mixture was stirred at <10°C for 3h before the precipitated solid was filtered off. The permeated solution was evaporated under vacuum and the residue was recovered by dissolving in ethyl acetate (10 mL). The insoluble solid was removed by filtration. The ethyl acetate solution was dried over anhydrous $MgSO_4$. Removal of solvent under vacuum gave the pure product as a white solid. Yield: 82%. ^{1}H-NMR (400 MHz, CD_3OD): δ/ppm = 2.93 (t, J = 2.48 Hz, 1H; ***H***≡CCR), 4.75 (d, J = 2.42 Hz, 2H; H≡CCC***H*****$_2$**OR), 7.29–7.72

(m, 4H; phenyl-*H*). MS (ESI+): m/z: Calc'd, 219.11; found, 242.27 $(M+Na)^+$, 270.24 $(M+MeOH+H_2O)^+$.

7.3.4 RP-HPLC analysis of "Clickable" affinity ligands

RP-HPLC was carried out on a Chromolite Performance column (RP-18e, from MERCK) mounted on a LaChrom L-7100 solvent delivery system. A L-7455 diode array detector was used to monitor the elution. Samples dissolved in acetonitrile were injected and eluted with water:acetonitrile (85:15) containing 0.1% trifluoroacetic acid.

7.3.5 Synthesis of epoxy-activated Sepharose

Sepharose 4B (10 ml) was washed with deionized water (10 mL) for three times before it was suspended in a mixture of 2.5 mL of deionized water and 2.5 mL of 2 M NaOH. Epichlorohydrin (3 mL, 40 mmol) was added into the suspended Sepharose 4B. The pH of the gel suspension was ~13. The mixture was rotated in a DNA hybridization oven set at 40°C overnight. The gel was then thoroughly washed with deionized water before the number of epoxide groups in the epoxy-activated Sepharose was determined using the method of Sundberg and Porath (244). The assay was based on the reaction between epoxide and sodium thiosulfate:

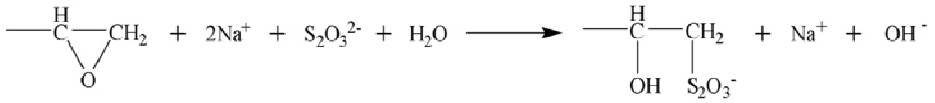

where where the released hydroxide ions were titrated with 1M hydrochloric acid.

The epoxy-activated Sepharose (100 μL) was added to 2 mL of 1.3 M sodium thiosulfate solution and subsequently titrated with hydrochloric acid until pH 7.0 using phenol red as an indicator. The amount of hydrochloric acid consumed was used to calculate the number of epoxy groups immobilized on the Sepharose gel.

7.3.6 Synthesis of azide-functionalized Sepharose (azide-Sepharose)

The epoxy-activated Sepharose (8 mL) was added into a 20 ml solution of sodium azide (910 mg, 14mmol) in deionized water. The mixture was rotated in a

DNA hybridization oven set at 25°C overnight. The gel was washed with 10 mL water for 5 times and kept in 10 ml water until further use.

7.3.7 Synthesis of PCAPBA-functionalized Sepharose (2-Sepharose) by click reaction

The azide-functionalized Sepharose (5 mL, containing ~0.4 mmol of azide groups) was suspended in 15 mL of methanol:water (1:1). To the suspension 3-PCAPBA (121 mg, 0.5 mmol mg) dissolved in 2 mL of methanol:water (1:1) was added, followed by addition of 10 μL of 100 mM $CuSO_4 \cdot 5H_2O$ solution. To this mixture 50 μL of 100 mM sodium ascorbate was finally added and the total volume of the mixture was adjusted to 25 mL by addition of water. The final concentration of $CuSO_4$ and sodium ascorbate in the mixture was 40 μM and 200 μM, respectively. The mixture was rotated in a DNA hybridization oven at room temperature overnight. The Sepharose gel was finally washed with deionized water (15 mL) for 5 times.

7.3.8 Synthesis of 3-APBA-functionalized Sepharose (APBA-Sepharose) by direct ring-opening reaction

The epoxy-activated Sepharose (5 mL, containing ~0.4 mmol of epoxide groups) was suspended in 18 mL of methanol:water (1:1). To the suspension 3-APBA monohydrate (121 mg, 0.5 mmol) dissolved in 2 mL of methanol:water (1:1) was added. The mixture was then rotated in a DNA hybridization oven at room temperature overnight. The gel was washed with water (15 mL × 5) and finally kept in 15 mL water until use.

7.3.9 Protein separation in batch mode

Different Sepharose gels (1 mL) were washed with 1 mL of binding buffer (PBS buffer pH 8.7, containing 20 mM $MgCl_2$) for 5 times. The gels were then mixed with different protein solutions of BSA and ovalbumin (10, 20, 40, 80 and 100 μM) dissolved in the binding buffer (500 μL) and rotated at room temperature for 3 h. After centrifugation, supernatant (500 μL) was collected for analysis of protein concentration.

To study competitive protein binding, Sepharose gels (1 mL) were washed in the binding buffer and mixed with 500 μL solution of protein mixture containing BSA (40 μM) and ovalbumin (40 μM) dissolved in the binding buffer. The samples were rotated at room temperature for 3 h and then centrifuged. The Sepharose gels were collected and washed with 1 mL of binding buffer for 5 times. Finally, the bound proteins were eluted with 0.5 mL of elution buffer (PBS buffer pH 7.2) and analyzed by SDS-PAGE.

The clicked boronic acid-Sepharose (**2**-Sepharose) was used to separate ovalbumin from BSA in a batch mode. The affinity gel was mixed with a solution of ovalbumin (40 μM), BSA (40 μM) and the *E. coli* protein extract in the binding buffer. The gel was washed with the binding buffer to remove non-specifically adsorbed protein before elution was carried out with 0.2 M sorbitol dissolved in PBS buffer at pH 7.2. SDS-PAGE was used to analyze the composition of the different fractions.

7.3.10 Protein separation by affinity chromatography

Escherichia coli BL21 (DE3) cells were grown in 25 mL of TB broth at 37°C with shaking at 160 rpm overnight. The cells were collected by centrifugation at 5000 rpm for 20 min at 4°C. Cell pellet was washed in 20 mL of binding buffer for 5 times and resuspended in 10 mL of binding buffer. The cells were disrupted by sonication. Cell debris was removed by centrifugation, the supernatant was passed through an Acrodisc syringe filter (pore size 0.45 μm, from Pall) to give crude *E. coli* extract as non-glycosylated proteins. The total protein concentration of the *E. coli* extract was 3.72 mg/ml. BSA (17.72 mg) and ovalbumin (8.92 mg) were added into 5 mL of the *E. coli* extract to give crude protein plus I, in which the final concentration of BSA and ovalbumin was 40 μM. To prepare crude protein plus II, ovalbumin (8.92 mg), RNase B (200 μg) and RNase A (2.5 mg) were added into 5 mL of the *E. coli* extract, giving a final concentration of the individual proteins: ovalbumin, 40 μM; RNase B, 2.67 μM; RNase A, 36.5 μM.

2-Sepharose was packed into a column (Ø 1 cm × 2 cm) that was equilibrated with at least 10 column volumes of binding buffer. The crude protein plus I or II was applied to the column and then washed with 10 column volumes of binding

buffer. The bound proteins were eluted with elution buffer (PBS buffer pH 7.2). The eluted fractions were collected and their UV absorbance at 280 nm deter- mined using a UV–Vis spectrophotometer. All the fractions were stored at −20°C until further analyzed.

7.3.11 Protein analysis

Protein concentration was determined with Bio-Rad Protein Assay (Bio-Rad Laboratories, USA) using BSA as standard. UV absorbance at 595 nm was measured using a Beckman Coulter DU 800 UV–Vis spectrophotometer. Fractions from the competitive binding test and the affinity chromatography with 3-PCAPBA-Sepharose were analyzed by SDS-PAGE. Polyacrylamide gel with a crosslinking density of 15% was prepared as described by Laemmli (245). The gels were stained with Coomassie Brilliant Blue after electrophoretic separation. PageRulerTM Unstained Protein Ladder (Fermentas) in the range from 10 kDa to 200 kDa was used for molecular mass determination.

7.4 Results and discussions

7.4.1 Synthesis and characterization of “clickable” boronic acid ligands

Two boronic acid ligands bearing acetylene moieties were obtained using synthetic approaches shown in Figure 7.1. Instead of using clickable azide group, as reported by Wang and coworkers in a previous study (246), terminal acetylene was linked to aminophenylboronic acid. The first ligand, OPAPBA was prepared by Michael addition reaction between 3-aminophenylboronic acid and propargyl acrylate under basic condition (Figure 7.1a). Under the reaction condition only mono-substituted product (**1**) was obtained, i.e. no further Michael addition between **1** and propargyl acrylate was observed. Purification of **1** using silica column chromatography did not give satisfactory result, therefore a further purification step was employed using reverse phase C_{18} RP-silica (Figure 7.2a). This purification procedure led to a poor product yield of ~10% (not optimized). The product turned out to be unstable and changed into reddish color after short storage, presumably caused by oxidation of the aromatic amine moiety.

The second ligand, PCAPBA (**2**) was synthesized by reacting 3-aminophenylboronic acid hemisulfate with propargyl chloroformate in the presence of $NaHCO_3$ (Figure 7.1b). The reaction product could be easily separated with satisfactory purity without tedious column purification (Figure 7.2b) and was found to be stable after long storage time (>6 months). Based on its simplicity of synthesis and stability, ligand **2** was selected as the "clickable" ligand to prepare affinity matrices for separation of glycoproteins.

7.4.2 Preparation of azide-Sepharose

To enable simple "click" reaction for immobilization of the boronic acid ligand, azide-functionalized Sepharose was prepared by firstly activating Sepharose with epichlorohydrin under basic condition, followed by a ring-opening reaction of the epoxide with sodium azide under neutral condition (Figure 7.3). The number of epoxide groups of the activated gel was determined via their reaction with sodium thiosulfate, with the released hydroxide ions being titrated with HCl (244). The titration result indicated that the number of epoxide groups in the activated gel was ~84 μmol/mL of gel. The epoxy-activated gel was treated with excess sodium azide in order to minimize the residual epoxide groups, which otherwise can react with proteins through their primary amino groups. No remaining epoxide group could be detected when the azide-functionalized Sepharose gel was treated with sodium thiosulfate, suggesting that all the epoxide groups were quantitatively converted into azide groups in the gel matrix.

7.4.3 Preparation of boronic acid-functionalized Sepharose (2-Sepharose and APBA-Sepharose)

Boronic acid ligand **2** was immobilized on azide-functionalized Sepharose using Cu(I)-catalyzed azide-alkyne cycloaddition reaction (Figure 7.3a). The Cu(I) catalyst was generated in situ by reducing $CuSO_4$ with sodium ascorbate in aqueous methanol. This click reaction afforded boronic acid ligand effectively immobilized on the hydrophilic sepharose gels via a 1,2,3-triazole spacer (**2**-Sepharose). Supposing quantitative conversion from epoxide to azide and during the click reaction, the boronate loading of **2**-Sepharose is approximately 84 μmol/mL gel.

For comparison, 3-aminophenylboronic acid was directly immobilized on epoxy-activated Sepharose according to Figure 7.3b. The immobilization was achieved by reacting the epoxide groups of the modified Sepharose with the aromatic amine in 3-APBA. After reacting with excess 3-APBA, no epoxide group could be detected when the gel was treated with sodium thiosulfate, suggesting that all the epoxide groups were quantitatively converted into boronic acid groups in the gel matrix (APBA-Sepharose).

The two types of affinity matrices displayed a quite different stability. While the affinity matrix **2**-Sepharose, obtained by the click reaction, did not show any obvious change, the color of APBA-Sepharose (obtained by the direct ring-opening reaction) eventually changed from white into yellowish after being kept in a refrigerator for one week (Figure 7.4), presumably caused by oxidation of the aromatic amine moiety. The higher stability of **2**-Sepharose can be explained by the more stable amide bond between the phenylboronic acid and the linker.

7.4.4 Protein binding characteristics

To evaluate the protein binding properties, the affinity gels obtained by the click reaction (**2**-Sepharose), the un-modified Sepharose as well as the azide-functionalized Sepharose (azide-Sepharose) were exposed to a model glycoprotein, ovalbumin and a non-glycoprotein, BSA in a weakly basic buffer. The different gel matrices were first exposed to protein solutions under alkaline condition (pH 8.7), which allowed boronate ester bond to be formed between the *cis*-diols of glycoprotein and the immobilized boronic acid. The unbound protein remaining in supernatant was measured by the Bio-Rad Protein Assay. As shown in Figure 7.5a, ovalbumin binding to **2**-Sepharose was significantly higher than those binding to the un-modified Sepharose and azide-Sepharose over a broad protein concentration range (10–100 μM). These results indicate that the Cu(I)-catalyzed click reaction was efficient to introduce phenylboronic acid ligand into hydrophilic Sepharose, resulting in effective binding for the model glycoprotein under weakly basic condition. For the un-modified Sepharose and the azide-functionalized Sepharose, some non-specific binding of ovalbumin was also observed.

To investigate the source of the non-specific binding, **2**-Sepharose was exposed to a model non-glycoprotein, BSA under the same condition. Compared to ovalbumin, BSA binding to **2**-Sepharose was significantly lower but nevertheless observable (Figure 7.5b). Interestingly, the non-specific binding of BSA to **2**-Sepharose has a profile similar to the non-specific binding of ovalbumin to the unmodified Sepharose and the azide-functionalized Sepharose (Figure 7.5a). This phenomenon may be explained if the non- specific protein binding is mainly caused by the Sepharose matrix itself rather than any of the immobilized small molecule ligand or the spacers.

Compared to the click approach for ligand immobilization (Figure 7.3a), phenylboronic acid can be directly immobilized on epoxy- activated Sepharose with fewer reaction steps (Figure 7.3b). However, the affinity matrix obtained through the direct immobilization has poor storage stability. To study the impact of matrix stability, APBA-Sepharose was stored at 4°C for one week before its binding characteristics for ovalbumin and BSA was tested. As shown in Figure 7.5c, APBA-Sepharose displayed much lower binding for ovalbumin than **2**-Sepharose. In fact, binding of glycoprotein (ovalbumin) to APBA-Sepharose is almost identical to the binding of the non- glycoprotein, BSA. The high stability of **2**-Sepharose and its clear preference to bind glycoprotein, as demonstrated in the batch mode experiments, make the clickable boronic acid ligand **2** attractive for practical applications.

The clicked boronic acid-Sepharose was further compared with a commercially available immobilized boronic acid gel. In this affinity material, the ligand 3-aminophenylboronic acid was immobilized on crosslinked polyacrylamide support (copolymer of 3-acrylamidophenyl-boronic acid and acrylamide). Ovalbumin binding to the commercial affinity gel was tested under the same batch condition as used for evaluating **2**-Sepharose. As shown in Figure 7.5c, the commercial gel displayed significantly lower binding for ovalbumin than **2**-Sepharose, despite the fact that the two matrices contained the same phenylboronic acid moiety. The high glycoprotein binding with the present clicked boronic acid gel may be explained in part by the lower crosslinking density of the Sepharose used. The longer triazole spacer in the present **2**-Sepharose may also reduce steric hindrance for binding large protein molecules.

7.4.5 Separation of glycoprotein in batch mode

The clicked boronic acid-Sepharose was used to separate ovalbumin from BSA in a batch mode. The affinity gel was mixed with a solution of ovalbumin (40 μM) and BSA (40 μM) in the binding buffer. To evaluate the influence of other non-glycosylated proteins, *E. coli* protein extract was also added into the test solution. The gel was washed with the binding buffer to remove non-specifically adsorbed protein before elution was carried out with PBS buffer at pH 7.2. This elution condition (with neutral buffer) was selected to maintain maximum protein stability. No competing reagent was needed in the elution buffer, as confirmed in a separate experiment where addition of 0.2 M sorbitol did not show any effect (Figure 7.6). SDS-PAGE was used to analyze the composition of the different fractions. As represented in Figure 7.7, the intensities of the protein bands in the SDS gel suggest that **2**-Sepharose bound preferentially ovalbumin over non-glycosylated BSA and *E. coli* proteins. The majority of the non-glycosylated proteins are found in unbound fraction (lane 5) and in the washing buffer (lane 6). In lane 7, an intense protein band corresponding to ovalbumin was observed. Some BSA still remained visible in the final elution however, suggesting that the washing condition was not able to remove all the non-specifically adsorbed proteins under the batch mode condition.

7.4.6 Separation of glycoproteins by affinity chromatography

To achieve more effective separation of glycoproteins, **2**-Sepharose was used as affinity matrix in a column mode to isolate ovalbumin from a mixture of *E. coli* extract and the non-glycosylated protein, BSA (Crude Protein Plus I). The sample was loaded into the affinity column and washed with the binding buffer at pH 8.7, before the glycoprotein was eluted with PBS buffer at pH 7.2 (Figure 7.8). Fractions 7 and 8 of the elution with the highest UV absorbance at 280 nm were pooled and subjected to SDS-PAGE analysis. As shown in Figure 7.9, the pooled elution fractions 7 and 8 (lane 8) contained dominantly ovalbumin (MW 45 kDa), although a very weak protein band corresponding to BSA (MW 70 kDa) was still visible. The protein bands in lane 8 should be compared with those from the original Crude Protein Plus I (lane 5), the break- through portion (lane 6) and the washing fractions (lane 7), which showed predominantly BSA and the *E. coli* proteins. The

result of the protein separation with this column chromatography is summarized in Table 7.1.

A more challenging test was performed by separating ovalbumin and RNase B from a mixture of *E. coli* extract and the non-glycosylated RNase A. The only difference between RNase B and RNase A is that the former ribonuclease contains a single glycosylation site at Asn34, otherwise the two enzymes have identical amino acid sequences and show the same basic catalytic activity (247). The protein sample (Crude Protein Plus II) containing ovalbumin, RNase B, RNase A and the *E. coli* extract was loaded to a **2**-Sepharose column, washed with the binding buffer before the glycosylated proteins were eluted at pH 7.2 and monitored with UV absorbance at 280 nm (Figure 7.10). The elution fractions 11–13 were combined and subjected to SDS-PAGE analysis. In Figure 7.11, the purified proteins in lane 9 show clearly the bands corresponding to the two glycosylated proteins, ovalbumin (lane 3) and RNase B (lane 5, MW ~15 kDa), whereas the original Crude Protein Plus II (lane 6), the breakthrough sample (lane 7) and the washing fractions (lane 8) showed mainly the *E. coli* protein and RNase A (MW ~13.7 kDa). The multiple bands observed for RNase B (lanes 5 and 9) may be explained by the existence of the different glycan variants of this particular enzyme. Collectively, the **2**-Sepharose column could effectively separate the two model glycoproteins from closely related non-glycosylated proteins in crude cellular extract.

In order to verify that the elution buffer at pH 7.2 is sufficient to recover all the glycoproteins from the affinity column, additional elution was performed using PBS buffer at pH 6.5 and all the fractions were monitored by UV absorbance at 280 nm. As shown in Figure 7.12, fractions 9-11 (measured pH 7.34) have the highest protein concentration, whereas fractions 15-17 (measured pH 6.61) had very low protein content. SDS-PAGE analysis of elution fractions 15-17 in Figure 7.13 showed no bands corresponding to any of the target glycoproteins (lane 10). Accordingly, the elution buffer at pH 7.2 was strong enough to remove all the target glycoproteins from the present boronic acid affinity column.

In summary of this work, we have developed a new clickable affinity ligand useful for effective separation of glycoproteins. The chemically stable boronic acid derivative **2** can be used as a modular ligand, to be easily linked to azide-

functionalized solid support via simple Cu(I)-catalyzed click reaction under very mild conditions. As demonstrated in this work, the hydrophilic Sepharose, after being modified with the clicked boronic acid, afforded the most efficient separation of model glycoproteins and outperformed the existing commercial immobilized boronic acid gel. Applying click chemistry to immobilize the developed ligand **2** also gave affinity medium with much improved stability compared to that obtained by directly coupling 3-aminophenylboronic acid with epoxy-activated support. Given that numerous small molecule ligands can be easily converted into clickable reagents bearing either acetylene or azide moieties, we believe a large variety of new clickable boronic ligands can be developed to simplify glycoprotein separation under physiological conditions.

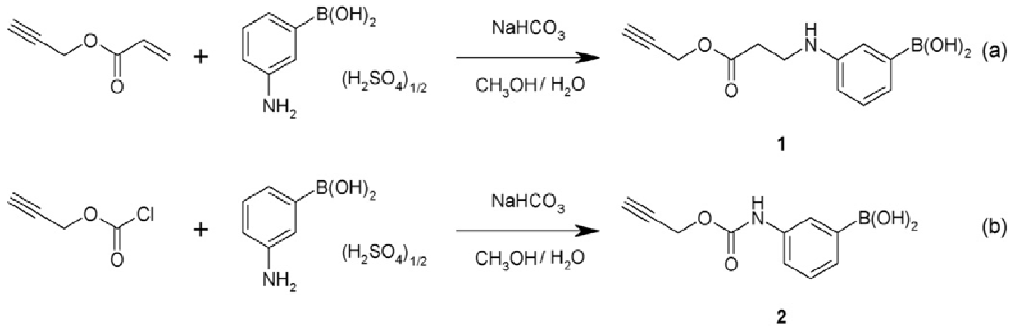

Figure 7.1. Syntheses of clickable boronic acid ligands by Michael addition (a) and nucleophilic acyl substitution (b).

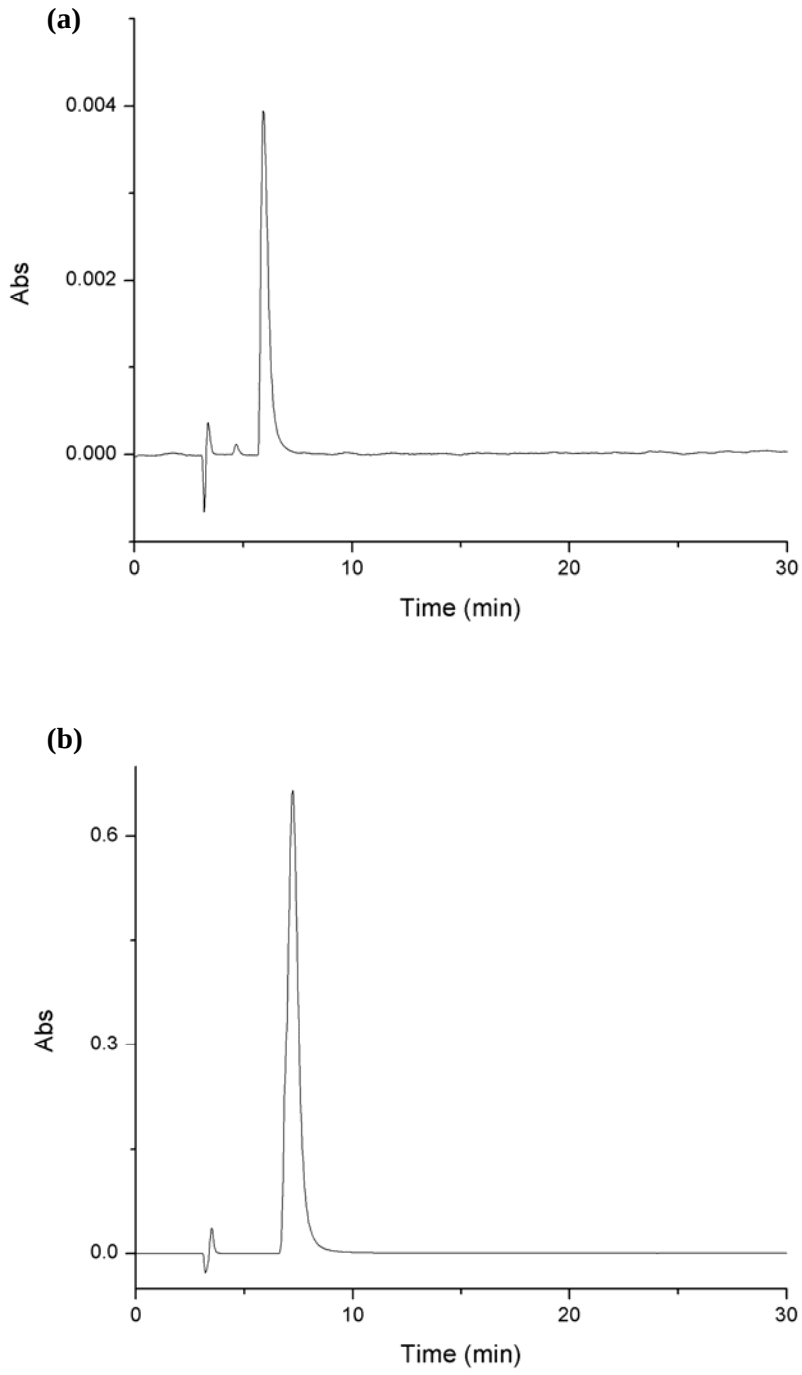

Figure 7.2. RP-HPLC chromatogram of OPAPBA (ligand **1**, UV absorbance 260 nm) (a) and PCAPBA (ligand **2**, UV absorbance 240 nm) (b).

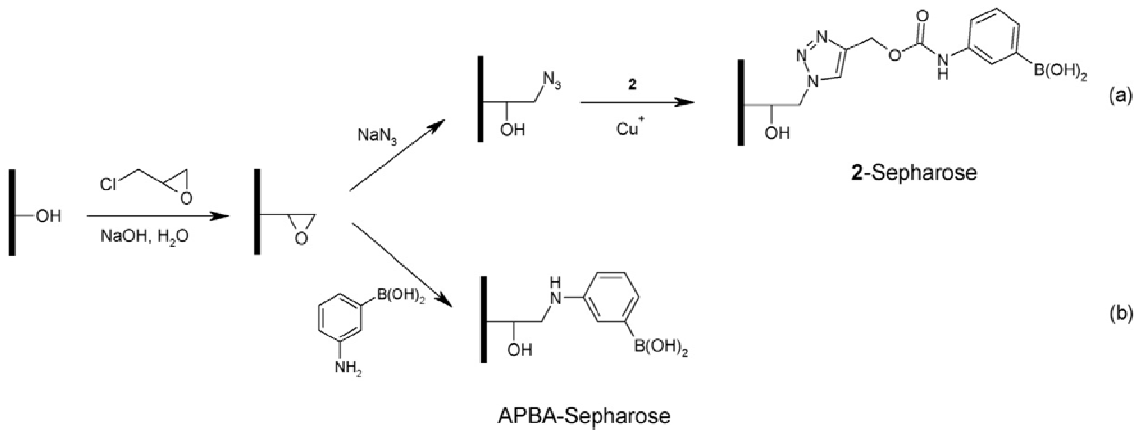

Figure 7.3. Immobilization of boronic acid ligands using click reaction (a) and direct ring opening of epoxide (b).

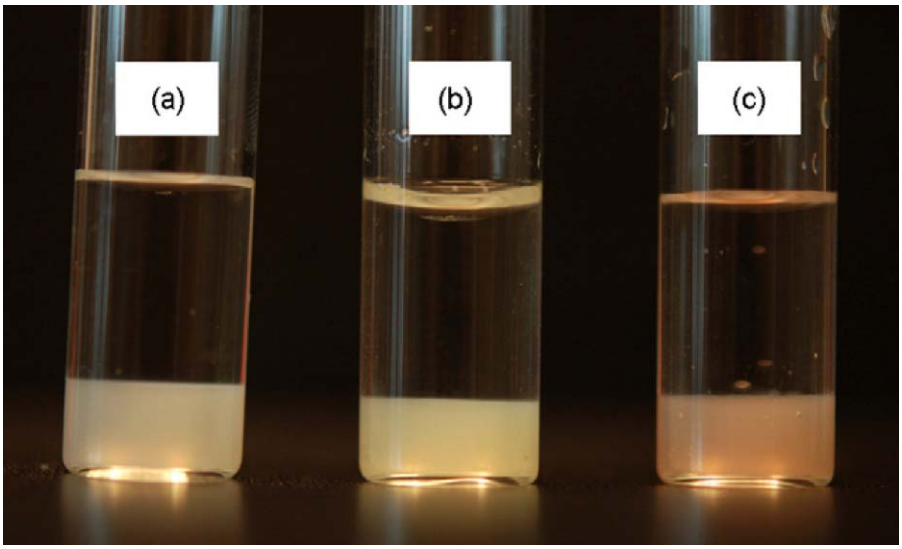

Figure 7.4. Comparison of gel stability: (a) azide-functionalized Sepharose, (b) clicked boronic acid-Sepharose and (c) boronic acid-Sepharose obtained by direct ring opening reaction.

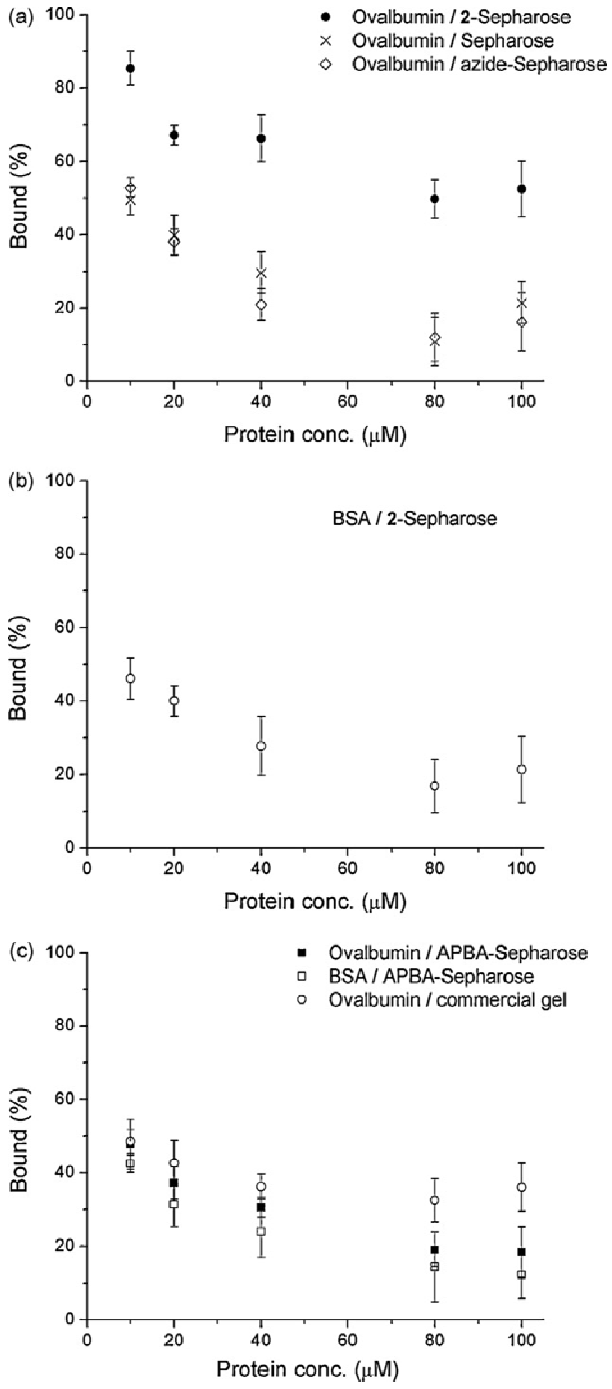

Figure 7.5. Evaluation of protein binding capabilities of different matrices. (a) Uptake of glycoprotein (ovalbumin) by different Sepharose gel, (b) Uptake of non-glycoprotein (BSA) by **2**-Sepharose, (c) Uptake of ovalbumin and BSA by the reference gels APBA-Sepharose and commercial immobilized boronic acid gel.

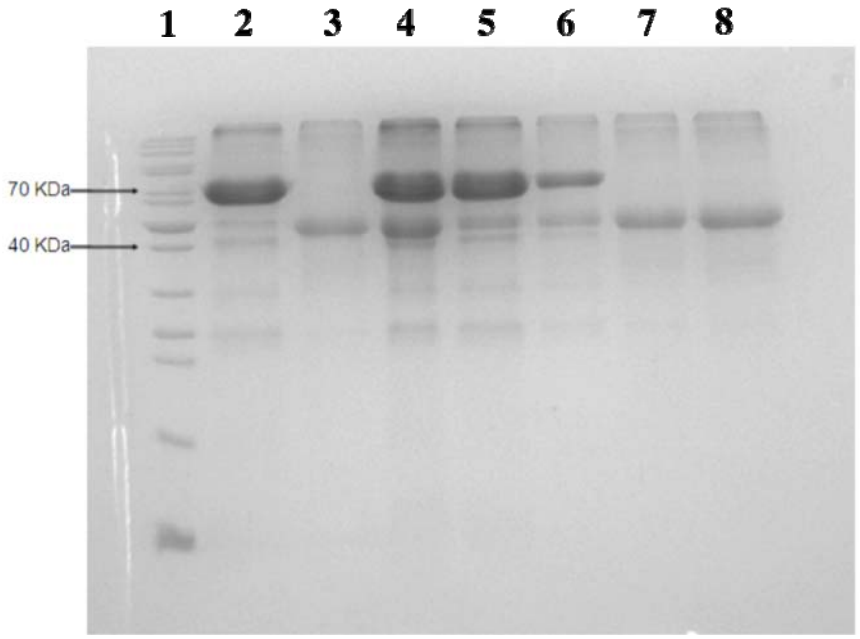

Figure 7.6. SDS analysis of protein fractions before and after treatment with **2**-Sepharose. Lane 1: protein molecular weight marker; Lane 2: BSA, 66 kDa; Lane 3: ovalbumin, 45 kDa; Lane 4: crude protein plus; Lane 5: supernatant; Lane 6: washed fraction; Lane 7: eluted fraction (pH 7.2); Lane 8: eluted fraction (0.2 M of sorbitol solution).

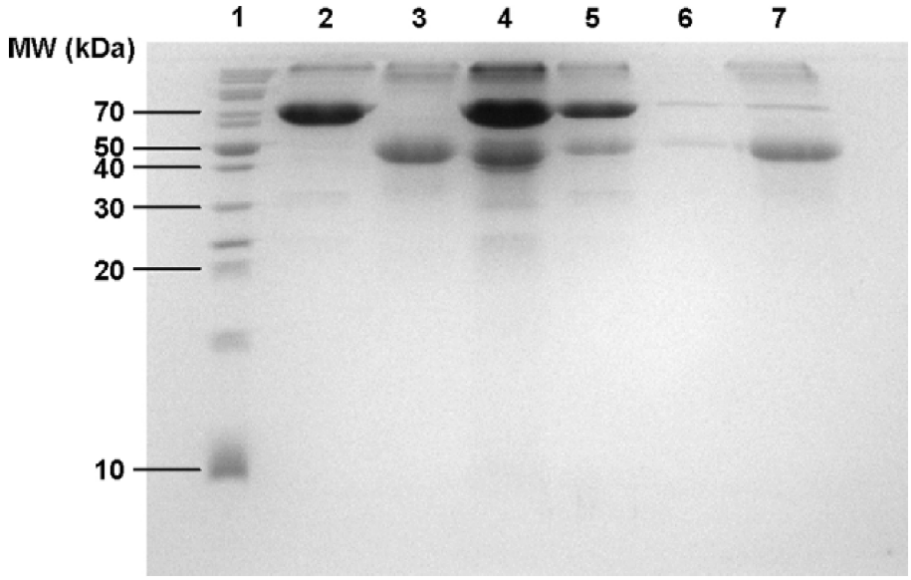

Figure 7.7. SDS-PAGE of protein fractions separated using **2**-Sepharose in batch mode. Lane 1: protein molecular weight marker; Lane 2: BSA, 66 kDa; Lane 3: ovalbumin, 45 kDa; Lane 4: crude protein plus; Lane 5: unbound fraction; Lane 6: washed fraction; Lane 7: eluted fraction

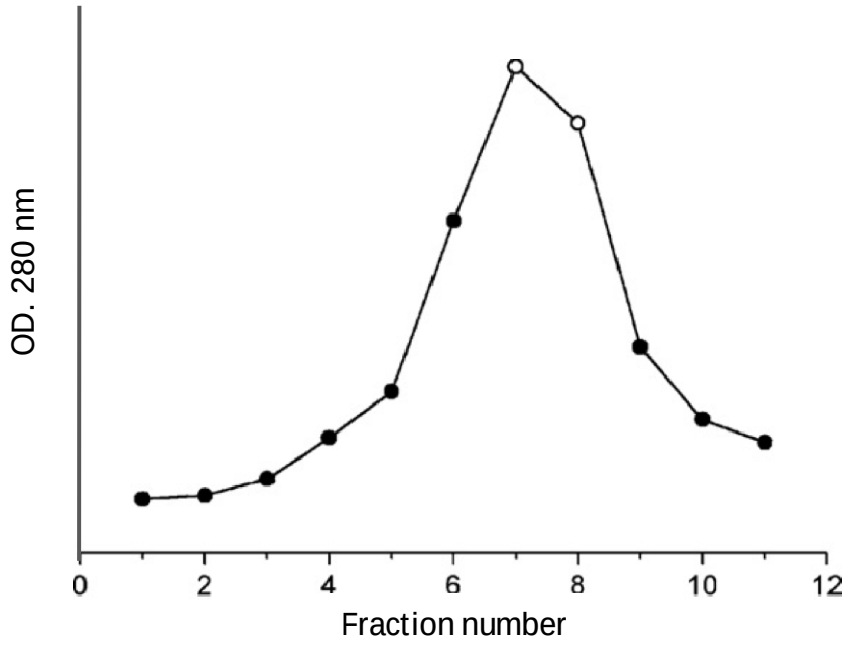

Figure 7.8. Elution profile monitored with UV 280 nm for the separation of ovalbumin from BSA and *E. coli* extract. The fractions marked with (o) were pooled as the purified product.

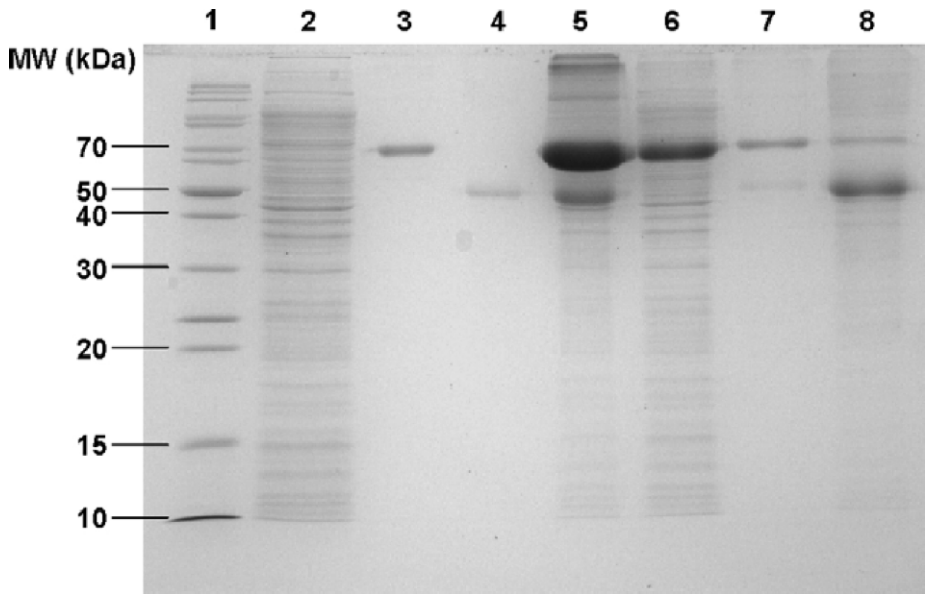

Figure 7.9. SDS-PAGE of protein fractions separated using **2**-Sepharose. Lane 1: protein molecular weight marker; Lane 2: crude *E. coli* extract; Lane 3: BSA, 66 kDa; Lane 4: ovalbumin, 45 kDa; Lane 5: crude protein plus I; Lane 6: flow through fraction; Lane 7: washed fraction; Lane 8: eluted fraction.

Table 7.1. Purification of ovalbumin from crude protein plus with **2**-Sepharose.

Purification step	Volume (ml)	Protein	
		Total (mg)	Conc. (mg/ml)
Crude Protein Plus I	5	28.2	5.64
Flow through	10	12.85	1.29
Washing	20	1.94	0.1
Elution	1.5	6.82	4.55

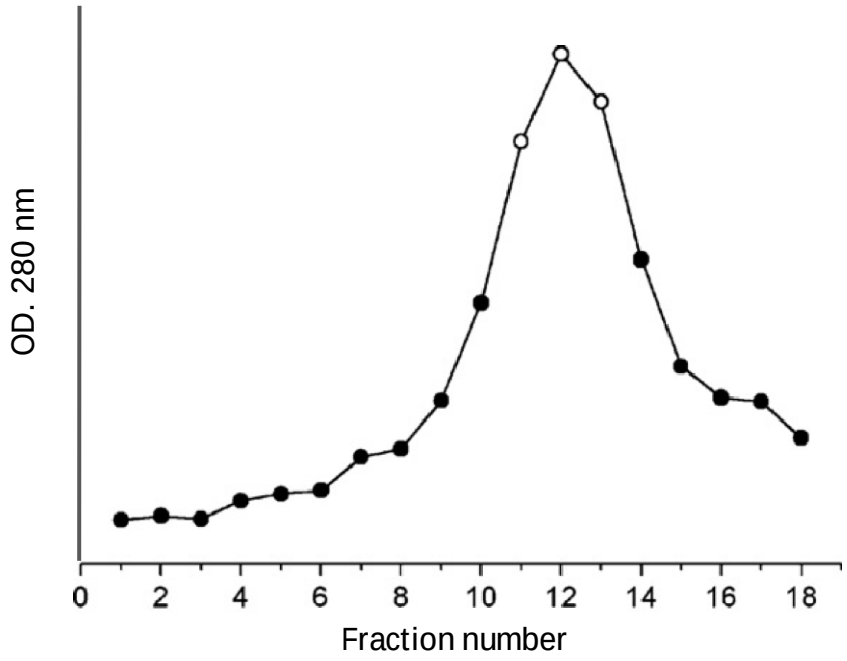

Figure 7.10. Elution profile monitored with UV 280 nm for the separation of ovalbumin and RNase B from RNase A and *E. coli* extract. The fractions marked with (o) were pooled as the purified product.

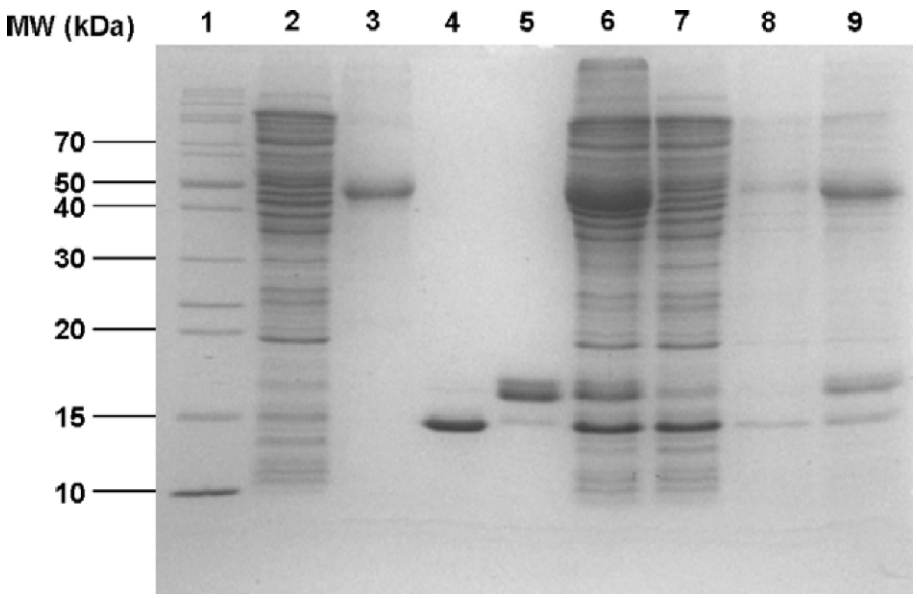

Figure 7.11. SDS-PAGE of protein fractions separated using **2**-Sepharose. Lane 1: protein molecular weight marker; Lane 2: crude *E. coli* protein; Lane 3: ovalbumin, 45 kDa; Lane 4: RNase A, 13.7 kDa; Lane 5: RNase B, 15 kDa; Lane 6: crude protein plus II; Lane 7: flow through fraction; Lane 8: washed fraction; Lane 9: eluted fraction.

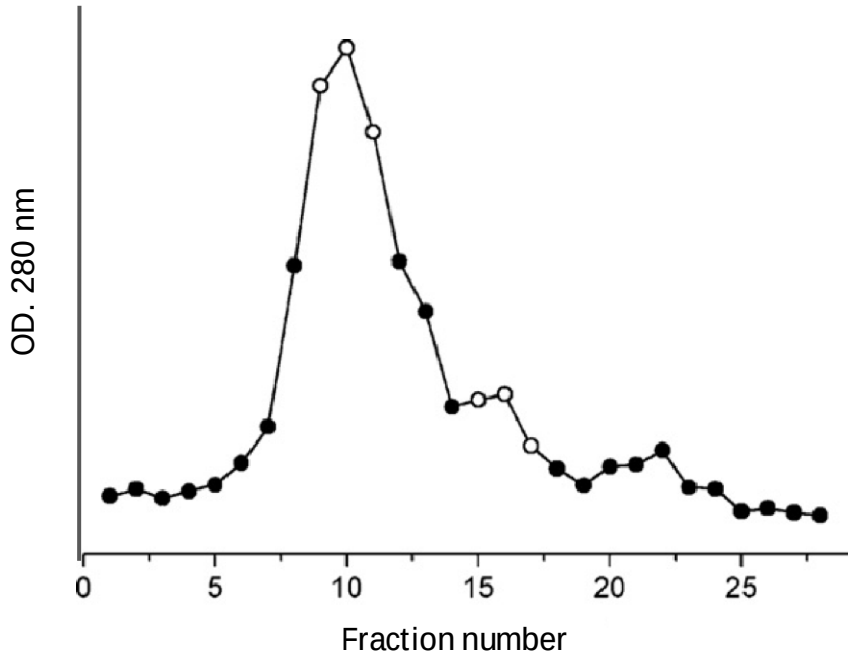

Figure 7.12. Elution profile monitored with UV 280 nm for the separation of ovalbumin and RNase B from RNase A and *E. coli* extract. The fractions eluted at pH 7.2 (fractions 9–11) and at pH 6.5 (fractions 15–17) marked with (o) were pooled and subjected to SDS-PAGE analysis.

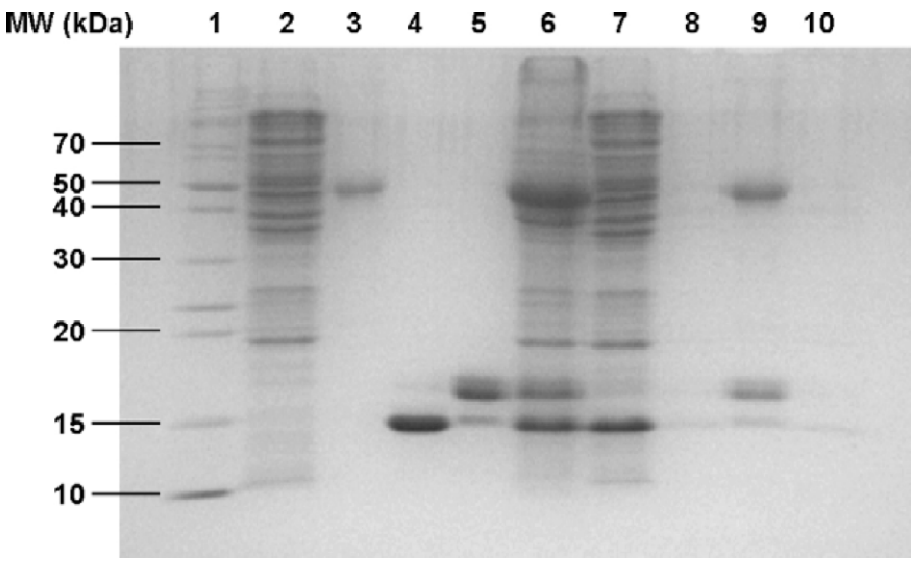

Figure 7.13. SDS-PAGE of protein fractions separated using **2**-Sepharose. Lane 1: protein molecular weight marker; Lane 2: crude *E. coli* protein; Lane 3: ovalbumin, 45 kDa; Lane 4, RNase A, 13.7 kDa; Lane 5: RNase B, 15 kDa; Lane 6: crude protein plus II; Lane 7: flow through fraction; Lane 8: washed fraction; Lane 9: eluted fractions 9–10 (pH 7.2); Lane 10: eluted fractions 15–17 (pH 6.5).

CHAPTER VIII
CONCLUSION AND FUTURE PERSPECTIVE

8.1. Superoxide dismutase mimetics

Superoxide dismutase (SOD) mimetics has been known for three decades as a potential candidate for antioxidative pharmaceutics. Since, the utilization in clinical trial of the native SOD has been reported causing variety of immunological responses particularly on the non-human derived enzyme. Penetration activity of enzyme to the target destructive oxidative site is as well a major concern for clinical application. Therefore, many SOD mimic have been designed from the active site of native enzymes that consist of metal center (Cu, Mn, Fe and Ni) and coordination sites of ligands containing nitrogen, oxygen and sulfur atoms. In 1980, the Fe-EDTA complex has been reported to exhibit only 0.01% activity as compare to the native enzyme. Later on variety of ligands have been used to improve the SOD mimetic activity e.g. Mn-OBTM-4-PyP (metalloporphyrin), Mn-EUK-8 (salen complex) and MnPAM (macrocyclic complex). However, the activity derived was still unsatisfaction. Additionally, free forms of the using ligands may cause unwanted effects to the host. Intention of generating was then turning to complexation of more general therapeutic drug such as aspirin and ibuprofen to complex with the copper ion.

Our studies herein, originally design to synthesize SOD mimics using general metabolites and essential vitamin complexed to copper ions. Those coordinating compounds were nicotinic acid (vitamin B3) and other bioactive compounds including phthalic acid (Ph), salicylic acid (Sal), anthranilic acid (Ant), 2-hydroxypyridine (2Hy), 2-aminopyridine (2Am) and picolinic acid (Pi). Therefore, in Chapter IV and V, copper complexes of nicotinic acid with their bioactive compounds were synthesized by the reaction of 1:1:1 ratio of copper ion: nicotinic acid: other bioactive compounds. The complexes were obtained in high yields (75-91%) as shown in Table 4.2 and 5.2. All complexes were characterized to be tetragonally distorted structures. Three copper complexes were formed by

monodentate coordination of ring N-atom of nicotinic acid as well as bidentate carboxylate ligands using two hydroxyls (Ph), phenolic carbonyl (Sal) and amino carbonyl (Ant) (Figure 4.1). Moreover, the other copper complexes were formed by bidentate nicotinic acid of the ring N-atom of pyridine and the carbonyl group of carboxylic acid. 2-Substituted pyridines were coordinated with copper ion by bidentate ligands using amino ketone (2Hy), amino pyridine (2Am) and carbonyl pyridine (Pi) (Figure 5.1). The SOD activity of the complexes displayed in the range of 34.42-130.20 μM. The copper complex of nicotinic acid with phthalic acid (CuNA/Ph) exhibited the greatest superoxide radical scavenging activity (Table 4.4 and 5.4). Additionally, all copper complexes were also demonstrated having antimicrobial activity against *B. subtilis* ATCC 6633 and *C. albicans* ATCC 90028 with the MIC range of 128-256 μg/mL (Table 4.5 and 5.5). A plausible explanation of antimicrobial activity of the copper complexes may cause by accumulation of hydrogen peroxide. The hydrogen peroxide is also catalyzed by Fenton's reaction to form hydroxyl radicals, which is harmful to bacterial cell.

Moreover, computational approach was employed to study correlation between SOD activity and theoretical parameters. This proposes was to find influent factors that affect superoxide-scavenging activity. The observation demonstrated that the electron affinity (EA; the electron transferring rate) provided positive correlation with SOD activity, where high EA gave rise to high SOD activity. This finding is inversely correlated with previously reports. However, such evidences could be inferred to the differences of geometric coordination of copper complex. Since, our complexes herein arranged in tetragonally distorted while in previous reports the copper complexes are distorted square planar and square pyramidal. In addition, the quantum chemical parameters consisting of HOMO and LUMO energies were also revealed. It is well established that HOMO accounts for the electron donating ability while LUMO characterizes the ability to accept electron. The calculated energies of HOMO and LUMO were significantly correlated with the SOD activity, which was represented as $-\log(1/IC_{50})$. The CuNA/Ph complex exhibited the lowest calculated values of both HOMO and LUMO. This is explained by inductive effect of the two carbonyl groups of the complex withdrawing electrons from the copper atom giving rise to low electron donating ability of the ligand as also indicated that by the lower

HOMO energy. Eventually, the bond length between copper and the coordination sites of the ligands was crucial for SOD activity. The longest axial bond lengths in CuNA/Ph were shown to possess the highest SOD activity.

8.2. Molecularly imprinted polymer (MIP)

Molecular imprinting is a technique to create template-shaped pockets in a polymer matrix that provides specific cavity for template molecules. Such cavities of imprinted polymer can be served as specific binding site in many applications and the binding is stereo-specific. Our study utilized tocopherol (vitamin E) and tocopherol acetate as templates. The preparations of molecularly imprinted polymer (MIP) using tocopherol and tocopherol acetate as the templates were described in Chapter VI. The tocopherol-imprinted polymer (MIP-TP) and the tocopherol acetate-imprinted polymer (MIP-TPA) were synthesized by traditional bulk polymerization method. It was observed that bulk polymers, both MIP-TP and MIP-TPA, displayed two-fold greater binding capacity than the corresponding non-imprinted polymer (Figure 6.3). To investigate the cross-selectivity of the bulk polymers, MIP-TP and MIP-TPA were cross-bound with the two template molecules; tocopherol and its derivative. The result showed that MIP-TPA can bind to tocopherol acetate (28.6%) at approximately half of the competing tocopherol (53.8%) as demonstrated in Figure 6.4. In addition, the MIP-TP was also performed by precipitation polymerization method to generate nanosphere polymers (Figure 6.5). The rebinding analysis of the nanosphere polymer showed that imprinted nanoshperes were able to bind the template approximately 1.22-1.57 times compared to non-imprinted nanospheres. To maximize the binding capacity of the nanosphere polymers, the optimal rebinding solvent was observed. The mixture of ethanol and water (8:2, v/v) exhibited the highest imprinted factor of 1.85 for imprinted and non-imprinted nanospheres as shown in Figure 6.7.

8.3. Clickable boronic acid particles

In Chapter VII, boronic acid was successfully bystanding onto Sepharose and subsequently applied as affinity chromatography to separate glycoproteins. Our study examined two general glycoproteins, the ovalbumin and RNase B. Generally, chemical reaction used for immobilization often requires harsh condition and are often

difficult to perform in the presence of biological molecules. Under the limitations, we applied the recently established “Click Chemistry” reaction to generate 1,2,3-triazole that covalently link with boronic acid. Thus, clickable affinity ligand based on boronic acid was synthesized in one step of the reaction to be coupled to azide-functionalized Sepharose by Cu(I)-catalyzed click reaction as described in Figure 7.1, 7.2 and 7.3. Glycoproteins (ovalbumin and RNase B) were used for binding separation while non-glycoproteins including BSA, RNase A and crude cellular proteins were utilized as the controls. The clickable ligand, 3-(prop-2-ynyloxy carbonylamino)phenylboronic acid (PCAPBA) and PCAPBA-Sepharose showed the more stable after long storage time (> 6 months) as shown in Figure 7.4. Our finding displayed that the clicked Sepharose possessed the high specific binding to glycoprotein as compared to the non-clicked Sepharose particles (Figure 7.5). To investigate the efficiency of glycoprotein separation from non-glycoproteins, the clicked Sepahrose was mixed with a solution mixture of the glycoproteins and the non-glycoproteins. It was clearly demonstrated that the clicked Sepharose could effectively separate the two glycoproteins from closely related non-glycoproteins in the absence and presence of crude cellular extract (Figure 7.6-7.13). Thus, new boronic acid derivative can be applied not only to improve glycoprotein separation in other formats, but can also be used as an affinity ligand to develop new chemical sensors for analysis of other glycated compounds. The notion should be made that this clickable boronic acid particles open up a new version of sorting for glycated and glycosylated bioactive molecules including proteins, metabolites and antioxidative compounds.

8.4. Further perspectives

All knowledge obtained from this study may be used to apply for designing superoxide radical scavengers and for extracting vitamins and bioactive compounds from natural resources and synthetic cocktails. Our metal complexes particularly those generated from nicotinic and aromatic carboxylic acids mimic potent SOD activity and antimicrobial activity. Further task then can be further synthesized more bioactive metal complex from other vitamins and general biometabolites. This will further develop more value-added metallovitamin-based therapeutic agents to

benefit the living host of unnecessary introduction of foreign unwanted chemicals to the body.

In molecular imprinting, the binding capabilities (imprinting factor) of the polymers remain unsatisfactory. However, the processes of imprinting for vitamin E will be maximized on most of the facets on polymerization condition, functional monomer, crosslinker, porogen, etc. Specific imprinting polymers for other vitamins and bioactive compounds for antioxidation are also included in the future plan.

Clickable boronic acid ligand and click chemistry are fantastic to be applied for separation of other molecules containing glycated and glycosylated residues, such as natural antioxidative agents.

REFERENCES

1. Afonso V, Champy R, Mitrovic D, Collin P, Lomri A. Reactive oxygen species and superoxide dismutases: Role in joint diseases. Joint Bone Spine. 2007;74(4):324-9.
2. Valko M, Leibfritz D, Moncol J, Cronin MTD, Mazur M, Telser J. Free radicals and antioxidants in normal physiological functions and human disease. The International Journal of Biochemistry & Cell Biology. 2007;39(1):44-84.
3. Xi H, Akishita M, Nagai K, Yu W, Hasegawa H, Eto M, et al. Potent free radical scavenger, edaravone, suppresses oxidative stress-induced endothelial damage and early atherosclerosis. Atherosclerosis. 2007;191(2):281-9.
4. Fearon IM, Faux SP. Oxidative stress and cardiovascular disease: Novel tools give (free) radical insight. Journal of Molecular and Cellular Cardiology. 2009;47(3):372-81.
5. Valko M, Rhodes CJ, Moncol J, Izakovic M, Mazur M. Free radicals, metals and antioxidants in oxidative stress-induced cancer. Chemico-Biological Interactions. 2006;160(1):1-40.
6. Almeida IF, Amaral MH, Costa PC, Bahia MF, Valentão P andrade PB, et al. Oak leaf extract as topical antioxidant: Free radical scavenging and iron chelating activities and in vivo skin irritation potential. BioFactors. 2008;33(4):267-79.
7. Rattan SIS. Theories of biological aging: Genes, proteins and free radicals. Free Radical Research. 2006;40(12):1230-8.
8. Supinski GS, Callahan LA. Free radical-mediated skeletal muscle dysfunction in inflammatory conditions. J Appl Physiol. 2007 May 1, 2007;102(5): 2056-63.
9. Dröge W. Redox regulation in anabolic and catabolic processes. Current Opinion in Clinical Nutrition & Metabolic Care. 2006;9(3):190-5.

10. Starkov AA. The Role of Mitochondria in Reactive Oxygen Species Metabolism and Signaling. Annals of the New York Academy of Sciences. 2008;1147(1):37-52.
11. Berner RA, VandenBrooks JM, Ward PD. Evolution: Oxygen and Evolution. Science. 2007 April 27, 2007;316(5824):557-8.
12. Falkowski PG, Katz ME, Milligan AJ, Fennel K, Cramer BS, Aubry MP, et al. The Rise of Oxygen over the Past 205 Million Years and the Evolution of Large Placental Mammals. Science. 2005 September 30, 2005;309(5744): 2202-4.
13. Raymond J, Segre D. The Effect of Oxygen on Biochemical Networks and the Evolution of Complex Life. Science. 2006 March 24, 2006;311(5768): 1764-7.
14. Shiva S. Mitochondria as metabolizers and targets of nitrite. Nitric Oxide. 2010;22(2):64-74.
15. Ji LL. Modulation of skeletal muscle antioxidant defense by exercise: Role of redox signaling. Free Radical Biology and Medicine. 2008;44(2):142-52.
16. Uttara B, Singh AV, Zamboni P, Mahajan RT. Oxidative stress and neurodegenerative diseases: a review of upstream and downstream antioxidant therapeutic options. Curr Neuropharmacol. 2009;7(1): 65-74.
17. Smith MW, Doolittle RF. A comparison of evolutionary rates of the two major kinds of superoxide dismutase. Journal of Molecular Evolution. 1992; 34(2):175-84.
18. Perry JJP, Shin DS, Getzoff ED, Tainer JA. The structural biochemistry of the superoxide dismutases. Biochimica et Biophysica Acta (BBA) - Proteins & Proteomics. 2010;1804(2):245-62.
19. Osman R, Basch H. On the mechanism of action of superoxide dismutase: a theoretical study. Journal of the American Chemical Society. 1984;106(19):5710-4.
20. Harris PL, Quaife ML, Swanson WJ. Vitamin E Content of Foods. J Nutr. 1950;40(3):367-81.

21. Kayden H, Traber M. Absorption, lipoprotein transport and regulation of plasma concentrations of vitamin E in humans. J Lipid Res. 1993;34(3):343-58.
22. Clarke MW, Burnett JR, Croft KD. Vitamin E in Human Health and Disease. Critical Reviews in Clinical Laboratory Sciences. 2008;45(5):417-50.
23. Dimitrios B. Sources of natural phenolic antioxidants. Trends in Food Science & Technology. 2006;17(9):505-12.
24. Huang C-C, Fang J-Y, Wu W-B, Chiang H-S, Wei Y-J, Hung C-F. Protective effects of (−)-epicatechin-3-gallate on UVA-induced damage in HaCaT keratinocytes. Archives of Dermatological Research. 2005;296(10): 473-81.
25. Leong AC-N, Kinjo Y, Tako M, Iwasaki H, Oku H, Tamaki H. Flavonoid glycosides in the shoot system of Okinawa Taumu (Colocasia esculenta S.). Food Chemistry. 2010;119(2):630-5.
26. Hollman PCH, Bijsman MNCP, van Gameren Y, Cnossen EPJ, de Vries JHM, Katan MB. The sugar moiety is a major determinant of the absorption of dietary flavonoid glycosides in man. Free Radical Research. 1999;31(6): 569-73.
27. Moon YJ, Wang X, Morris ME. Dietary flavonoids: effects on xenobiotic and carcinogen metabolism. Toxicol In Vitro. 2006;20(2):187-210.
28. Olthof MR, Hollman PCH, Katan MB. Chlorogenic Acid and Caffeic Acid Are Absorbed in Humans. J Nutr. 2001;131(1):66-71.
29. Ross JA, Kasum CM. Dietary flavonoids: bioavailability, metabolic effects and safety. Annu Rev Nutr. 2002;22:19-34.
30. Stobiecki M. Application of mass spectrometry for identification and structural studies of flavonoid glycosides. Phytochemistry. 2000;54(3):237-56.
31. Diguiseppi J, Fridovich I. Putative superoxide dismutase activity of iron-EDTA: A reexamination. Arch Biochem Biophy. 1980;203(1):145-50.
32. Gauter-Fleckenstein B, Fleckenstein K, Owzar K, Jiang C, Batinic-Haberle I, Vujaskovic Z. Comparison of two Mn porphyrin-based mimics of superoxide dismutase in pulmonary radioprotection. Free Radical Biology and Medicine. 2008;44(6):982-9.

33. Doctrow SR, Huffman K, Marcus CB, Tocco G, Malfroy E, Adinolfi CA, et al. Salen−Manganese Complexes as Catalytic Scavengers of Hydrogen Peroxide and Cytoprotective Agents: Structure−Activity Relationship Studies. J Med Chem. 2002;45(20):4549-58.
34. Harper H, Rodwell V, Mayes P. Review of Physiological Chemistry. J Am Med Assoc. 1952;148(6):499-b-.
35. Sharman IM. Vitamins: essential dietary constituents discovered. Endeavour. 1977;1(3-4):97-102.
36. Rosenfeld L. Vitamine-vitamin: The early years of discovery. Clin Chem. 1997; 43(4):680-5.
37. Bogan KL, Brenner C. Nicotinic Acid, Nicotinamide and Nicotinamide Riboside: A Molecular Evaluation of NAD+ Precursor Vitamins in Human Nutrition. Annu Rev Nutr. 2008;28(1):115-30.
38. Benavente CA, Jacobson MK, Jacobson EL. NAD in Skin: Therapeutic Approaches for Niacin. Current Pharmaceutical Design. 2009;15:29-38.
39. Basu TK, Donaldson D. Intestinal absorption in health and disease: micronutrients. Best Practice & Research Clinical Gastroenterology. 2003;17(6):957-79.
40. Moffett JR, Namboodiri MAA. Tryptophan and the immune response. Immunol Cell Biol. 2003;81(4):247-65.
41. Xu P, Sauve AA. Vitamin B3, the nicotinamide adenine dinucleotides and aging. Mechanisms of Ageing and Development. 2010;131(4):287-98.
42. Yang T, Chan NY-K, Sauve AA. Syntheses of nicotinamide riboside and derivatives: effective agents for increasing nicotinamide adenine dinucleotide concentrations in mammalian cells. J Med Chem. 2007; 50(26):6458-61.
43. Chapman MJ. How does nicotinic acid modify the lipid profile? Eur Heart J Suppl. 2006;8(suppl F):F54-F9.
44. Coggan SE, Smythe GA, Bilgin A, Grant RS. Age and circadian influences on picolinic acid concentrations in human cerebrospinal fluid. J Neurochem. 2009;108:1220-5.

45. You Z-L, Zhang L, Shi D-H, Ni L-L. Synthesis and crystal structure of a novel one-dimensional silver(I) complex with high urease inhibitory activity. Inorg Chem Commu. 2009;12(12):1231-3.
46. Abdullah A, Huq F, Chowdhury A, Tayyem H, Beale P, Fisher K. Studies on the synthesis, characterization, binding with DNA and activities of two cis-planaramineplatinum(II) complexes of the form: cis-PtL(NH3)Cl2 where L = 3-hydroxypyridine and 2,3-diaminopyridine. BMC Chem Bio. 2006; 6(1):3.
47. Lv Z, Sheng C, Wang T, Zhang Y, Liu J, Feng J, et al. Design, synthesis and antihepatitis B virus activities of novel 2-pyridone derivatives. J Med Chem. 2009;53(2):660-8.
48. Hopkins AL, Clarke J. Episodic cerebellar dysfunction in a bichon frise: a canine case of episodic ataxia? Journal of Small Animal Practice. 2010;51(8):444-6.
49. Odenike O, Larson R, Gajria D, Dolan M, Delaney S, Karrison T, et al. Phase I study of the ribonucleotide reductase inhibitor 3-aminopyridine-2-carboxaldehyde-thiosemicarbazone (3-AP) in combination with high dose cytarabine in patients with advanced myeloid leukemia. Investigational New Drugs. 2008;26(3):233-9.
50. Štastná M, Trávníček M, Šlais K. New azo dyes as colored isoelectric point markers for isoelectric focusing in acidic pH region. Electrophoresis. 2005;26(1):53-9.
51. Acker R-d, Hamprecht G. Preparation of 2-aminopyridine derivatives. United States Patent 4395555. 1983.
52. Carlucci G, Colanzi A, Mazzeo P, Quaglia MG. Determination of 2-aminopyridine in piroxicam by derivative UV-spectrophotometry. International J Pharm. 1989;53(3):257-9.
53. Dickson S, Paterson M, Willans C anderson K, Steed J. Anion Binding and Luminescent Sensing using Cationic Ruthenium(II) Aminopyridine Complexes. Chemistry – A European Journal. 2008;14(24):7296-305.
54. Hossain B, Islam MS, Hassan N, Yousuf MA, Salam MA. Antifungal activity of mixed ligand transition metal complexes of some dibasic acid and

heterocyclic bases. Daffodil International University Journal of Science and Technology. 2009;4(21):57-9.

55. Chi J. Phthalate acid esters in Potamogeton crispus L from Haihe River, China. Chemosphere. 2009;77(1):48-52.

56. Dinarello CA. Anti-inflammatory Agents: Present and Future. Cell. 2010;140(6): 935-50.

57. Zhang C, Sun A, Zhang P, Wu C, Zhang S, Fu M, et al. Aspirin for primary prevention of cardiovascular events in patients with diabetes: A meta-analysis. Diabetes Research and Clinical Practice. 2010;87(2):211-8.

58. Mahdi JG, Mahdi AJ, Bowen ID. The historical analysis of aspirin discovery, its relation to the willow tree and antiproliferative and anticancer potential. Cell Proliferation. 2006;39(2):147-55.

59. Djurendić E, Dojčinović-Vujašković S, Sakač M, Jovin E, Kojić V, Bogdanović G, et al. X-ray structural analysis, antioxidant and cytotoxic activity of newly synthesized salicylic acid derivatives. Structural Chemistry. 2010; 21(1):67-78.

60. McLauchlan CC, Hooker JD, Jones MA, Dymon Z, Backhus EA, Greiner BA, et al. Inhibition of acid, alkaline and tyrosine (PTP1B) phosphatases by novel vanadium complexes. J Inorg Biochem. 2010;104(3):274-81.

61. Lycka A, Lustinec D, Holecek J, Nádvorník M, Holcapek M. ^{27}Al, ^{15}N, ^{13}C and ^{1}H NMR spectra and negative-ion electrospray mass spectra of the 2:1 aluminium(III) complexes of azo dyes derived from anthranilic acid. Dyes and Pigments. 2001;50(3):203-9.

62. Chaskes S, Tyndall RL. Pigmentation and autofluorescence of Cryptococcus species after growth on tryptophan and anthranilic acid media. Mycopathologia. 1978;64(2):105-12.

63. Vaclavik VA, Christian EW. Sugars, Sweeteners and Confections. Essentials of Food Science: Springer New York; 2008. p. 331-48.

64. Breslow R. Binding and catalysis with flexible locks and flexible keys 1. Supramolecular Chemistry. 1995;6(1):41 - 7.

65. Piletsky SA, Panasyuk TL, Piletskaya EV, Nicholls IA, Ulbricht M. Receptor and transport properties of imprinted polymer membranes-a review. J Mem Sci. 1999;157(2):263-78.

66. Haupt K, Mosbach K. Molecularly Imprinted Polymers and Their Use in Biomimetic Sensors. Chem Rev. 2000;100(7):2495-504.

67. Rajkumar R, Warsinke A, Möhwald H, Scheller FW, Katterle M. Development of fructosyl valine binding polymers by covalent imprinting. Biosen Bioelec. 2007;22(12):3318-25.

68. Zhang H, Ye L, Mosbach K. Non-covalent molecular imprinting with emphasis on its application in separation and drug development. J Mol Recogn. 2006;19(4):248-59.

69. Ou J, Dong J, Tian T, Hu J, Ye M, Zou H. Enantioseparation of tetrahydropalmatine and Tröger's base by molecularly imprinted monolith in capillary electrochromatography. J Biochem Biophys Methods. 2007; 70(1):71-6.

70. Weiss R, Molinelli A, Jakusch M, Mizaikoff B. Molecular imprinting and solid phase extraction of flavonoid compounds. Bioseparation. 2001;10(6):379-87.

71. Greene NT, Shimizu KD. Colorimetric Molecularly Imprinted Polymer Sensor Array using Dye Displacement. J Am Chem Soc. 2005;127(15):5695-700.

72. Tong K, Xiao S, Li S, Wang J. Molecular Recognition and Catalysis by Molecularly Imprinted Polymer Catalysts: Thermodynamic and Kinetic Surveys on the Specific Behaviors. Journal of Inorganic and Organometallic Polymers and Materials. 2008;18(3):426-33.

73. Rathbone DL. Molecularly imprinted polymers in the drug discovery process. Advanced Drug Delivery Reviews. 2005;57(12):1854-74.

74. Ye L, Haupt K. Molecularly imprinted polymers as antibody and receptor mimics for assays, sensors and drug discovery. Anal Bioanal Chem. 2004;378(8):1887-97.

75. Ye L, Mosbach K. Molecular imprinting: Synthetic materials as substitutes for biological antibodies and receptors. Chem Mater. 2008;20(3):859-68.

76. Regev R, Katzir H, Yeheskely-Hayon D, Eytan GD. Modulation of P-glycoprotein-mediated multidrug resistance by acceleration of passive drug permeation across the plasma membrane. FEBS J. 2007;274(23): 6204-14.

77. Hocking AM, Shinomura T, McQuillan DJ. Leucine-rich repeat glycoproteins of the extracellular matrix. Matrix Biol. 1998;17(1):1-19.

78. Miller DS, Bauer B, Hartz AMS. Modulation of P-glycoprotein at the blood-brain barrier: opportunities to Improve central nervous system pharmacotherapy. Pharmacological Reviews. 2008;60(2):196-209.

79. Gamblin DP, Scanlan EM, Davis BG. Glycoprotein Synthesis: An Update. Chem Rev. 2008;109(1):131-63.

80. Olofsson S, Bergström T. Glycoconjugate glycans as viral receptors. Annals of Medicine. 2005;37(3):154-72.

81. Warren JD, Miller JS, Keding SJ, Danishefsky SJ. Toward fully synthetic glycoproteins by ultimately convergent routes: A solution to a long-standing problem. J Am Chem Soc. 2004;126(21):6576-8.

82. Yang X, Su K, Roos MD, Chang Q, Paterson AJ, Kudlow JE. O-linkage of N-acetylglucosamine to Sp1 activation domain inhibits its transcriptional capability. Proceedings of the National Academy of Sciences of the United States of America. 2001;98(12):6611-6.

83. Arnold JN, Wormald MR, Sim RB, Rudd PM, Dwek RA. The Impact of Glycosylation on the Biological Function and Structure of Human Immunoglobulins. Annu Rev Immunol. 2007;25(1):21-50.

84. Brockmann E-C, Vehniäinen M, Pettersson K. Use of high-capacity surface with oriented recombinant antibody fragments in a 5-min immunoassay for thyroid-stimulating hormone. Anal Biochem. 2010;396(2):242-9.

85. Dierich A, Sairam MR, Monaco L, Fimia GM, Gansmuller A, LeMeur M, et al. Impairing follicle-stimulating hormone (FSH) signaling in vivo: Targeted disruption of the FSH receptor leads to aberrant gametogenesis and hormonal imbalance. Proceedings of the National Academy of Sciences of the United States of America. 1998;95(23):13612-7.

86. van Koppen C, Zaman G, Timmers C, Kelder J, Mosselman S, van de Lagemaat R, et al. A signaling-selective, nanomolar potent allosteric low molecular weight agonist for the human luteinizing hormone receptor. Naunyn-Schmiedeberg's Archives of Pharmacology. 2008;378(5):503-14.
87. Ebe Y, Kuno A, Uchiyama N, Koseki-Kuno S, Yamada M, Sato T, et al. Application of lectin microarray to crude samples: differential glycan profiling of lec mutants. J Biochem. 2006;139(3):323-7.
88. Ohtsubo K, Marth JD. Glycosylation in Cellular Mechanisms of Health and Disease. Cell. 2006;126(5):855-67.
89. Liu XC, Scouten WH. Boronate affinity chromatography. Methods in molecular biology. 2000;147:119-28.
90. Liu S, Bakovic L, Chen A. Specific binding of glycoproteins with poly(aniline boronic acid) thin film. J Electroanal Chem. 2006;591(2):210-6.
91. Preinerstorfer B, Lämmerhofer M, Lindner W. Synthesis and application of novel phenylboronate affinity materials based on organic polymer particles for selective trapping of glycoproteins. J Sep Sci. 2009;32(10):1673-85.
92. Ren L, Liu Z, Dong M, Ye M, Zou H. Synthesis and characterization of a new boronate affinity monolithic capillary for specific capture of cis-diol-containing compounds. J Chrom A. 2009;1216(23):4768-74.
93. Liu X-C. Boronic Acids as Ligands for Affinity Chromatography. Chinese J Chrom. 2006;24(1):73-80.
94. Kolb HC, Finn MG, Sharpless KB. Click chemistry: diverse chemical function from a few good reactions. Angew Chem Int Ed. 2001;40(11):2004-21.
95. Kolb HC, Sharpless KB. The growing impact of click chemistry on drug discovery. Drug Discovery Today. 2003;8(24):1128-37.
96. Hein C, Liu X-M, Wang D. Click Chemistry, A Powerful Tool for Pharmaceutical Sciences. Pharm Res. 2008;25(10):2216-30.
97. Helms B, Mynar JL, Hawker CJ, Fréchet JMJ. Dendronized Linear Polymers via "Click Chemistry". J Am Chem Soc. 2004;126(46):15020-1.
98. Michel O, Ravoo BJ. Carbohydrate Microarrays by Microcontact "Click" Chemistry. Langmuir. 2008;24(21):12116-8.

99. O'Reilly RK, Joralemon MJ, Wooley KL, Hawker CJ. Functionalization of Micelles and Shell Cross-linked Nanoparticles Using Click Chemistry. Chem Mater. 2005;17(24):5976-88.

100. Tron GC, Pirali T, Billington RA, Canonico PL, Sorba G, Genazzani AA. Click chemistry reactions in medicinal chemistry: Applications of the 1,3-dipolar cycloaddition between azides and alkynes. Med Res Rev. 2008;28(2):278-308.

101. Friesner RA. Ab initio quantum chemistry: Methodology and applications. Proceedings of the National Academy of Sciences of the United States of America. 2005;102(19):6648-53.

102. Ramachandran KI, Gopakumar D, Namboori K. Quantum Mechanics: A Brief Introduction. Computational Chemistry and Molecular Modeling: Springer Berlin Heidelberg; 2008. p. 37-52.

103. Depeint F, Bruce WR, Shangari N, Mehta R, O'Brien PJ. Mitochondrial function and toxicity: Role of the B vitamin family on mitochondrial energy metabolism. Chemico-Biological Interactions. 2006;163(1-2):94-112.

104. Hageman GJ, Stierum RH. Niacin, poly(ADP-ribose) polymerase-1 and genomic stability. Mutation Research - Fundamental and Molecular Mechanisms of Mutagenesis. 2001;475(1-2):45-56.

105. Carlson LA. Nicotinic acid: The broad-spectrum lipid drug: A 50th anniversary review. Journal of Internal Medicine. 2005;258(2):94-114.

106. Kamanna VS, Kashyap ML. Mechanism of Action of Niacin. Am J Cardiol. 2008;101(8 SUPPL. 1).

107. Gross MD. Lipids, Oxidation and Cardiovascular Disease. In: Holtzman JL, editor. Atherosclerosis and Oxidant Stress: Springer US; 2008. p. 79-95.

108. Spasojević I, Chen Y, Noel TJ, Yu Y, Cole MP, Zhang L, et al. Mn porphyrin-based superoxide dismutase (SOD) mimic, MnIIITE-2-PyP5+, targets mouse heart mitochondria. Free Radical Biology and Medicine. 2007;42(8):1193-200.

109. Piacham T, Isarankura-Na-Ayudhya C, Nantasenamat C, Yainoy S, Ye L, Bülow L, et al. Metalloantibiotic Mn(II)-bacitracin complex mimicking

manganese superoxide dismutase. Biochem Biophys Res Commun. 2006; 341(4):925-30.

110. Singh R, Rao RSS. Synthesis and characterization of divalent manganese, cobalt, nickel, copper and zinc complexes with nicotinic acid. J Mol Struct. 1981;71(C):23-30.
111. El-Saadani MA, Nassar AY, El-Ela SHA, Metwally TH, Nafady AM. The protective effect of copper complexes against gastric mucosal ulcer in rats. Biochem Pharm. 1993;46(6):1011-8.
112. Salama RHM, Nassar AYA, Nafady AAM, Mohamed HHT. A novel therapeutic drug (copper nicotinic acid complex) for non-alcoholic fatty liver. Liver Int. 2007;27(4):454-64.
113. Huh HS, Lee SW. Copper coordination polymers containing pyridinecarboxylate and multicarboxylate: $[Cu_{1.5}(ina)(btcH)]\bullet H_2O$, $[Cu_2(ina)_2(bdc)_{0.5}(\mu 3\text{-}OH)]$ and [Cu(ina)(na)] (inaH=4-pyridinecarboxylic acid, $btcH_3$=1,3,5-benzene tricarboxylic acid, $bdcH_2$ = 1,3-benzenedicarboxylic acid, naH = 3-pyridinecarboxylic acid). J Mol Struct. 2007;829(1-3):44-50.
114. Yeh C-W, Suen M-C, Hu H-L, Chen J-D, Wang J-C. Synthesis and structural characterization of two new chiral coordination polymers of $Cu(nicotinate)_2(H_2O)$ and $Co(nicotinate)_2$. Polyhedron. 2004;23(11): 1947-52.
115. Dutta S, Padhye S, McKee V. Structural characterization and SOD activity of copper-oxaprozinate. Inorg Chem Commun. 2004;7(9):1071-4.
116. Kostyuk VA, Potapovich AI, Strigunova EN, Kostyuk TV, Afanas'ev IB. Experimental evidence that flavonoid metal complexes may act as mimics of superoxide dismutase. Arch Biochem Biophys. 2004;428(2):204-8.
117. Mahal HS, Kapoor S, Satpati AK, Mukherjee T. Radical scavenging and catalytic activity of metal-phenolic complexes. J Phys Chem B. 2005; 109(50):24197-202.
118. Devereux M, O'Shea D, O'Connor M, Grehan H, Connor G, McCann M, et al. Synthesis, catalase, superoxide dismutase and antitumour activities of copper(II) carboxylate complexes incorporating benzimidazole, 1,10-phenanthroline and bipyridine ligands: X-ray crystal structures of

[$Cu(BZA)_2(bipy)(H_2O)$], [$Cu(SalH)_2(BZDH)_2$] and [$Cu(CH_3COO)_2$(5,6-DMBZDH)$_2$] ($SalH_2$ = salicylic acid; BZAH = benzoic acid; BZDH = benzimidazole and 5,6-DMBZDH = 5,6-dimethylbenzimidazole). Polyhedron 2007;26:4073-84.

119. Harris RM, Hawker RJ, Langman MJS, Singh S, Waring RH. Inhibition of phenolsulphotransferase by salicylic acid: A possible mechanism by which aspirin may reduce carcinogenesis. Gut. 1998;42(2):272-5.
120. Schindler U, Strobel H, Schönafinger K, Linz W, Ľohn M, Martorana PA, et al. Biochemistry and pharmacology of novel anthranilic acid derivatives activating heme-oxidized soluble guanylyl cyclase. Mol Pharm. 2006; 69(4):1260-8.
121. Bo S, Durazzo M, Gambino R, Berutti C, Milanesio N, Caropreso A, et al. Associations of dietary and serum copper with inflammation, oxidative stress and metabolic variables in adults. J Nutr. 2008;138(2):305-10.
122. Olivares M, Uauy R. Copper as an essential nutrient. Am J Clin Nutr. 1996; 63(5).
123. Koca E, Buyukasik Y, Cetiner D, Yilmaz R, Sayinalp N, Yasavul U, et al. Copper deficiency with increased hematogones mimicking refractory anemia with excess blasts. Leukemia Res. 2008;32(3):495-9.
124. Twomey PJ, Reynolds TM, Wierzbicki AS, Viljoen A. The relationship between serum copper and ceruloplasmin in routine clinical practice. International J Clin Pract. 2008;62(3):485-7.
125. Cramer CJ. Essentials of Computational Chemistry: Theories and Models. 2nd ed. West Sussex, U.K: John Wiley & Sons, Ltd; 2004.
126. Karawajczyk A, Drgan V, Medic N, Oboh G, Passamonti S, Novič M. Properties of flavonoids influencing the binding to bilitranslocase investigated by neural network modelling. Biochem Pharm. 2007;73(2):308-20.
127. Nantasenamat C, Isarankura-Na-Ayudhya C, Naenna T, Prachayasittikul V. Prediction of bond dissociation enthalpy of antioxidant phenols by support vector machine. J Mol Graph Model. 2008;27(2):188-96.

128. Cabelli DE, Guan Y, Leveque V, Hearn AS, Tainer JA, Nick HS, et al. Role of tryptophan 161 in catalysis by human manganese superoxide dismutase. Biochem. 1999;38(36):11686-92.

129. Prachayasittikul S, Suksrichavalit T, Isarankura-Na-Ayudhya C, Ruchirawat S, Prachayasittikul V. Antimicrobial and antioxidative activities of 1-adamantylthio derivatives of 3-substituted pyridines. EXCLI J. 2008; 7:63-70.

130. Dennington R, Keith T, Millam J, Eppinnett K, Hovell WL, Gilliland R. GaussView, version 3.09; Semichem, Inc, Shawnee Mission, KS, 2003.

131. Stephens PJ, Devlin FJ, Chabalowski CF, Frisch MJ. Ab Initio calculation of vibrational absorption and circular dichroism spectra using density functional force fields. Journal of Physical Chemistry®. 1994;98(45): 11623-7.

132. Hay PJ, Wadt WR. Ab initio effective core potentials for molecular calculations. Potentials for the transition metal atoms Sc to Hg. J Chem Phys. 1985; 82(1):270-83.

133. Hay PJ, Wadt WR. Ab initio effective core potentials for molecular calculations. Potentials for K to Au including the outermost core orbitale. J Chem Phys. 1985;82(1):299-310.

134. Wadt WR, Hay PJ. Ab initio effective core potentials for molecular calculations. Potentials for main group elements Na to Bi. J Chem Phys. 1985;82(1): 284-98.

135. Frisch MJ, Trucks GW, Schlegel HB, Scuseria GE, Robb MA, Cheeseman JR, Montgomery J, Pople JA. (2004) Gaussian 03, Revision C.02. Gaussian, Inc., Wallingford, CT.

136. Foresman JB, Frisch A. Exploring Chemistry with Electronic Structure Methods. Gaussian I, editor. Pittsburgh2000.

137. Han P, Chen CQ, Zhang CL, Song KK, Zhou HT, Chen QX. Inhibitory effects of 4-chlorosalicylic acid on mushroom tyrosinase and its antimicrobial activities. Food Chemistry. 2008;107(2):797-803.

138. De-Oliveira G, Martin JML, De Proft F, Geerlings P. Electron affinities of the first- and second-row atoms: Benchmark ab initio and density-functional

calculations. Physical Review A - Atomic, Molecular and Optical Physics. 1999;60(2):1034-45.

139. Ji HF, Zhang HY. A Theoretical Study on Cu(II) Binding Modes and Antioxidant Activity of Mammalian Normal Prion Protein. Chemical Research in Toxicology. 2004;17(4):471-5.
140. Ji HF, Zhang HY. A new strategy to combat Alzheimer's disease. Combining radical-scavenging potential with metal-protein-attenuating ability in one molecule. Bioorganic and Medicinal Chemistry Letters. 2005;15(1):21-4.
141. Shen L, Zhang HY, Ji HF. Computational note on the SOD-like antioxidant potential of nicotine-copper(II) complexes. J Mol Struct: THEOCHEM. 2007;817(1-3):161-2.
142. Branco RJF, Fernandes PA, Ramos MJ. Density-functional calculations of the Cu, Zn superoxide dismutase redox potential: The influence of active site distortion. J Mol Struct: THEOCHEM. 2005;729(1-2 SPEC. ISS.):141-6.
143. Branco RJF, Fernandes PA, Ramos MJ. Cu, Zn Superoxide dismutase: Distorted active site binds substrate without significant energetic cost. Theoretical Chemistry Accounts. 2006;115(1):27-31.
144. Karelson M, Lobanov VS, Katritzky AR. Quantum-chemical descriptors in QSAR/QSPR studies. Chem Rev. 1996;96(3):1027-43.
145. Guo P, Chen W, Song J, Cao W, Tian C. A DFT study of the interaction between butein anion and metal cations (M = Mg^{2+}, Cr^{2+}, Fe^{2+} and Cu^{2+}): Taking an insight into its chelating property. J Mol Struct: THEOCHEM. 2008;849(1-3):33-6.
146. Sun R, Ge J, Yao J, Li S, Shen H, Gu R. Predicting the binding capability of benzothiazoline-2-thione and its derivatives with gold: A DFT and FT-Raman combined studies. Spectrochimica Acta - Part A: Mol Biomol Spect. 2008;71(4):1535-9.
147. Li QX, Luo QH, Li YZ, Shen MC. A study on the mimics of Cu-Zn superoxide dismutase with high activity and stability: Two copper(II) complexes of 1,4,7-triazacyclononane with benzimidazole groups. Dalton Transactions. 2004(15):2329-35.

148. Garbutt JT, Morehouse AL, Hanson AM. Feed additives: Metal binding properties of bacitracin. Journal of Agricultural and Food Chemistry. 1961;9(4):285-9.

149. Banerjee A, Dasgupta N, De B. In vitro study of antioxidant activity of Syzygium cumini fruit. Food Chem. 2005;90(4):727-33.

150. Sakurai T, He G, Matsuzawa A, Yu GY, Maeda S, Hardiman G, et al. Hepatocyte Necrosis Induced by Oxidative Stress and IL-1α Release Mediate Carcinogen-Induced Compensatory Proliferation and Liver Tumorigenesis. Cancer Cell. 2008;14(2):156-65.

151. Cathcart MK. Regulation of Superoxide Anion Production by NADPH Oxidase in Monocytes/Macrophages: Contributions to Atherosclerosis. Arteriosclerosis, Thrombosis and Vascular Biology. 2004;24(1):23-8.

152. Andreadis AA, Hazen SL, Comhair SAA, Erzurum SC. Oxidative and nitrosative events in asthma. Free Radical Biology and Medicine. 2003;35(3):213-25.

153. Emerit J, Edeas M, Bricaire F. Neurodegenerative diseases and oxidative stress. Biomedicine and Pharmacotherapy. 2004;58(1):39-46.

154. Hearn AS, Tu C, Nick HS, Silverman DN. Characterization of the product-inhibited complex in catalysis by human manganese superoxide dismutase. Journal of Biological Chemistry. 1999;274(35):24457-60.

155. Wang Y, Yang ZY, Wang BD. Synthesis, characterization and anti-oxidative activity of cobalt(II), nickel(II) and iron(II) Schiff base complexes. Transition Metal Chemistry. 2005;30(7):879-83.

156. Suksrichavalit T, Prachayasittikul S, Piacham T, Isarankura-Na-Ayudhya C, Nantasenamat C, Prachayasittikul V. Copper Complexes of Nicotinic-Aromatic Carboxylic Acids as Superoxide Dismutase Mimetics. Molecules. 2008;13(12):3040-56.

157. Bodor ET, Offermanns S. Nicotinic acid: An old drug with a promising future. British Journal of Pharmacology. 2008;153(SUPPL. 1).

158. Brown BG, Zhao XQ. Nicotinic Acid, Alone and in Combinations, for Reduction of Cardiovascular Risk. American Journal of Cardiology. 2008;101(8 SUPPL. 1).

159. Aggett PJ, Fenwick PK, Kirk H. An in vitro study of the effect of picolinic acid on metal translocation across lipid bilayers. Journal of Nutrition. 1989; 119(10):1432-7.

160. Heffernan MP, Nelson MM, Anadkat MJ. A pilot study of the safety and efficacy of picolinic acid gel in the treatment of acne vulgaris. British Journal of Dermatology. 2007;156(3):548-52.

161. Shrivastava R, Nagar R, Ravishankar GA, Upreti RK, Chaturvedi UC. Effect of pretreatment with chromium picolinate on haematological paramters during dengue virus infection in mice. Indian Journal of Medical Research. 2007;126(5):440-6.

162. Abe S, Hu W, Ishibashi H, Hasumi K, Yamaguchi H. Augmented inhibition of Candida albicans growth by murine neutrophils in the presence of a tryptophan metabolite, picolinic acid. Journal of Infection and Chemotherapy. 2004;10(3):181-4.

163. Tomioka H, Shimizu T, Tatano Y. Effects of picolinic acid on the antimicrobial functions of host macrophages against Mycobacterium avium complex. International Journal of Antimicrobial Agents. 2007;29(4):460-4.

164. Fernandez-Pol JA, Klos DJ, Hamilton PD. Antiviral, cytotoxic and apoptotic activities of picolinic acid on human immunodeficiency virus-1 and human herpes simplex virus-2 infected cells. Anticancer Research. 2001;21(6 A):3773-6.

165. Mucci A, Varesio L, Neglia R, Colombari B, Pastorino S, Blasi E. Antifungal activity of macrophages engineered to produce IFN-γ: Inducibility by picolinic acid. Medical Microbiology and Immunology. 2003;192(2):71-8.

166. Rawson JM, Winpenny REP. The coordination chemistry of 2-pyridone and its derivatives. Coordination Chemistry Reviews. 1995;139:313-74.

167. Cheng H, Huq F, Beale P, Fisher K. Synthesis, characterization, activities, cell uptake and DNA binding of trinuclear complex: [{*trans*-$PtCl(NH_3)$}$_2$ μ-{*trans*-$Pt(NH_3)$(2-hydroxypyridine)-$(H_2N(CH_2)6NH_2)_2$]Cl_4. Eur J Med Chem. 2005;40(8):772-81.

168. Huq F, Tayyem H, Beale P, Yu JQ. Studies on the activity of three palladium(II) compounds of the form: *Trans*-PdL_2Cl_2 where L = 2-hydroxypyridine,

3-hydroxypyridine and 4-hydroxypyridine. J Inorg Biochem. 2007;101(1): 30-5.

169. Zhao G, Lin H, Yu P, Sun H, Zhu S, Su X, et al. Ethylenediamine-palladium(II) complexes with pyridine and its derivatives: Synthesis, molecular structure and initial antitumor studies. J Inorg Biochem. 1999;73(3):145-9.
170. Hyvelin JM, Gautier M, Lemaire MC, Bonnet P, Eder V. Adaptative modifications of right coronary myocytes voltage-gated K+ currents in rat with hypoxic pulmonary hypertension. Pflugers Archiv Eur J Phys. 2009; 457(4):721-30.
171. Williams JLR, Fyfe GK, Sibley CP, Baker PN, Greenwood SL. K+ channel inhibition modulates the biochemical and morphological differentiation of human placental cytotrophoblast cells in vitro. American Journal of Physiology - Regulatory Integrative and Comparative Physiology. 2008;295(4).
172. Molgo J, Lemeignan M, Peradejordi F, Lechat P. Presynaptic effects of aminopyridines at the neuromuscular junction in vertebrates. Effects Presynaptiques Des Aminophyridines LA Junction Neuromusculaire De Vertebres. 1985;16(2):109-44.
173. Pashkov VN, Hemmings Jr HC. The effects of general anesthetics on norepinephrine release from isolated rat cortical nerve terminals. Anesthesia and Analgesia. 2002;95(5):1274-81.
174. Mohan G, Nagar R, Agarwal SC, Mehta KA, Rao CS. Syntheses and anti-inflammatory activity of diphenylamine-2,2′-dicarboxylic acid and its metal complexes. Journal of Enzyme Inhibition and Medicinal Chemistry. 2005;20(1):55-60.
175. Prachayasittikul S, Buraparuangsang P, Worachartcheewan A, Isarankura-Na-Ayudhya C, Ruchirawat S, Prachayasittikul V. Antimicrobial and antioxidative activities of bioactive constituents from Hydnophytum formicarum Jack. Molecules. 2008;13(4):904-21.

176. Thimmaiah KN, Lloyd WD, Chandrappa GT. Stereochemistry and fungitoxicity of complexes of p-anisaldehydethiosemicarbazone with Mn(II), Fe(II), Co(II) and Ni(II). Inorganica Chimica Acta. 1985;106(2):81-3.

177. Ahmed SM, Ismail DA. Synthesis and biological activity of 8-hydroxyquinoline and 2-hydroxypyridine quaternary ammonium salts. Journal of Surfactants and Detergents. 2008;11(3):231-5.

178. Lagutkin NA, Mitin NI, Zubairov MM, Dorokhov VA, Mikhailov BM. Antiviral activity of boron chelates obtained from 2-aminopyridine. Pharmaceutical Chemistry Journal. 1983;16(6):464-7.

179. Schepetkin I, Potapov A, Khlebnikov A, Korotkova E, Lukina A, Malovichko G, et al. Decomposition of reactive oxygen species by copper(II) bis(1-pyrazolyl) methane complexes. Journal of Biological Inorganic Chemistry. 2006;11(4):499-513.

180. Cappellani EP, Drouin SD, Jia G, Maltby PA, Morris RH, Schweitzer CT. Effect of the ligand and metal on the pKa values of the dihydrogen ligand in the series of complexes $[M(H_2)H(L)_2]^+$, M = Fe, Ru, Os, containing isosteric ditertiaryphosphine ligands. J Am Chem Soc. 1994;116(8):3375-88.

181. Bóka B, Myari A, Sóvágó I, Hadjiliadis N. Copper(II) and zinc(II) complexes of the peptides Ac-HisValHis-NH_2 and Ac-HisValGlyAsp-NH_2 related to the active site of the enzyme CuZnSOD. J Inorg Biochem. 2004;98(1):113-22.

182. Lonn E. Effects of long-term vitamin E supplementation on cardiovascular events and cancer: A randomized controlled trial. J Am Med Assoc. 2005; 293(11):1338-47.

183. Coulter ID, Hardy ML, Morton SC, Hilton LG, Tu W, Valentine D, et al. Antioxidants vitamin C and vitamin E for the prevention and treatment of cancer. Journal of General Internal Medicine. 2006;21(7):735-44.

184. Burton GW, Doba T, Gabe EJ, Hughes L, Lee FL, Prasad L, et al. Autoxidation of biological molecules 4 Maximizing the antioxidant activity of phenols. Journal of the American Chemical Society. 1985;107(24):7053-65.

185. Mustacich DJ, Bruno RS, Traber MG. Vitamin E. 2007. p. 1-21.

186. Neužil J, Witting PK, Stocker R. α-Tocopheryl hydroquinone is an efficient multifunctional inhibitor of radical-initiated oxidation of low density

lipoprotein lipids. Proceedings of the National Academy of Sciences of the United States of America. 1997;94(15):7885-90.

187. Nagao T, Kobayashi T, Hirota Y, Kitano M, Kishimoto N, Fujita T, et al. Improvement of a process for purification of tocopherols and sterols from soybean oil deodorizer distillate. Journal of Molecular Catalysis B: Enzymatic. 2005;37(1-6):56-62.
188. Martins PF, Batistella CB, Maciel-Filho R, Wolf-Maciel MR. Comparison of two different strategies for tocopherols enrichment using a molecular distillation process. Industrial and Engineering Chemistry Research. 2006;45(2):753-8.
189. Nagesha GK, Subramanian R, Udaya Sankar K. Processing of tocopherol and FA systems using a nonporous denser polymeric membrane. JAOCS, Journal of the American Oil Chemists' Society. 2003;80(4):397-402.
190. King JW, Favati F, Taylor SL. Production of tocopherol concentrates by supercritical fluid extraction and chromatography. Separation Science and Technology. 1996;31(13):1843-57.
191. Bergmann NM, Peppas NA. Molecularly imprinted polymers with specific recognition for macromolecules and proteins. Progress in Polymer Science (Oxford). 2008;33(3):271-88.
192. Ghasemzadeh N, Nyberg F, Hjertén S. Highly selective artificial gel antibodies for detection and quantification of biomarkers in clinical samples. I. Spectrophotometric approach to design the calibration curve for the quantification. Journal of Separation Science. 2008;31(22):3945-53.
193. Piacham T, Josell A, Arwin H, Prachayasittikul V, Ye L. Molecularly imprinted polymer thin films on quartz crystal microbalance using a surface bound photo-radical initiator. Analytica Chimica Acta. 2005;536(1-2):191-6.
194. Turiel E, Tadeo JL, Cormack PAG, Martin-Esteban A. HPLC imprinted-stationary phase prepared by precipitation polymerisation for the determination of thiabendazole in fruit. Analyst. 2005;130(12):1601-7.
195. Haginaka J. Molecularly imprinted polymers for solid-phase extraction. Analytical and Bioanalytical Chemistry. 2004;379(3):332-4.

196. Mosbach K, Yu Y andersch J, Ye L. Generation of new enzyme inhibitors using imprinted binding sites: The anti-idiotypic approach, a step toward the next generation of molecular imprinting. Journal of the American Chemical Society. 2001;123(49):12420-1.
197. Hillberg AL, Brain KR, Allender CJ. Molecular imprinted polymer sensors: Implications for therapeutics. Advanced Drug Delivery Reviews. 2005;57(12):1875-89.
198. Vlatakis G andersson LI, Muller R, Mosbach K. Drug assay using antibody mimics made by molecular imprinting. Nature. 1993;361(6413):645-7.
199. Hart BR, Shea KJ. Synthetic peptide receptors: Molecularly imprinted polymers for the recognition of peptides using peptide-metal interactions. Journal of the American Chemical Society. 2001;123(9):2072-3.
200. Boonpangrak S, Prachayasittikul V, Bülow L, Ye L. Molecularly imprinted polymer microspheres prepared by precipitation polymerization using a sacrificial covalent bond. J Appl Pol Sci. 2006;99(4):1390-8.
201. Boonpangrak S, Whitcombe MJ, Prachayasittikul V, Mosbach K, Ye L. Preparation of molecularly imprinted polymers using nitroxide-mediated living radical polymerization. Biosen Bioelec. 2006;22(3):349-54.
202. Allender CJ, Richardson C, Woodhouse B, Heard CM, Brain KR. Pharmaceutical applications for molecularly imprinted polymers. International J Pharm. 2000;195(1-2):39-43.
203. Sellergren B, Allender CJ. Molecularly imprinted polymers: A bridge to advanced drug delivery. Adv Drug Del Rev. 2005;57(12):1733-41.
204. Sellergren B, Karmalkar RN, Shea KJ. Enantioselective ester hydrolysis catalyzed by imprinted polymers. J Org Chem. 2000;65(13):4009-27.
205. Piacham T, Isarankura Na-Ayudhya C, Prachayasittikul V, Bülow L, Ye L. A polymer supported manganese catalyst useful as a superoxide dismutase mimic. Chem Commun (Cambridge, England). 2003(11):1254-5.
206. Wulff G. Enzyme-like catalysis by molecularly imprinted polymers. Chem Rev. 2002;102(1):1-27.
207. Ye L, Cormack PAG, Mosbach K. Molecularly imprinted monodisperse microspheres for competitive radioassay. Anal Commun. 1999;36(2):35-8.

208. Puoci F, Cirillo G, Curcio M, Iemma F, Spizzirri UG, Picci N. Molecularly imprinted solid phase extraction for the selective HPLC determination of α-tocopherol in bay leaves. Anal Chim Acta. 2007;593(2):164-70.
209. Faizal CKM, Kikuchi Y, Kobayashi T. Molecular imprinting targeted for α-tocopherol by calix-resorcarenes derivative in membrane scaffold prepared by phase inversion. J Mem Sci. 2009;334(1-2):110-6.
210. Faizal CKM, Kobayashi T. Tocopherol-targeted membrane adsorbents prepared by hybrid molecular imprinting. Pol Eng Sci. 2008;48(6):1085-93.
211. Puoci F, Cirillo G, Curcio M, Iemma F, Parisi OI, Castiglione M, et al. Molecularly imprinted polymers for α-tocopherol delivery. Drug Del. 2008;15(4):253-8.
212. Andersson LI. Application of molecular imprinting to the development of aqueous buffer and organic solvent based radioligand binding assays for (S)-propranolol. Anal Chem. 1996;68(1):111-7.
213. Haginaka J. Monodispersed, molecularly imprinted polymers as affinity-based chromatography media. J Chrom B: Analytical Technologies in the Biomedical and Life Sciences. 2008;866(1-2):3-13.
214. Yoshimatsu K, Reimhult K, Krozer A, Mosbach K, Sode K, Ye L. Uniform molecularly imprinted microspheres and nanoparticles prepared by precipitation polymerization: The control of particle size suitable for different analytical applications. Anal Chim Acta. 2007;584(1):112-21.
215. Cacho C, Turiel E, Martin-Esteban A, Pérez-Conde C, Cámara C. Characterisation and quality assessment of binding sites on a propazine-imprinted polymer prepared by precipitation polymerisation. J Chrom B: Analytical Technologies in the Biomedical and Life Sciences. 2004;802(2):347-53.
216. Sajonz P, Kele M, Zhong G, Sellergren B, Guiochon G. Study of the thermodynamics and mass transfer kinetics of two enantiomers on a polymeric imprinted stationary phase. J Chrom A. 1998;810(1-2):1-17.
217. Pérez-Moral N, Mayes AG. Novel MIP formats. Biosep. 2001;10(6):287-99.

218. Pérez-Moral N, Mayes AG. Comparative study of imprinted polymer particles prepared by different polymerisation methods. Anal Chim Acta. 2004;504(1):15-21.

219. Oxelbark J, Legido-Quigley C, Aureliano CSA, Titirici MM, Schillinger E, Sellergren B, et al. Chromatographic comparison of bupivacaine imprinted polymers prepared in crushed monolith, microsphere, silica-based composite and capillary monolith formats. J Chrom A. 2007;1160 (1-2):215-26.

220. Nicholls IA, Adbo K andersson HS andersson PO, Ankarloo J, Hedin-Dahlström J, et al. Can we rationally design molecularly imprinted polymers? Anal Chim Acta. 2001;435(1):9-18.

221. Isarankura-Na-Ayudhya C, Nantasenamat C, Buraparuangsang P, Piacham T, Ye L, Bülow L, et al. Computational insights on sulfonamide imprinted polymers. Molecules. 2008;13(12):3077-91.

222. Nantasenamat C, Isarankura-Na-Ayudhya C, Naenna T, Prachayasittikul V. Quantitative structure-imprinting factor relationship of molecularly imprinted polymers. Biosen Bioelec. 2007;22(12):3309-17.

223. Nantasenamat C, Naenna T, Isarankura Na-Ayudhya C, Prachayasittikul V. Quantitative prediction of imprinting factor of molecularly imprinted polymers by artificial neural network. J Computer-Aided Mol Design. 2005;19(7):509-24.

224. Nantasenamat C, Tantimongcolwat T, Naenna T, Isarankura-Na-Ayudhya C, Prachayasittikul V. Prediction of selectivity index of pentachlorophenol-imprinted polymers. EXCLI J. 2006;5:150-63.

225. Nantasenamat C, Isarankura-Na-Ayudhya C, Tansila N, Naenna T, Prachayasittikul V. Prediction of GFP spectral properties using artificial neural network. J Comp Chem. 2007;28(7):1275-89.

226. Nantasenamat C, Naenna T, Isarankura-Na-Ayudhya C, Prachayasittikul V. Recognition of DNA splice junction via machine learning approaches. EXCLI J. 2005;4:114-29.

227. Thippakorn C, Suksrichavalit T, Nantasenamat C, Tantimongcolwat T, Isarankura-Na-Ayudhya C, Naenna T, et al. Modeling the LPS neutralization activity of anti-endotoxins. Molecules. 2009;14(5):1869-88.
228. Worachartcheewan A, Nantasenamat C, Naenna T, Isarankura-Na-Ayudhya C, Prachayasittikul V. Modeling the activity of furin inhibitors using artificial neural network. Eur J Med Chem. 2009;44(4):1664-73.
229. Nantasenamat C, Isarankura-Na-Ayudhya C, Naenna T, Prachayasittikul V. A practical overview of quantitative structure-activity relationship. EXCLI J. 2009;8:74-88.
230. Hanski C, Drechsler K, Hanisch FG, Sheehan J, Manske M, Ogorek D, et al. Altered glycosylation of the MUC-1 protein core contributes to the colon carcinoma-associated increase of mucin-bound sialyl-Lewis(x) expression. Cancer Res. 1993;53(17):4082-8.
231. Hawkins CJ, Lavin MF, Parry DL, Ross IL. Isolation of 3,4-dihydroxyphenylalanine-containing proteins using boronate affinity chromatography. Anal Biochem. 1986;159(1):187-90.
232. Ren L, Liu Y, Dong M, Liu Z. Synthesis of hydrophilic boronate affinity monolithic capillary for specific capture of glycoproteins by capillary liquid chromatography. J Chrom A. 2009;1216(47):8421-5.
233. Dou P, Liang L, He J, Liu Z, Chen HY. Boronate functionalized magnetic nanoparticles and off-line hyphenation with capillary electrophoresis for specific extraction and analysis of biomolecules containing cis-diols. J Chrom A. 2009;1216(44):7558-63.
234. He J, Liu Z, Dou P, Liu J, Ren L, Chen HY. Electrochemically deposited boronate affinity extracting phase for covalent solid phase microextraction of cis-diol biomolecules. Talanta. 2009;79(3):746-51.
235. Jin S, Choudhary G, Cheng Y, Dai C, Li M, Wang B. Fluoride protects boronic acids in the copper(I)-mediated click reaction. Chem Commun. 2009(35):5251-3.
236. Kuzimenkova MV, Ivanov AE, Thammakhet C, Mikhalovska LI, Galaev IY, Thavarungkul P, et al. Optical responses, permeability and diol-specific

reactivity of thin polyacrylamide gels containing immobilized phenylboronic acid. Polymer. 2008;49(6):1444-54.

237. Shinkai S, Takeuchi M. Molecular design of synthetic receptors with dynamic, imprinting and allosteric functions. Biosen Bioelec. 2004;20(6):1250-9.
238. Zhang J, Geddes CD, Lakowicz JR. Complexation of polysaccharide and monosaccharide with thiolate boronic acid capped on silver nanoparticle. Anal Biochem. 2004;332(2):253-60.
239. Zhang L, Xu Y, Yao H, Xie L, Yao J, Lu H, et al. Boronic acid functionalized core-satellite composite nanoparticles for advanced enrichment of glycopeptides and glycoproteins. Chem Eur J. 2009;15(39):10158-66.
240. Rostovtsev VV, Green LG, Fokin VV, Sharpless KB. A stepwise huisgen cycloaddition process: Copper(I)-catalyzed regioselective "ligation" of azides and terminal alkynes. Angew Chem Int Ed. 2002;41(14):2596-9.
241. Tornøe CW, Christensen C, Meldal M. Peptidotriazoles on solid phase: [1,2,3]-Triazoles by regiospecific copper(I)-catalyzed 1,3-dipolar cycloadditions of terminal alkynes to azides. J Org Chem. 2002;67(9):3057-64.
242. Best MD. Click chemistry and bioorthogonal reactions: Unprecedented selectivity in the labeling of biological molecules. Biochem. 2009;48(28):6571-84.
243. Kurpiers T, Mootz HD. Bioorthogonal ligation in the spotlight. Angew Chem Int Ed. 2009;48(10):1729-31.
244. Sundberg L, Porath J. Preparation of adsorbents for biospecific affinity chromatography I Attachment of group-containing ligands to insoluble polymers by means of bifunctional oxiranes. J Chrom A. 1974;90(1):87-98.
245. Laemmli UK. Cleavage of structural proteins during the assembly of the head of bacteriophage T4. Nature. 1970;227(5259):680-5.
246. Lin N, Yan J, Huang Z, Altier C, Li M, Carrasco N, et al. Design and synthesis of boronic-acid-labeled thymidine triphosphate for incorporation into DNA. Nucleic Acids Res. 2007;35(4):1222-9.

247. Grafl R, Lang K, Vogl H, Schmid FX. The mechanism of folding of pancreatic ribonucleases is independent of the presence of covalently linked carbohydrate. J Biol Chem. 1987;262(22):10624-9.

BIOGRAPHY

NAME Mr. Thummaruk Suksrichavalit

DATE OF BIRTH 15 February 1982

PLACE OF BIRTH Nakhon Sawan, Thailand

INSTITUTIONS ATTENDED Mahidol University, 2000-2003:
Bachelor of Science (Medical Technology)
Mahidol University, 2004-2010:
Doctor of Philosophy (Medical Technology)

HOME ADDRESS 44/3 Phayuha, Phayuha Khiri,
Nakhon Sawan 60130 Thailand
E-mail: rukmu47@gmail.com

SCHOLARSHIP The Ministry Staff Development Project
by the Ministry of Education, Thailand

PUBLICATIONS

1. Suksrichavalit T, Prachayasittikul S, Piacham T, Isarankura-Na-Ayudhya C, Nantasenamat C, Prachayasittikul V. Copper complexes of nicotinic acid-aromatic carboxylic acids as superoxide dismutase mimetics. Molecules. 2008; 13: 3040-56.
2. Suksrichavalit T, Prachayasittikul S, Isarankura-Na-Ayudhya C, Nantasenamat C, Prachayasittikul V. Copper complexes of pyridine derivatives with superoxide scavenging and antimicrobial activities. Eur J Med Chem. 2009; 44: 3259-65.
3. Piacham T, Nantasenamat C, Suksrichavalit T, Puttipanyalears C, Pissawong T, Maneewas S, Isarankura-Na-Ayudhya C, Prachayasittikul V. Synthesis and theoretical study of molecularly imprinted nanospheres for recognition of tocopherols. Molecules. 2009; 14: 2985-02.

4. Suksrichavalit T, Yoshimatsu K, Prachayasittikul V, Bülow L, Ye L. “Clickable” affinity ligands for effective separation of glycoproteins. J Chromatogr A. 2010; 1217: 3635-41.

PUBLICATION NOT INCLUDED IN THIS THESIS;

1. Thippakorn C, Suksrichavalit T, Nantasenamat C, Tantimongcolwat T, Isarankura-Na-Ayudhya C, Naenna T, Prachayasittikul V. Modeling the LPS neutralization activity of anti-endotoxins. Molecules. 2009; 14(5): 1869-88.